INVESTIGATION OF ATMOSPHERIC OZONE FORMATION POTENTIALS OF C_{12} - C_{16} N-ALKANES

Report to
The Aluminum Association
Contract AA1345

by
William P. L. Carter, Dongmin Luo, and Irina L. Malkina

October 28, 1996

College of Engineering
Center for Environmental Research and Technology
University of California
Riverside, California 92521

96:AP:022:R

ABSTRACT

A series of environmental chamber experiments and computer model calculations were carried out to asses the atmospheric ozone formation potentials of the C_{12} through C_{16} n-alkanes. The experiments consisted of determining the effects of adding n-C_{12}, n-C_{14}, n-C_{15}, or n-C_{16} on NO oxidation, ozone formation and integrated OH radical levels in simulated model photochemical smog systems. Either blacklights or xenon arc lamps were used as the light source, two different surrogate mixtures were used to represent the reactive organic gases (ROGs) present in the atmosphere, and the ROG/NO_x ratio was also varied. The C_{12+} n-alkanes were found to inhibit integrated OH levels and initial rates of NO oxidation and ozone formation in all experiments, but the inhibiting effect on ozone decreased with time in the runs with the more realistic ROG surrogate and the lower NO_x levels, and in some cases slightly higher levels of ozone were eventually formed by the end of the experiment.

An updated detailed gas-phase mechanism gave good fits to data in model simulations of the experiments with n-C_{12}, but tended to underpredict the radical and ozone inhibition in some experiments with the C_{14+} n-alkanes. Somewhat better fits to those runs were obtained in a modified mechanism where ~20% higher alkyl nitrate yields, and thus more radical and NO_x inhibition, was assumed. It is concluded that for the C_{14+} n-alkanes the likely atmospheric reactivities will be somewhere between those predicted by the standard mechanism and the mechanism assuming the ~20% higher nitrate yields.

These mechanisms were then used to estimate the ozone impacts of the higher n-alkanes for a variety of atmospheric conditions. These were compared with ozone impacts calculated for ethane (the compound the EPA uses as the borderline for determining "negligible" ozone reactivity) and the mixture of all emitted VOCs. The results indicated that, regardless of which mechanism was used, the relative ozone impacts of the C_{12+} n-alkanes were highly dependent on atmospheric conditions, and also on whether ozone impacts were measured by effects on peak ozone levels, or on integrated ozone over the standard. Under some conditions the C_{12+} n-alkanes inhibited ozone, while under others they formed more ozone than ethane, depending on how ozone was quantified. Overall, for a majority of the atmospheric conditions examined the C_{12+} n-alkanes were calculated to be slightly more reactive than ethane in terms of their effects on maximum ozone yields, and to be of comparable or lesser reactivity than ethane in terms of their effects on integrated ozone over the standard.

ACKNOWLEDGEMENTS

The authors gratefully acknowledge Mr. Dennis Fitz for assistance in administering this program Mr. Kurt Bumiller and Ms. Kathalena Smihula for assistance in carrying out the experiments. We also thank the Aluminum Associations's VOC Ad Hoc Work group for helpful discussions and their assistance in the design of this program. We acknowledge the National Renewable Energy Laboratory for providing funding for the xenon arc light source used in some of the experiments carried out for this program.

This work was funded by the Aluminum Association through contract number AA 1345. However, the opinions and conclusions expressed in this report are entirely those of the primary author, Dr. William P. L. Carter. Mention of trade names or commercial products does not constitute endorsement or recommendation for use.

EXECUTIVE SUMMARY

Emissions of volatile organic compounds (VOCs) are subject to regulations because they can react in the atmosphere in the presence of oxides of nitrogen (NO_x) and sunlight to form ground-level of ozone (O_3) in photochemical smog. Individual types of VOCs can differ significantly in their effects on ozone formation (i.e., their "reactivities") because of differences in their reaction rates, the types of reactions they undergo, and how their reactions affect the reactions of other VOCs. Therefore, it is more effective to regulate emissions of some types of VOCs as ozone precursors than it is for others. In recognition of this, the EPA has exempted certain compounds from regulation as a VOC ozone precursor on the basis of having "negligible" reactivity. Although the EPA has no formal policy in this regard, in practice the reactivity of ethane is used as the standard because ethane is the most reactive of the compounds the EPA has exempted to date.

In an initial evaluation of ozone impacts of aluminum cold rolling mill emissions, we estimated the ozone impacts of 20 representative rolling lubricant constituents, including C_{12} - C_{22} n-alkanes, C_{10} - C_{26}, C_{20+} olefins, and several other compounds. Of these, we estimated that the C_{12+} n-alkanes were the most likely to have sufficiently low ozone impacts to be likely candidates for VOC exemption. However, the estimated atmospheric reaction mechanisms for these compounds were quite uncertain, and the limited available data were insufficient to support the validity of ozone estimates based on them. Because of this, the ozone impact were too uncertain to serve as a basis for regulatory decision-making.

To improve the reliability of ozone impact assessments of the C_{12+} normal alkanes, the Aluminum Association contracted with us to carry out the environmental chamber experiments needed to provide an experimental basis to support the chemical mechanisms used to calculate their atmospheric ozone impacts. These consisted primarily of measurements of effects of adding the C_{12+} n-alkanes on ozone formation, on rates of NO oxidation, and on rates of consumption of other VOCs under various simulated atmospheric conditions. This involves two types of irradiations of model photochemical smog mixtures. The first is a "base case" experiment where a mixture of reactive organic gases representing those present in polluted atmospheres (the "ROG surrogate") is irradiated in the presence of oxides of nitrogen (NO_x) in air. The second is the "test" experiment which consists of repeating the base case irradiation except that the VOC whose reactivity is being assessed is added. The differences between the results of these experiments provide a measure of the atmospheric impact of the test compound, and the difference relative

to the amount added is a measure of its reactivity. To provide data concerning the reactivities of the test compounds under varying atmospheric conditions, three types of base case experiments were carried out, with both the nature of the ROG surrogate and the ROG surrogate/NO_x ratio varied.

In all cases the addition of the C_{12+} n-alkanes caused a decrease in the rates of ozone formation and NO oxidation in the initial periods of the experiments, and also inhibited levels of hydroxyl (OH) radicals, the primary species oxidizing most VOCs in the atmosphere. However, the inhibiting effect on ozone decreased with time, especially in the runs with the more complex (and realistic) ROG surrogate and the lower NO_x levels, and in some cases slightly higher levels of ozone were eventually formed by the end of the experiment.

The results of these experiments were compared with the predictions of two sets of chemical mechanisms describing the atmospheric reactions of the C_{12+} n-alkanes. The first set, referred to as the "standard" mechanisms, was the set of mechanisms we had estimated previously based on extrapolations from mechanistic data for C_8 and lower n-alkanes. The second set, referred to as the "high nitrate" mechanisms, was based on assuming ~20% higher organic nitrate formation in the photooxidations of these compounds. The assumed amount of organic nitrate formation is an important parameter affecting predictions of ozone reactivity because its formation is a radical termination process which tends to reduce ozone formation, and it is an uncertain parameter because it cannot be measured directly for alkanes larger than n-octane.

The standard mechanism was found to perform quite well in simulating the results of the chamber experiments for n-C_{12}, tending to validate its ability to predict ozone impacts of this compound when modeling atmospheric conditions. However, the standard mechanism tended to underpredict the radical and ozone inhibition effects of the C_{14+} n-alkanes in some experiments, suggesting that it may tend to overpredict their atmospheric ozone impacts. Somewhat better fits to the chamber data for the C_{14+} n-alkanes were obtained if the high nitrate mechanisms were assumed, which predict somewhat lower atmospheric ozone impacts. It is concluded that the actual ozone impacts for the C_{14+} n-alkanes are probably somewhere between those predicted by the standard and the high nitrate mechanisms.

The experimentally evaluated mechanisms were then used to calculate the ozone impacts for the C_{12+} n-alkanes for model air pollution scenarios representing one day ozone episodes in 39 different ozone nonattainment areas throughout the United States, and for three "averaged conditions" scenarios representing three different conditions of NO_x availability. These included the relatively high NO_x

Maximum Incremental Reactivity (MIR) scenario which represents conditions where VOC emissions have the greatest impact on ozone levels, the Maximum Ozone Reactivity (MOR) scenario which represents the intermediate NO_x conditions which are optimum for ozone formation, and the Equal Benefit Incremental Reactivity (EBIR) scenario which represents NO_x conditions where reducing VOC and reducing NO_x emissions are equally effective in reducing ozone formation. Ozone impacts were quantified either by the effect of adding the VOC on the peak instantaneous ozone concentration achieved in the one-day simulation, or by its effect on the ozone concentration integrated over time for the period when the ozone concentrations exceeded the U.S. air quality standard of 0.12 ppm.

Selected results of the atmospheric ozone impact calculations for ethane and representative C_{12+} n-alkanes, relative to the average of all other emitted VOCs, are shown on Table EX-1. The relative ozone impacts of the higher n-alkanes were found to be quite variable, indicating a significant dependence on conditions and on how ozone impacts are quantified. This variability was much greater than differences between calculations using the standard or the high nitrate mechanisms, suggesting atmospheric variability is a larger factor complicating quantifications of ozone impacts of these compounds than mechanistic uncertainty. In some scenarios the higher n-alkanes inhibited ozone formation, and thus had negative incremental reactivity. However, in most scenarios the C_{12+} n-alkanes were calculated to have

Table EX-1. Summary of atmospheric ozone impact estimates for ethane and selected C_{12+} n-alkanes.

Scenario	Ozone Impact relative to Average of All Emitted VOCs (gram basis)			
	Ethane	n-C_{12}	n-C_{14} [a]	n-C_{16} [a]
Impacts on Peak Ozone				
Averaged Conditions MIR (High NO_x)	0.08	0.15	0.11 - 0.13	0.10 - 0.12
Averaged Conditions MOR (Medium NO_x)	0.15	0.29	0.23 - 0.26	0.21 - 0.23
Averaged Conditions EBIR (Low NO_x)	0.19	0.27	0.19 - 0.24	0.18 - 0.22
Highest in 39 Scenarios	0.27	0.42	0.34 - 0.37	0.33 - 0.34
Lowest in 39 scenarios	0.05	-0.08	-0.22 - -0.06	-0.15 - -0.04
Impacts on Integrated Ozone				
Averaged Conditions MIR (High NO_x)	0.07	0.14	0.09 - 0.12	0.08 - 0.11
Averaged Conditions MOR (Medium NO_x)	0.10	0.16	0.10 - 0.14	0.09 - 0.12
Averaged Conditions EBIR (Low NO_x)	0.12	0.12	0.03 - 0.10	0.02 - 0.08
Highest in 39 Scenarios	0.19	0.22	0.15 - 0.20	0.15 - 0.18
Lowest in 39 scenarios	0.05	-0.13	-0.34 - -0.14	-0.27 - -0.13

[a] Range of results for the standard and the high nitrate mechanisms. In all cases, the higher number is that calculated using the standard mechanism.

positive ozone impacts, and in extreme cases they were as high as ~40% of the average reactivity of all reactive VOC emissions, or ~3 times the reactivity of ethane. Overall, we would conclude that in a majority of conditions these C_{12+} n-alkanes probably are slightly more reactive than ethane in terms of their effects on maximum ozone yields, but are of comparable or lower reactivity than ethane in terms of their effects on integrated ozone over the standard.

TABLE OF CONTENTS

LIST OF TABLES

LIST OF FIGURES

TABLE OF ACRONYMS

Abbreviation	Meaning
CE-CERT	University of California at Riverside College of Engineering Center for Environmental Resesarch and Technology
CTC	CE-CERT Xenon Arc Teflon Chamber
CARB	California Air Resources Board
DTC	CE-CERT Dividible Teflon Chamber (blacklight light source)
d(O_3-NO)	Sum of ozone formed + NO oxidized, or change in ([O_3] - [NO]) during an experiment.
ECD	Electron Capture Detection (for gas chromatographs)
EKMA	Emperical Kinetic Modeling Approach. (In the context of this report, refers to a type of model used to represent air pollultion episodes by a single box with varying inversion heights, emissions, etc.)
EPA	United States Environmental Protection Agency
FID	Flame Ionization Detection (for gas chromatographs)
GC	Gas Chromatograph
INTOH	Integrated hydroxyl radical levels.
IR	Incremental reactivity. Change in some measure of air quality (O_3, IntOH, d(O_3-NO), etc.) caused by adding a compound, divided by the amount added.
kOH	Rate constant for reaction with hydroxyl (OH) radicals.
MIR	Maximum Incremental Reactivity. Can refer either to airshed scenarios with NO_x conditions such that VOCs have their highest incremental reactivities, or the set of incremental reactivities for MIR scenarios.
MOIR	Maximum Ozone Incremental Reactivlty. Set of incremental reactivities for airshed scenarios where NO_x conditions are most favorable for ozone formation.
MOR	Maximum Ozone Reactivity. Airshed scenarios with NO_x conditions most favorable for ozone formation.
NMOC	Non-methane organic compounds.
NO	Nitric oxide.
NO_2	Nitrogen dioxide
NO_x	Sum of NO + NO_2.
O_3	Ozone

Abbreviation	Meaning
OH	Hydroxyl radicals. The primary reactive species oxidizing alkanes and most other VOCs in the atmosphere.
PPB	Parts per billion.
PPM	Parts per million
ROG	Reactive Organic Gases
SAPRC	Statewide Air Pollution Research Center at the University of California at Riverside
SCAQS	Southern California Air Quality Study
VOC	Volatile organic compound.

INTRODUCTION

Ozone in photochemical smog is formed from the gas-phase reactions of volatile organic compounds (VOCs) and oxides of nitrogen (NO_x) in sunlight. Although Los Angeles has the worst ozone problem in the United States, other areas of the country also have episodes where ozone exceeds the federal air quality standard of 0.12 ppm. Ozone control strategies in the past have focused primarily on VOC controls, though the importance of NO_x control has become recognized in recent years. VOC and NO_x controls have differing effects on ozone formation. NO_x is required for ozone formation, and if the levels of NO_x are low compared to the levels of reactive VOCs, then changing VOC emissions will have relatively little effect on ozone. Since NO_x is removed from the atmosphere more rapidly than VOCs, ozone in areas far downwind from the primary sources tends to be more NO_x limited, and thus less responsive to VOC controls. VOC controls tend to reduce the rate that O_3 is formed when NO_x is present, so VOC controls are the most beneficial in reducing O_3 in the urban source areas, where NO_x is relatively plentiful, and where O_3 is determined primarily by how rapidly it is being formed. Because of this, any comprehensive ozone control strategy must involve reduction of emissions of both NO_x and VOCs.

Many different types of VOC compounds are emitted into the atmosphere, each reacting at different rates and having a different mechanism for its reactions. Because of this, they can differ significantly in their effects on ozone formation, or their "reactivity". Some compounds, such as CFCs, do not react in the lower atmosphere at all, and thus make no contribution to ground-level ozone formation. Others, such as methane, react and contribute to ozone formation, but react so slowly that their practical effect on ozone formation is negligible. Obviously, it does not make sense to regulate such compounds as ozone precursors. In recognition of this, the EPA has exempted certain compounds from such regulations on the basis of having "negligible" effects on ozone formation. Although the EPA has no formal policy on what constitutes "negligible" reactivity, in practice it has used the ozone formation potential of ethane as the standard in this regard. This is because ethane is the most reactive of the compounds the EPA has exempted to date. Therefore, the ozone formation potential of a compound relative to ethane is of particular interest when assessing whether it might be a likely candidate for exemption from regulation as an ozone precursor.

For example, several years ago our laboratory undertook an experimental and modeling study funded by the Chemical Manufactures Association to provide data needed by the EPA to assess whether

For example, several years ago our laboratory undertook an experimental and modeling study funded by the Chemical Manufactures Association to provide data needed by the EPA to assess whether acetone should be exempted as a VOC ozone precursor (Carter et al., 1993a). The EPA scientist responsible for advising the policy office on this issue made it clear that the decision would hinge largely on the ozone impact of acetone relative to ethane (Dimitriades, private communication, 1993). The result of our study showed that the relative impacts of acetone and ethane (on an ozone formed per gram emitted basis) varied depending on atmospheric conditions, with acetone forming more ozone under some conditions, and ethane forming more under others. The final conclusion was that "acetone and ethane can be considered to have essentially the same reactivity to within their variability with environmental conditions". On this basis, the EPA went forward and ultimately granted a VOC exemption for acetone. This exemption provides a significant precedent because it showed that it is not necessary to show that a compound will always have less of an ozone impact than ethane for it to be considered for exemption.

Aluminum cold rolling mills are regulated as sources of ozone-producing VOCs because their operations involve the use of various organic lubricants which have the potential to be emitted into the atmosphere and promote ozone formation. Since the control equipment required to reduce these emissions is costly, the Aluminum industry has an obvious interest in evaluating whether these emissions do, in fact, promote sufficient ozone for the regulations to be justified on this basis. In an initial evaluation of the atmospheric ozone impacts of aluminum cold rolling mill emissions, Carter and Venkataraman (1995) estimated the ozone impacts of 20 representative rolling lubricant constituents, which consisted of representative C_{12} - C_{22} n-alkanes, C_{10} - C_{26}, C_{20+} olefins, and several other compounds. While some of these compounds were estimated to have insufficient volatility to contribute significantly to ozone formation, most were sufficiently volatile that their reactivities needed to be considered. The ozone impacts of these compounds were then calculated using the chemical mechanism and modeling methodology used to develop general reactivity scales for VOC ozone reactivity assessment (Carter, 1994a), and used in our previous assessment of the reactivity of acetone (Carter et al, 1993a). The result was that while some of the constituents were calculated to be relatively reactive, the C_{12+} normal alkanes were estimated to have ozone impacts quite comparable to that of ethane. This suggests that they, like acetone, might be candidates for exemption on the basis of low reactivity. However, as discussed by Carter and Venkataraman (1995), the estimated atmospheric reaction mechanisms for these high molecular weight compounds were quite uncertain, and the limited available data were insufficient to support the validity of these calculations. Without such data, the estimates of Carter and Venkataraman (1995) were too uncertain to serve as a basis for regulatory decision-making.

To improve the reliability of reactivity assessments of the C_{12+} normal alkanes, the Aluminum Association contracted the College of Engineering Center for Environmental Research and Technology (CE-CERT) to carry out the environmental chamber experiments needed to provide an experimental basis to support the chemical mechanisms used to calculate their atmospheric ozone impacts. The results of this program are documented in this report.

EXPERIMENTAL AND DATA ANALYSIS METHODS

Overall Experimental Approach

The environmental chamber experiments consisted primarily of measurements of "incremental reactivities" of the selected C_{12+} n-alkanes under various conditions. These involve two types of irradiations of model photochemical smog mixtures. The first is a "base case" experiment where a mixture of reactive organic gases (ROGs) representing those present in polluted atmospheres (the "ROG surrogate") is irradiated in the presence of oxides of nitrogen (NO_x) in air. The second is the "test" experiment which consists of repeating the base case irradiation except that the VOC whose reactivity is being assessed is added. The differences between the results of these experiments provide a measure of the atmospheric impact of the test compound, and the difference relative to the amount added is a measure of its reactivity.

To provide data concerning the reactivities of the test compounds under varying atmospheric conditions, three types of base case experiments were carried out:

1. Mini-Surrogate Experiments. This base case employed a simplified ROG surrogate and relatively low ROG/NO_x ratios. Low ROG/NO_x ratios represent "maximum incremental reactivity" (MIR) conditions, which are most sensitive to VOC effects. This is useful because it provides a sensitive test for the model, and also because it is most important that the model correctly predict a VOC's reactivity under conditions where the atmosphere is most sensitive to the VOCs. The ROG mini-surrogate mixture employed consisted of ethene, n-hexane, and m-xylene. This same surrogate was employed in our previous studies (Carter et al, 1993a,b; 1995a,b.), and was found to provide a more sensitive test to the mechanism than the more complex surrogates which more closely represent atmospheric conditions (Carter et al, 1995b). This high sensitivity to mechanism differences made this type of experiment most useful for mechanism evaluation.

2. Full Surrogate Experiments. This base case employed a more complex ROG surrogate under somewhat higher, though still relatively low, ROG/NO_x conditions. While less sensitive to the mechanism employed, experiments with a more representative ROG surrogate are needed to evaluate the mechanism under conditions more closely resembling the atmosphere. The ROG surrogate employed was the same 8-component "lumped molecule" surrogate as employed in our previous study (Carter et al., 1995b), and consists of n-butane, n-octane, ethene, propene, trans-2-butene, toluene, m-xylene, and formaldehyde.

Calculations have indicated that use of this 8-component mixture will give essentially the same results in incremental reactivity experiments as use of actual ambient mixtures (Carter et al., 1995b).

3. Full Surrogate, low NO_x Experiments. This base case employed the same 8-component lumped molecule surrogate as the above set, except that lower NO_x levels (higher ROG/NO_x ratios) were employed to represent NO_x-limited conditions. Such experiments are necessary to assess the ability of the model to properly simulate reactivities under conditions where NO_x is low. The conditions employed were comparable to those employed in our previous studies (Carter et al. 1995b).

In addition to varying the nature of the ROG surrogate and the ROG/NO_x ratios, experiments with different types of light sources were also carried out. Experiments using a blacklight light source were carried out because they give a reasonably good simulation of sunlight in the important UV region affecting most of the atmospherically-important photoreactive species, allow use of a relatively larger volume chamber (which might be important for studies of lower volatility compounds which might tend to adsorb on the surfaces), and are relatively inexpensive to operate, allowing the most experiments to be conducted for a given level of funding. However, blacklights do not give a good representation of sunlight in the λ>400 nm region of the spectrum, which affects atmospheric reactions of some photoreactive species, particularly aromatic ring fragmentation products. Although long-chain alkanes are not expected to form such products in their atmospheric photolysis, it is prudent to include experiments using such a light source to insure that there are not unexpected light-source dependant effects which the model being evaluated is not correctly accounting for. Previous studies have indicated that xenon arcs provide the most realistic representation of sunlight that is attainable for an artificial light source (Carter et al, 1995c). Therefore, a limited number of experiments employing a xenon arc light source were included in this study. This also allowed testing whether the mechanism can adequately simulate the effects of changing light conditions.

An appropriate set of control and characterization experiments necessary to assure data quality and characterizing the conditions of the runs for mechanism evaluation were also carried out. These are discussed where relevant in the results or modeling methods sections.

Environmental Chambers

The two chamber systems employed in this study were the CE-CERT “Dividable Teflon Chamber” (DTC) with the blacklight light source and the CE-CERT Dividable Xenon-arc Teflon Chamber (CTC). Both of these are designed to allow simultaneous irradiations of the base case and the test experiments

under the same reaction conditions. Each chamber is actually two adjacent FEP Teflon reaction bags which can be simultaneously irradiated using the same light source and the same temperature control system. These are referred to as the two "sides" of the chamber (Side A and Side B) in the subsequent discussion. The sides are interconnected with two ports, each with a box fan, which rapidly exchanges their contents to insure that reactants which are desired to have equal concentrations in each side are equalized. In addition, a fan is located in each of the reaction bags to rapidly mix the reactants within each chamber. The ports connecting the two reactors can then be closed to allow separate injections on each side, and separate monitoring of each. This design is optimized for carrying outincremental reactivity experiments such as those for this program.

The CE-CERT DTC consists of two ~5000-liter 2-mil heat-sealed FEP Teflon reaction bags located adjacent to each other and fitted inside an 8'x8'x8' framework, and which uses two diametrically opposed banks of 32 Sylvania 40-W BL blacklights as the light source. Because this has the largest volume of all the indoor chambers currently used at CE-CERT, it is well suited for studies of relatively low volatile compounds such as the C_{12+} n-alkanes. The lighting system in the DTC was found to provide so much intensity that only half the lights were used for the blacklights. The unused blacklights were covered with aluminum sheet, and were used to bring the chamber up to the temperature it will encounter during the irradiation before the uncovered lights are turned on. The air conditioner for thechamber room was turned on before and during the experiments. Four air blowers which are locatedin the bottom of the chamber were used to help cool the chamber and to mix the contents of the chamber. The CE-CERT DTC is very similar to the SAPRC DTC which is described in detail elsewhere (Carter et al, 1995b,d).

Like the DTC, the CTC consists of two reaction bags constructed of the same FEP Teflon material and located next to each other. The reaction bags are in one end of a ~9'x14' room. All surfaces are covered with reflectively polished aluminum paneling and have four 6.3 kw adjustable Xenon Arc lights mounted on the wall opposite the reactors. The radiative power per lamp using borosilicate inner and outer lamp filters was stated as 114,350 microwatts per square centimeter at 48 cm from the light. The lamps were operated at a constant power setting of 4.0 kw for all experiments discussed here, which is ~60% of maximum. The air conditioner for the CTC room was turned on before and during the experiment. The four lamps were turned on to warm up the lamps and to preheat the chamber at least 30 minutes prior to irradiation. A shutter was used to shield the chamber from the lights when they were warming up. It was raised to begin the irradiation. Four blowers located on the ceiling were turned on to force cooling air down into the chamber room to cool the chamber during the irradiation. The CTC is very similar to the SAPRC XTC which is described in detail elsewhere (Carter et al, 1995c,d).

Experimental Procedures

Similar experimental procedures were employed for both chamber systems. The reaction bags were flushed with dry purified air for 14 hours (6pm-8am) on the nights before experiments. An AADCO air purification system was employed. The continuous monitors were connected prior to reactant injection and the data system began logging data from the continuous monitoring systems. The reactants were injected as described below (see also Carter et al, 1993a,, 1995d). The common reactants were injected in both sides simultaneously using a three-way (one inlet and two outlets connected to side A and B respectively) bulb of 2 liters in the injection line and were well mixed before the chamber was divided. The contents of each side were blown into the other using two box fans located between them. Mixing fans were used to mix the reactants in the chamber during the injection period, but these were turned off prior to the irradiation. The sides were then separated by closing the ports which connected them, after turning all the fans off to allow their pressures to equalize. After that, reactants for specific sides (the test compound in the case of reactivity experiments) were injected and mixed. The irradiation began by turning on the lights and proceeded for 6 hours. In the case of the CTC, the sliding panel was lowered between the lights and the reaction bags, and the lights were turned on and allowed to stabilize for 30 minutes prior to the irradiation being started by raising the panel. After the run, the chamber was emptied by allowing the bag to collapse, and then flushed with purified air. The contents of the reactors were vented into a fume hood.

The procedures for injecting the various types of reactants were as follows. The NO and NO_2 were prepared for injection using a high vacuum rack. Known pressure of NO, measured with MKS Baratron capacitance manometers, were expanded into Pyrex bulbs with known volumes, which were then filled with nitrogen (for NO) or oxygen (for NO2). The contents of the bulbs were then flushed into the chamber with ADDCO air. The other gas reactants were prepared for injection either using a high vacuum rack or using gas-tight syringes. The gas reactants in a gas-tight syringe were usually diluted to 100-ml with nitrogen in the syringe. The volatile liquid reactants were injected, using a micro syringe, into a 1-liter Pyrex bulb equipped with stopcocks on each end and a port for the injection of the liquid. The port was then closed and one end of the bulb was attached to the injection port of the chamber and the other to a dry air source. The stopcocks were then opened, and the contents of the bulb were flushed into the chamber with a dry air for approximately 5 minutes, while being heated with a heat gun. In the case of high boiling point chemicals like the C_{12+} n-alkanes, a three-way glass tube (one port for the liquid injection) surrounded with heat tape was used instead. Formaldehyde, which is the only solid compound used in this study, was prepared in a vacuum rack system by heating paraformaldehyde in an evacuated bulb until the pressure corresponded to the desired amount of formaldehyde. The bulb was then closed

and detached from the vacuum system and its contents were flushed into the chamber with dry air through the injection port.

Analytical Methods

Ozone and nitrogen oxides (NOx) were continuously monitored using commercially available continuous analyzers with Teflon sampling lines inserted directly into the chambers. The sampling lines from each side of the chamber were connected to solenoids which switched from side to side every 10 minutes, so the instruments alternately collected data from each side. Ozone was monitored using a Dasibi 1003AH UV photometric ozone analyzer and NO and total oxides of nitrogen (including HNO3 and organic nitrates) were monitored using a Teco Model 14B chemiluminescent NO/NOx monitor. The output of these instruments, along with that from the temperature and formaldehyde instruments were attached to a computer data acquisition system, which recorded the data at 10 minute intervals for ozone, NO and temperature (and at 15 minutes for formaldehyde), using 30 second averaging times. This yielded a sampling interval of 20 minutes to take data from each side.

The Teco instrument and Dasibi CO analyzer were calibrated with a certified NO and CO source and CSI gas-phase dilution system. It was done prior to the chamber experiment for each run. The NO2 converter efficiency check was carried out on regular intervals. The Dasibi ozone analyzer was calibrated against a transfer standard ozone analyzer approximately every three months. In addition, for each experiment the Dasibi was checked with a CSI ozone generator (set to 400 ppb) to insure that the instrument worked properly. The details were discussed elsewhere (Carter et al, 1995d)

Organic reactants other than formaldehyde were measured by gas chromatography with FID or ECD detectors as described elsewhere (Carter et al., 1993a). GC samples were taken for analysis at intervals from 20 minutes to 30 minutes either using 100 ml gas-tight glass syringes or by collecting the 100 ml sample from the chamber onto a Tenax-GC solid adsorbent cartridge. These samples were taken from ports directly connected to the chamber after injection and before irradiation and at regular intervals after irradiation. Two sampling methods were employed for injecting the sample onto the GC column, depending on the volatility or "stickiness" of the compound. For analysis of the more volatile species (which includes all the components of the base case surrogates employed in this study), the contents of the syringe were flushed through a 2 ml or 3 ml stainless steel or 1/8" Teflon tube loop and subsequently injected onto the column by turning a gas sample valve. This is referred to as the "loop" analysis method. For the analysis of lower volatility or more "sticky" compounds, such as the C_{12+} n-alkanes in this study, the contents of the syringe were first trapped in a 1/4" id x 3" long tube filled with Tenax absorbent. The

Tenax filled tube was then placed in series with the GC column, then heated to 300°C to desorb the sample, which was then cryofocused on the column. This is referred to as the "tenax" analysis method. For some compounds, particularly n-hexane, n-octane, toluene and m-xylene, data could be obtained using both methods. In those cases, except when problems were encountered as discussed below, the loop analysis method was employed when analyzing the data for modeling because it usually gives more precise data.

The calibrations for the GC analyses for most compounds were carried out by sampling from chambers or vessels of known volume into which known amounts of the reactants were injected, as described previously (Carter et al, 1995d). However, this method was not considered reliable for the C_{12+} n-alkanes because of uncertainties in quantitatively injecting such low volatility compounds completely into the gas phase. For these compounds, known concentrations were prepared in methanol solution, and known volumes of this solution were placed on the tenax cartridges using a microliter syringe, whose contents were then injected onto the column using the procedures discussed above. The FID calibration per-carbon responses observed for these high molecular weight compounds using this methanol/tenax calibration method were consistent with those for lower molecular weight compounds calibrated using the gas-phase tenax analysis method.

Characterization Methods

Three temperature thermocouples for each chamber were used to monitor the chamber temperature, two of which were located in the sampling line of continuous analyzers to monitor the temperature in each side. The third one was located in the chamber to monitor chamber temperature. The temperatures in these experiments were typically 21-25° C for DTC and 25-30° C for CTC.

The light intensity in the DTC chamber was monitored by periodic NO2 actinometry experiments utilizing the quartz tube method of Zafonte et al (1977), with the data analysis method modified as discussed by Carter et al. (1995d). The results of these experiments were tracked over time in this chamber since it was first constructed in early 1994. The measured NO_2 photolysis rates were fit by a curve where the NO_2 photolysis rate decayed relatively rapidly from its initial value of ~0.31 min^{-1} when the chamber and lights were new, leveling off to ~0.22 min^{-1} by the time of these experiments. The results of the actinometry experiments carried out in the DTC during this study were consistent with the predictions of this curve to within the variability of these determinations, which is ±3%. The spectrum of the blacklight source was measured using a LiCor LI-1200 spectra radiometer, and found to be

essentially the same as the general blacklight spectrum recommended by Carter et al (1995d) for use in modeling blacklight chamber experiments.

The light intensity in the CTC chamber was monitored using several methods, summarized below. In addition, the spectra of the xenon arc lights were measured five times during each experiment, and the averages of these spectra were used for calculating the photolysis rates for modeling, as discussed by Carter et al (1995c,d). Periodic NO_2 actinometry experiments were conducted using the quartz tube method as employed for the DTC, but the results were not considered as a reliable indicator of the average light intensity in the reactor because of the inhomogeneity of the light source in the room, and the fact that the tube had to be located closer to the lights than the chamber. These data were used therefore to determine relative trends in the intensity over time. Even more precise indications of relative trends in light intensity were obtained from the data from the LI-1200 spectra radiometer, since such data were obtained several times during an experiment. These relative trend data were then placed on an absolute basis from "steady state" actinometry experiments where NO, NO_2 and O_3 were simultaneously monitored in the reaction bags, as discussed by Carter et al (1995c,d) for a similar xenon arc Teflon chamber. The quartz tube actinometry experiments were found to give measurements which were consistently a factor of 1.2 higher than those of the steady state actinometry runs. Thus, a factor of 1/1.2 was used to correct the quartz tube data for the purpose of establishing NO_2 photolysis rates in the chamber for modeling purposes. For the period of these experiments, the NO_2 photolysis rate based on the corrected trend data was 0.19 $min^{-1.}$

More recently, the light intensity in the CTC was determined by measuring the rate of decay of n-butane in irradiations of Cl_2 - n-butane mixtures. Model simulations indicate that reaction with n-butane is the dominant fate of the Cl atoms formed in the photolysis of Cl_2 in that system, and that this was also the dominant process consuming the n-butane. These data can thus be used to derive the Cl_2 photolysis rate in the chamber. The results were in good agreement with those calculated from the light intensity and spectrum and absorption cross sections of Cl_2 (Atkinson et al. 1996), assuming unit quantum yields, and thus tended to support the validity of our light intensity determinations for this chamber.

The dilution of the DTC chamber due to sampling is expected to be small because the flexible reaction bags can collapse as sample is withdrawn for analysis. However, some dilution occurs with the age of reaction bags because of small leaks. Information concerning dilution in an experiment can be obtained from relative rates of decay of added VOCs which react with OH radicals with differing rate constants (Carter et al., 1993b; 1995d). All experiments had more s reactive compound such as m-xylene

or n-octane, present either as a reactant or added in trace amounts to monitor OH radical levels. Trace amounts (~0.1 ppm) of n-butane was added to experiments if needed to provide a less reactive compound for the purposes of monitoring dilution. In addition, specific dilution check experiments such as CO-NO were carried out and based on the results, the dilution rate was found to be 0.3% per hour in side A, which is slightly higher than the dilution rate of 0.1% in side B. The dilution rate in the CTC chamber was expected to be even less because the chamber framework design was such that any leakage tended to cause the reactors to collapse rather than fill with outside air.

Reactivity Data Analysis Methods

As indicated above, most of the experiments for this program consisted of simultaneous irradiation of a "base case" reactive organic gas (ROG) surrogate - NO_x mixture in one of the dual reaction chambers, together with an irradiation, in the other reactor, of the same mixture with a n-C_{12+} n-alkane added. The results were analyzed to yield two measures of VOC reactivity: the effect of the added VOC on the amount of NO reacted plus the amount of ozone formed, and integrated OH radical levels. These are discussed in more detail below.

The first measure of reactivity is the effect of the VOC on the change in the quantity $[O_3]$-[NO], or $([O_3]_t$-$[NO]_t)$-$([O_3]_0$-$[NO]_0)$, which is abbreviated as d(O_3-NO) in the subsequent discussion. As discussed elsewhere (e.g., Johnson, 1983; Carter and Atkinson, 1987; Carter and Lurmann, 1990, 1991, Carter et al, 1993b, 1995a), this gives a direct measure of the amount of conversion of NO to NO_2 by peroxy radicals formed in the photooxidation reactions, which is the process that is directly responsible for ozone formation in the atmosphere. (Johnson calls it "smog produced" or "SP".) The incremental reactivity of the VOC relative to this quantity, which is calculated for each hour of the experiment, is given by

$$IR[d(O_3\text{-}NO)]_t^{VOC} = \frac{d(O_3\text{-}NO)_t^{test} - d(O_3\text{-}NO)_t^{base}}{[VOC]_0} \qquad (I)$$

where $d(O_3\text{-}NO)_t^{test}$ is the d(O_3-NO) measured at time t from the experiment where the test VOC was added, $d(O_3\text{-}NO)_t^{base}$ is the corresponding value from the corresponding base case run, and $[VOC]_0$ is the amount of test VOC added. An estimated uncertainty for IR[d(O_3-NO)] is derived based on assuming a ~3% uncertainty or imprecision in the measured d(O_3-NO) values. This is consistent with the results of the side equivalency test, where equivalent base case mixtures are irradiated on each side of the chamber.

Note that reactivity relative to $d(O_3\text{-NO})$ is essentially the same as reactivity relative to O_3 in experiments where O_3 levels are high, because under such conditions $[NO]_t^{base} \approx [NO]_t^{test} \approx 0$, so a change $d(O_3\text{-NO})$ caused by the test compound is due to the change in O_3 alone. However, $d(O_3\text{-NO})$ reactivity has the advantage that it provides a useful measure of the effect of the VOC on processes responsible for O_3 formation even in experiments where O_3 formation is suppressed by relatively high NO levels.

The second measure of reactivity is the effect of the VOC on integrated hydroxyl (OH) radical concentrations in the experiment, which is abbreviated as "IntOH" in the subsequent discussion. This is an important factor affecting reactivity because radical levels affect how rapidly all VOCs present, including the base ROG components, react to form ozone. If a compound is present in the experiment which reacts primarily with OH radicals, then the IntOH at time t can be estimated from

$$IntOH_t = \int_0^t [OH]_\tau d\tau = \frac{ln\left(\frac{[tracer]_0}{[tracer]_t}\right) - Dt}{kOH^{tracer}} , \qquad (II)$$

where $[tracer]_0$ and $[tracer]_t$ are the initial and time=t concentrations of the tracer compound, kOH^{tracer} is its OH rate constant, and D is the dilution rate in the experiments. The latter was found to be small and was assumed to be negligible in our analysis. The concentration of tracer at each hourly interval was determined by linear interpolation of the experimentally measured values. M-xylene was used as the OH tracer in these experiments because it is a surrogate component present in all experiments, its OH rate constant is known (the value used was 2.36×10^{-11} cm^3 $molec^{-1}$ s^{-1} [Atkinson, 1989]), and it reacts relatively rapidly.

The effect of the VOC on OH radicals can thus be measured by its IntOH incremental reactivity, which is defined as

$$IR[IntOH]_t^{VOC} = \frac{IntOH_t^{test} - IntOH_t^{base}}{[VOC]_0} \qquad (III)$$

where $IntOH_t^{test}$ and $IntOH_t^{base}$ are the IntOH values measured at time t in the added VOC and the base case experiment, respectively. The results are reported in units of 10^6 min. The uncertainties in IntOH and IR[IntOH] are estimated based on assuming a ~2% imprecision in the measurements of the m-xylene concentrations. This is consistent with the observed precision of results of replicate analyses of this compound.

CHEMICAL MECHANISMS AND MODELING METHODS

General Atmospheric Photooxidation Mechanism

The chemical mechanism used in the environmental chamber and atmospheric model simulations in this study is given in Appendix A to this report. This mechanism is based on that documented by Carter (1990), with a number of updates as discussed below. It can explicitly represent a large number of different types of organic compounds, but it lumps together species reacting with similar rate constants and mechanisms in atmospheric simulations, and it uses a condensed representation for many of the reactive organic products. The reactions of inorganics, CO, formaldehyde, acetaldehyde, peroxyacetyl nitrate, propanaldehyde, peroxypropionyl nitrate, glyoxal and its PAN analog, methylglyoxal and several other product compounds are represented explicitly. In addition, the reactions of unknown photoreactive products formed in the reactions of aromatic hydrocarbons are represented by a model species "AFG2", whose yields and photolysis parameters are adjusted based on fits of model simulations to environmental chamber experiments. A chemical operator approach is used to represent peroxy radical reactions, as discussed in detail by Carter (1990). Generalized reactions with variable rate constants and product yields are used to represent the primary emitted alkane, alkene, aromatic and other VOCs (with rate constants and product yields appropriate for the individual compounds being represented in each simulation); The tables in the Appendix list only those VOCs (or groups of VOCs) used in the simulations in this work. Most of the higher molecular weight oxygenated product species are represented using the "surrogate species" approach, where simpler molecules such as propanaldehyde or 2-butanone are used to represent the reactions of higher molecular weight analogues that are assumed to react similarly.

Several aspects of the Carter (1990) mechanism were updated prior to this work to account for new kinetic and mechanistic information for certain classes of compounds as described by Carter et. al. (1993a) and Carter (1995). In addition, further modifications were made to the uncertain portions of the mechanisms for the aromatic hydrocarbons to satisfactorily simulate results of experiments carried out using the chamber and light source employed in this study. The previously optimized aromatic mechanisms tended to underpredict the rates of NO oxidation and O_3 formation in the aromatic - NO_x experiments carried out in the chamber employed in this study (Carter et al, 1995c), so the aromatic mechanisms were reoptomized, by adjusting yields of model species used to represent uncharacterized ring-opening products (AFG2 and MGLY), to satisfactorily fit the chamber data. Note that while in the previous mechanisms the MGLY model species represented methylglyoxal alone, in the reoptimized

mechanism it is being used to represent uncharacterized products as well. The reoptimized MGLY and AFG2 yields for toluene were changed from respectively 0.13 and 0.49 to 0.85 and 0.27, and those for m-xylene were changed from 0.37 and 0.75 to 1.55 and 0.51, and the AFG2 photolysis rate was reduced by a factor of 2, relative to those used by the 1993 version of the mechanism (Carter et al, 1993a; Carter 1995). These updated aromatic mechanisms are still being developed, and a more detailed discussion of them is beyond the scope of this paper. The reactions of the species of particular interest in this study are discussed in more detail below.

Atmospheric Reactions of Alkanes

The only significant gas-phase atmospheric reaction of alkanes is the reaction with OH radicals (Atkinson, 1989, 1990). Alkanes do not absorb light in the wavelength region provided by ground-level sunlight ($\lambda \geq 300$ nm) (Calvert and Pitts, 1966), and rate constants for their reactions with other reactive atmospheric species (e.g., O_3, NO_3 radicals, $O(^3P)$ atoms) are too low for them to be of significance (Atkinson and Carter, 1984; Atkinson, 1991; Atkinson, 1990). Rate constants for OH radical reactions have been measured for the n-alkanes up to C_{13}, and for various branched alkane isomers up to ~C_8. Based on this information, Atkinson (1987) developed a structure-estimation method which can be used to derive rate constants for other compounds which (for alkanes at least) is probably good to within ±50%. (This is based on assigning a group rate constant for each $-CH_3$, $>CH_2$, and >CH- group, with corrections for the types of "neighbor" groups adjacent to each.) The OH radical rate constants used for n-C_{12} and n-C_{13} were the experimentally-measured values reported by Atkinson (1989), while those used for n-C_{14+} are estimated. Since the estimates agreed with the measurements for n-C_{12} and n-C_{13} to within 5%, the estimates for n-C_{14+} are not considered to be highly uncertain.

The major processes by which ethane reacts in the atmosphere are as follows:

$$\cdot OH + CH_3CH_3 \rightarrow H_2O + CH_2CH_2\cdot \quad (1)$$

$$CH_2CH_2\cdot + O_2 \rightarrow CH_2CH_2OO\cdot \quad (2)$$

$$CH_2CH_2OO\cdot + NO \rightarrow CH_2CH_2O\cdot + NO_2 \quad (3a)$$

$$CH_2CH_2O\cdot + O_2 \rightarrow CH_3CHO + HO_2\cdot \quad (4a)$$

$$HO_2\cdot + NO \rightarrow NO_2 + \cdot OH \quad (5)$$

The net effect of these processes is the conversion of two molecules of NO to NO_2, the oxidation of ethane to acetaldehyde, and no net change in OH radical levels. The conversion of NO to NO_2 is the process directly responsible for ozone formation. Since acetaldehyde is a fairly reactive compound which

also causes ozone formation, this means that ethane is a moderately efficient compound towards forming ozone once it reacts. Its relatively low overall reactivity is due primarily to its relatively low reaction rate, and not to its relatively efficient reaction mechanism.

In many respects the reactions of the higher alkanes are very similar to those shown above for ethane, but the larger radicals involved have available additional reaction routes which will affect the distribution of oxidized products formed, the number of molecules of NO converted to NO_2, and the effect of the overall processes on OH radical levels. The atmospheric reactions of higher molecular weight alkanes have been discussed in detail elsewhere (Carter and Atkinson, 1985), and only the major features will be summarized here. The initial reaction routes are directly analogous to those shown above, the primary process is abstraction by OH from a C-H bond forming an alkyl radical, which then reacts rapidly with O_2 to form a peroxy radical, which, in the presence of NO_x, reacts primarily with NO. Most (though not all — see below) proceed analogously to reactions (1-3a) above, giving rise to an alkoxy ($RO\cdot$) radical. However, higher molecular weight alkoxy radicals in general have two other types of possible reaction routes besides the O_2 reaction analogous to reaction (4a). One is decomposition via β-scission, whose net effect is formation of lower molecular weight oxidized products, and conversion of additional molecules of NO to NO_2. For example,

$$\begin{array}{c} R'C(O\cdot)CHR \rightarrow R'CHO + R\cdot \\ R\cdot + O_2 \rightarrow RO_2 \\ RO_2 + NO \rightarrow NO_2 + RO\cdot. \\ RO\cdot \rightarrow \rightarrow \text{(etc)} \end{array} \qquad \text{(4b)}$$

Another is isomerization via a 1,4-hydrogen shift to form polyfunctional oxygenates, and also cause additional NO to NO_2 conversions. For example,

$$RCH_2CH_2CH_2CH_2CH(O\cdot)R' \rightarrow RCH(\cdot)RCH_2CH_2CH(OH)R' \qquad \text{(4c)}$$

$$RCH(\cdot)RCH_2CH_2CH(OH)R' + O_2 \rightarrow RCH(OO\cdot)RCH_2CH_2CH(OH)R'$$

$$RCH(OO\cdot)RCH_2CH_2CH(OH)R' + NO \rightarrow RCH(O\cdot)RCH_2CH_2CH(OH)R' + NO_2 \qquad \text{(3a')}$$

$$RCH(OO\cdot)RCH_2CH_2CH(OH)R' + NO \rightarrow RCH(ONO_2)RCH_2CH_2CH(OH)R'. \qquad \text{(3b')}$$

$$RCH(O\cdot)RCH_2CH_2CH(OH)R' \rightarrow RCH(OH)RCH_2CH_2C(\cdot)(OH)R'$$

$$RCH(OH)RCH_2CH_2C(\cdot)(OH)R' + O_2 \rightarrow RCH(OH)RCH_2CH_2C(=O)R' + HO_2$$

$$HO_2 + NO \rightarrow NO_2 + HO\cdot.$$

Decomposition processes (e.g., reaction 4b) tend to be relatively more important for the branched alkanes because radicals with substituents are more likely to split off. Hydrogen shift isomerization processes (via a 6-member ring transition state, e.g, reaction 4c) are more important with the n- and other longer-chain

alkanes, and generally dominate over decomposition for those straight-chain radicals where such hydrogen shift isomerizations are possible. Both isomerization and decomposition have similar net effects on ozone formation in that they cause additional NO to NO_2 conversions compared to cases where the O_2 reaction (e.g, 4a) dominate. The main difference is that decomposition causes formation of lower molecular weight oxidized products, while isomerization is believed to form polyfunctional compounds which are more likely to undergo condensation. Isomerization may be relatively less important for cycloalkanes (e.g., napthenics) because of ring strain considerations; there is no information available concerning this.

If these were the only factors involved, then the higher alkanes would be relatively efficient ozone precursors because of the additional NO to NO_2 conversions. However, there is an additional factor which turns out to be even more important in affecting the ozone reactivity of these compounds. In the case of ethane and most other low molecular weight compounds, the reaction of NO with peroxy ($ROO\cdot$) radicals involves primarily formation of alkoxy radicals and NO_2, as shown in reaction (3a), above. Thus, no net loss of radicals or NO_x is involved. However, for the alkanes at least, it is now known that as the size of the peroxy radical increases, a competing process, alkyl nitrate formation via

$$ROO\cdot + NO \rightarrow RONO_2 \qquad (3b)$$

becomes increasingly important (Atkinson, 1990; Carter and Atkinson, 1985, 1989b). This can have a strong effect on the VOC's reactivity because it removes both radicals and NO_x from the system. As discussed above, if a VOC's reactions cause radical removal, it reduces the rate of ozone formation from all other VOCs, and, if sufficiently important, can more than compensate for the O_3 formed from the VOC's direct reactions. The NO_x removal effect of this process can also reduce the ultimate amount of O_3 which can be formed in environments where O_3 formation is NO_x-limited.

Thus, the $k_{3b}/(k_{3a}+k_{3b})$ ratio, or the "nitrate formation yield", tends to be the dominant factor affecting a high molecular weight alkane's reactivity. If sufficiently high, it would cause the alkane to have a lower incremental reactivity than ethane despite its higher atmospheric reaction rate and greater number of NO to NO_2 conversions, and it may even cause the alkane to have a negative effect on ozone. How high is "sufficient" in this regard will be discussed later in conjunction with the calculations of atmospheric reactivity.

The extent of alkyl nitrate formation via reactions such as (3b) has been quantified by measuring yields of alkyl nitrate isomers in the OH/NO_x/air reactions of various normal and branched alkanes. Such

measurements have been made for all the n-alkanes from propane through n-octane, and for a number of C_5 and C_6 branched alkanes (Carter and Atkinson, 1989b and references therein). Based on these data, Carter and Atkinson (1989b) derived a general estimation method for alkyl nitrate yields from reactions of NO with various alkanes. The yields were found to be dependent on both temperature and pressure, and increased monotonically with the number of carbons, though tending to level out for the larger radicals. For example, Figure 1 shows a plot of the alkyl nitrate yield as a function of carbon number for the n-alkanes, where the points show the experimental data, and the curve shows the estimate based on the functional fit derived by Carter and Atkinson (1989b). Note that since there are no data for n-alkanes greater than n-octane, the estimates for the yields for all the higher n-alkanes are extrapolations. The dotted line gives our estimate of the likely upper limit of the overall nitrate formation yields, based on the results of modeling the experiments in this study which are discussed later in this report.

An additional question is the extent of nitrate formation in the reactions of NO with the oxidized peroxy radicals believed to be formed following the isomerization of the longer-chain alkoxy radicals, shown as Reaction (3b') above. Since all the data concerning nitrate formation in these reactions is based on measurements of the alkyl nitrates formed from the initially formed alkyl peroxy radicals, there is no information concerning these processes. If alkyl nitrate formation from these OH-substituted radicals were as important as from the initially formed ones, the total radical termination from nitrate-forming reactions from n-alkanes could be up to 75% higher in the case of the C_{12+} n-alkanes. However, the previously available environmental chamber data for n-octane (Carter et al, 1993b, 1995b) and n-pentadecane (Carter, 1987; Carter and Venkataraman, 1995), as well as the results of this study (discussed below) are inconsistent with this assumption. Therefore, nitrate formation from the oxidized radicals formed following isomerization (e.g. from Reaction (3b'), appears to be much less important than nitrate formation from the primarily formed radicals.

The mechanisms the C_{12+} n-alkanes used as in this study (and shown in Appendix A) have been derived based on the considerations above. Specifically, the extrapolations of Carter and Atkinson (1989b) were used to estimate the nitrate yields in the initially formed peroxy radicals, but alkyl nitrate formation from the reactions of NO hydroxy-substituted radicals formed in the isomerization reactions is assumed to be negligible. Based on the estimates of Carter and Atkinson (1985), isomerizations are assumed to be the dominant reactions of the long-chain alkoxy radicals, and thus the major products formed, other than the organic nitrates, are δ-hydroxy carbonyls such as $RCH(OH)RCH_2CH_2C(=O)R'$.

Figure 1. Plot of experimental and estimated alkyl nitrate yields in the reactions of OH radicals with the n-alkanes.

Following the "lumped molecule" approach of general mechanism for representing most oxygenated product species (Carter, 1990), these products are represented in the model as either the generic higher aldehyde (RCHO) or the generic higher ketone (MEK) species, depending on whether it is an aldehyde or ketone. Likewise, the C_{12+} alkyl nitrate products are represented by the generic alkyl nitrate species RCHO. This product representation is clearly highly approximate (since the reactions of these generic products are based on much lower molecular weight compounds), but calculations have shown that alkane reactivities are not highly sensitive to this aspect of the mechanism (unpublished results from this laboratory).

This mechanism with the nitrate yields estimated using the extrapolations of Carter and Atkinson (1989b) is referred to as the "standard" mechanism. As discussed below, model simulations of some of the C_{14+} n-alkane experiments suggest that the standard mechanism may be biased toward overpredicting

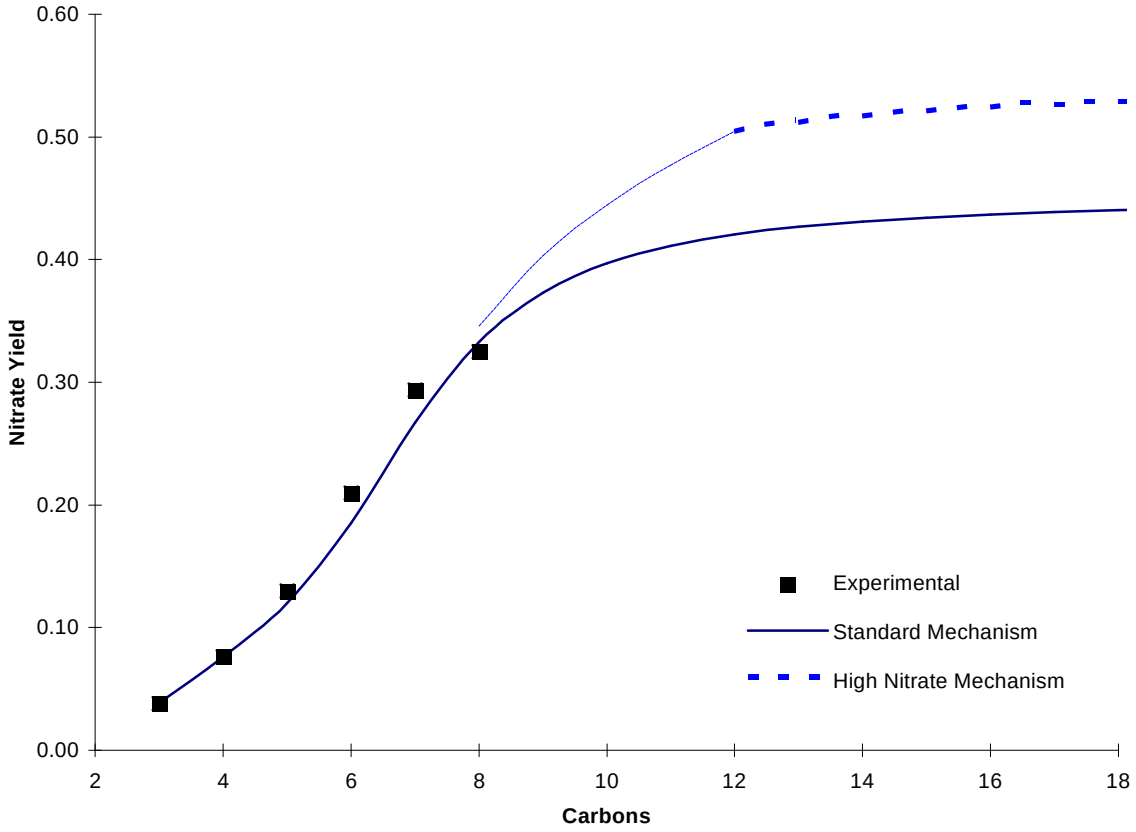

Figure 1. Plot of experimental and estimated alkyl nitrate yields in the reactions of OH radicals with the n-alkanes.

the reactivity (underestimating the radical inhibition) of these compounds. This would be the case if the extrapolated alkyl nitrate yields were low. To assess this, we derived an alternative "high nitrate mechanism" for the C_{12+} n-alkanes where the overall nitrate yields were assumed to be ~20% higher than those in the standard mechanism. The reactions in this mechanism are also included in Appendix A.

Environmental Chamber Simulations

The ability of the chemical mechanisms to appropriately simulate the atmospheric impacts of the C_{12+} n-alkane reactions was evaluated by conducting model simulations of the environmental chamber experiments from this study. This requires including in the model appropriate representations of chamber-dependent effects such as wall reactions and characteristics of the light source. The methods used are based on those discussed in detail by Carter and Lurmann (1990, 1991), updated as discussed by Carter et al (1995c,d). The photolysis rates were derived from results of NO_2 actinometry experiments and direct measurements of the spectra of the light source. In the case of the blacklights used in the DTC, the spectrum was assumed to be constant and the blacklight spectrum given by Carter et al (1995c,d) was employed. In the case of the xenon arc light source in the CTC, rate constants were calculated using averages of spectral measurements made during each experiment, similar to the methods used for a comparable chamber as described by Carter et al. (1995c,d). The thermal rate constants were calculated using the temperatures measured during the experiments, with the small variations of temperature with time during the experiment being taken into account. The computer programs and modeling methods employed are discussed in more detail elsewhere (Carter et al, 1995d). The specific values of the chamber-dependent parameters used in the model simulations of the experiments for this study are given in Appendix A.

Atmospheric Reactivity Simulations

To estimate its effects on ozone formation under conditions more representative of polluted urban atmospheres, incremental reactivities, defined as the change in O_3 caused by adding small amounts of a compound to the emissions, were calculated for ethane, the n-C_{12+} n-alkanes, and several other representative compounds for various simulated atmospheric pollution scenarios. Carter (1994a) used a series of single-day EKMA box model scenarios (EPA, 1984) derived by the EPA to represent 39 different urban ozone exceedence areas around the United States (Baugues, 1990), to develop various reactivity scales to quantify impacts of VOCs on ozone formation in various environments. It was found NO_x levels is the most important factor affecting differences in relative ozone impacts among VOCs, and that the ranges of relative reactivities in the various scales can be reasonably well represented by ranges in relative reactivities in three "averaged conditions" scenarios representing three different NO_x conditions. These

scenarios were derived by averaging the inputs to the 39 EPA scenarios, except for the NO_x emissions. In the "maximum reactivity" scenario, the NO_x inputs were adjusted such that the final O_3 level was most sensitive to changes in VOC emissions; in the "maximum ozone" scenario the NO_x inputs were adjusted to yield the highest daily maximum O_3 concentration; and in the "equal benefit" scenario the NO_x inputs were adjusted such that relative changes in VOC and NO_x emissions had equal effect on ozone formation. As discussed by Carter (1994a), these represent respectively the high, medium and range of NO_x conditions which are of relevance when assessing VOC control strategies for reducing ozone.

The chemical mechanisms used for these atmospheric simulations were the same as used to simulate the chamber experiments, except that the reactions representing chamber effects were removed, and the reactions for the full variety of VOCs emitted into the scenarios (Carter, 1994a) were represented (see Appendix A). Most of the emitted VOCs (other than the test compound whose reactivity is being calculated) are not represented in the model explicitly, but are represented using lumped model species whose rate constants and product yield parameters are derived based on the mixture of compounds they represent. The rate constants and mechanistic parameters for the emitted species in the scenarios were the same as those used previously (Carter, 1994a; Carter et al, 1993a), except for the aromatics, whose unknown photoreactive product yields were reoptimized in a manner analogous to that discussed above for toluene and m-xylene (unpublished results from this laboratory). The listings in Appendix A give the lumped model species used to represent the emissions in the scenarios and indicate the types of species each is used to represent, and give the rate constants and product yield parameters for each.

RESULTS AND DISCUSSION

Summary of Experiments

Tables 1 and 2 give chronological listings of all the experiments carried out for this program for each of the two chambers. These consisted primarily of incremental reactivity experiments, whose conditions and selected results are summarized in more detail in Table 3. In addition, several characterization runs were carried out to determine chamber-dependent inputs needed for the model simulations of the experiments, control experiments were conducted to insure consistency with previous results, and side equivalency tests were conducted to insure that essentially equivalent results were obtained when equal mixtures were simultaneously irradiated in each of the dual reaction bags. Comments on the tables summarize the results obtained for the characterization and control runs.

Except as noted, the results of the characterization and control runs were generally as expected based on our previous experience with these and similar chambers in our laboratories (Carter et al., 1995d and references therein). Good side equivalency was observed when equivalent surrogate - NO_x, propene - NO_x or n-butane - NO_x mixtures were simultaneously irradiated in the dual reactors. The only exception in this regard was one pure air run (CTC161), which apparently had a small amount of NO_x contamination in one side. This level of contamination, which was not indicated by modeling the other pure air runs, is not sufficient to significantly affect the reactivity experiments carried out for this program. The results of the n-butane - NO_x and CO - NO_x experiments, which are highly sensitive to the magnitude of the chamber radical source assumed in the model (see Table A-4 in Appendix A), were sufficiently well simulated by the model to indicate that the model is appropriately representing this effect for these runs. The actinometry results in the blacklight (DTC) and xenon arc (CTC) chamber were respectively slightly lower or slightly higher than the extrapolated values based on results of previous determinations (see Table A-4), but were within the variability and uncertainties of these determinations. They were not sufficiently different from the estimated NO_2 photolysis rates based on the longer-term trends in these chambers to justify using different values when modeling these experiments.

Injecting the C_{12+} n-alkanes into the gas phase was an area of concern because of their relatively low volatility. A useful method for assessing this is to compare the measured gas-phase concentration of the compound in the chamber with the expected amount based on the amount injected. This is summarized in Table 3 for each incremental reactivity experiment. Except for several anomalous runs,

Table 1. Chronolological listing of all the DTC experiments carried out for this program

RunID	Date	Title	Comments
DTC245	8/28/95	NO2 ACTINOMETRY	NO2 photolysis rate was 0.225 min-1, in good agreement with the extrapolation from previou determinations.
DTC246	8/15/95	PROPENE + NOx	Control run for comparison with other propene runs carried out in this and other chambers. The model slightly overpredicts ozone formation rate, but results in the normal range. Good side equivalency.
DTC247	8/16/95	ACETALDEHYDE + AIR	Background O3 formation rate is ~3 ppb/hour. This is attributed to NOx offgasing. Model slightly underpredicts background rate of ozone formation, but results are within offset uncertainty in ozone measurement.
DTC253		N-BUTANE + NOx	This run is highly sensitive to the chamber radical source. The observed rates of NO oxidation and OH radical tracer consumption are consistent with the predictions of the chamber model.
DTC254			
DTC258	9/1/95	LOW NOx FULL SURROGATE	The same surrogate - NOx mixture was irradiated in both sides. to test side equivalency. Good side equivalency was observed.
DTC270	9/26/95	FORMALDEHYDE + NOx	
DTC271	10/3/95	MINI-SURROGATE + n-C12(B) + NOx	Problems with calibration factor for m-xylene for GC loop analysis through run 279. Tenax sampling analysis used as primary method for determining concentration. Runs still usable.
DTC272	10/4/95	FULL SURROGATE + n-C12(A) + NOx	
DTC273	10/5/95	MINI-SURROGATE + n-C12(A) + NOx	
DTC274	10/6/95	FULL SURROGATE + n-C12(B) + NOx	
DTC275	10/10/95	MINI-SURROGATE + N-C14(A) + NOx	n-C14 data somewhat more scattered than usual., but run still usable.
DTC276	10/11/95	FULL SURROGATE + n-C14(B) + NOx	
DTC277	10/12/95	MINI-SURROGATE + n-C14(B) + NOx	
DTC278	10/13/95	FULL SURROGATE + n-C14(A) + NOx (Rejected)	The measured initial n-C14 was ~60% of the calculated amount injected. Because of this, it i concluded that the initial n-C14 is too uncertain for the run to be useful for reactivity assessment and modeling.
DTC279	10/17/95	MINI-SURROGATE + n-C15(B) + NOx	
DTC280	10/18/95	FULL SURROGATE + n-C15(A) + NOx (Rejected)	The measured initial n-C15 was ~35% of the calculated amount injected. Because of this, it i concluded that the initial n-C15 is too uncertain for the run to be useful for reactivity assessment and modeling.
DTC281	10/19/95	FULL SURROGATE + n-C16(B) + NOx	
DTC282	10/20/95	MINI-SURROGATE + n-C16(A) + NOx (Rejected)	The measured initial n-C16 was ~45% of the calculated amount injected. Because of this, it i concluded that the initial n-C16 is too uncertain for the run to be useful for reactivity assessment and modeling.
DTC283	10/24/95	MINI-SURROGATE + n-C12(B) + NOx	
DTC284	10/25/95	FULL SURROGATE + n-C12(A) + NOx	
DTC285	10/26/95	N-BUTANE + NOx	The observed rates of NO oxidation and OH radical tracer consumption are consistent with the predictions of the chamber model.
DTC286	10/27/95	PURE AIR IRRADIATION	Approximately 40 ppb of O3 was formed in 6 hours. The chamber model gave a good fit to this result.
DTC287	10/30/95	NO2 ACTINOMETRY	NO2 photolysis rate was 0.220 min-1, in good agreement with previous determinations.
DTC288	10/31/95	PROPENE + NOX	Model slightly overpredicts ozone formation rate, but results in the normal range. Good side equivalency.
DTC289	11/1/95	MINI-SURROGATE + n-C14(B) + NOx	
DTC290	11/2/95	FULL-SURROGATE + n-C14(A) + NOx (Rejected)	The measured initial n-C14 was ~55% of the calculated amount injected. Because of this, it i concluded that the initial n-C14 is too uncertain for the run to be useful for reactivity assessment and modeling.
DTC291	11/3/95	MINI-SURROGATE + n-C16(B) + NOx	
DTC292	11/14/95	FULL-SURROGATE + n-C16(B) + NOx	
DTC293	11/15/95	FULL-SURROGATE + N-C12 (A) + NOx	
DTC297	11/27/95	NO2 ACTINOMETRY	NO2 photolysis rate was 0.211 min-1, slightly lower than the estimate based on previous determinations, but within the uncertainty of these measurements.
DTC298	11/28/95	Low NOx full surrogate + n-C16	
DTC299	11/29/95	N-BUTANE + NOx	Apparent leak in Side A. The NO oxidation rate was somewhat higher in Side A than in Side B. The chamber model gave a better fit to the side A results, but the results for Side B were within the acceptable range.
DTC300	1/19/96	NO2 ACTINOMETRY	NO2 photolysis rate was 0.216 min-1, slightly lower than the estimate based on previous determinations, but within the uncertainty of these measurements.
DTC301	1/24/96	PROPENE + NOX	Results similar to other propene runs. No apparent leak problems.

Table 2. Chronological listing of the all the CTC experiments carried out for this program.

RunID	Date	Title	Comments
CTC145	11/30/95	NO2 ACTINOMETRY	NO2 photolysis rate determined by tube method was 0.260 min-1, which yields a corrected value of 0.22 min^{-1}. This is slightly higher than 0.19 min^{1} predicted by the trend with the LiCor measurements, but within the scatter of the data.
CTC146	12/4/95	PURE AIR IRRADIATION	Approximately 25 ppb O3 formed in 6 hours. Results consistent with prediction of chamber model.
CTC147	12/5/95	PROPENE + NOx	Results in good agreement with model predictions. Good side equivalency.
CTC148	12/6/95	N-BUTANE + NOx	Rate of NO oxidation is slightly less than the predictions of the chamber model, but the results are within the normal range. Data fit if the chamber radical input rates are reduced by ~25%.
CTC149	12/8/95	FULL SURROGATE + NOx	Same surrogate - NOx mixture irradiated in each of two reactors. Good side equivalency observed.
CTC150	12/12/95	FULL SURROGATE + N-C12 (B)	
CTC151	12/13/95	FULL SURROGATE + N-C14 (A)	
CTC152	12/14/95	FULL SURROGATE + N-C16 (B)	
CTC153	1/3/96	PROPENE + NOX	Results in good agreement with model predictions. Good side equivalency.
CTC154	1/4/96	FULL SURROGATE + N-C12 (A)	
CTC155	1/5/96	N-BUTANE + NOx	Rate of NO oxidation is slightly less than the predictions of the chamber model, but the results are within the normal range. Data fit if the chamber radical input rates are reduced by ~20%.
CTC156	1/9/96	FULL SURROGATE + N-C16 (B)	
CTC157	1/10/96	NO2 ACTINOMETRY	NO2 photolysis rate determined by tube method was 0.254 min-1, which yields a corrected value of 0.21 min^{-1}. This is slightly higher than 0.19 min^{1} predicted by the trend with the LiCor measurements, but within the scatter of the data.
CTC158	1/11/96	FULL SURROGATE + N-C14 (A)	
CTC161	1/18/96	PURE AIR IRRADIATION	Sides differ in ozone formation. Side A forms ~30 ppb O3 in 6 hours, in good agreement wit chamber model predictions. Side B forms ~40 ppb O3, which is consistent with chamber model predictions if ~1 ppb of NO is assumed to be present initially.
CTC162	2/6/96	CO - AIR IRRADIATION	Run conducted to measure dilution due to leakage, which was found to be negligible.
CTC163	3/13/96	PROPENE + NOx	Results in good agreement with model predictions. Good side equivalency.
CTC164	3/14/96	PURE AIR IRRADIATION	Approximately 35 ppb O3 formed on each side in 6 hours, somewhat more than predicted by chamber model.
CTC165	3/15/96	FULL SURROGATE + NOx	Good side equivalency.
CTC166	3/18/96	NO2 ACTINOMETRY	NO2 photolysis rate determined by tube method was 0.256 min-1, which yields a corrected value of 0.21 min^{-1}. This is slightly higher than 0.19 min^{1} predicted by the trend with the LiCor measurements, but within the scatter of the data.

Table 3. Summary of conditions and results of the incremental reactivity experiments.

Run	Run Type	Initial Reactants (ppm)			Meas./Inj.	t=2 d(O_3-NO) (ppm)			t=5 d(O_3-NO) (ppm)			t=5 IntOH (10^{-6} min)		
		NOx	Surg [a]	Alkane	Alkane [b]	Base	Test	IR	Base	Test	IR	Base	Test	IR
n-C_{12}														
DTC-273 (A)	Mini-Surg	0.31	5.6	0.10	92%	0.14	0.09	-0.41	0.49	0.38	-1.13	17	10	-58
DTC-271 (B)	Mini-Surg	0.30	5.6	0.18	95%	0.12	0.07	-0.29	0.43	0.29	-0.74	17	11	-34
DTC-283 (B)	Mini-Surg	0.33	5.5	0.23	99%	0.12	0.06	-0.24	0.45	0.26	-0.82	15	5	-41
DTC-274 (B)	Full Surg	0.16	3.8	0.11	95%	0.30	0.28	-0.17	0.46	0.45	-0.07	31	24	-65
DTC-272 (A)	Full Surg	0.14	3.7	0.16	85%	0.26	0.24	-0.13	0.40	0.38	-0.13	29	22	-44
DTC-284 (A)	Full Surg	0.15	3.8	0.19	103%	0.31	0.28	-0.14	0.48	0.45	-0.12	28	19	-48
DTC-293 (A)	Low NOx Surg	0.08	3.9	0.20	105%	0.28	0.26	-0.11	0.32	0.31	-0.04	20	16	-24
CTC-150 (B)	CTC Full Surg	0.41	5.2	0.27	91%	0.36	0.30	-0.20	0.68	0.66	-0.05	22	15	-24
CTC-154 (A)	CTC Full Surg	0.44	5.2	0.60	102%	0.41	0.32	-0.14	0.70	0.70	-0.01	24	14	-15
n-C_{14}														
DTC-277 (B)	Mini-Surg	0.31	5.1	0.11	98%	0.13	0.07	-0.47	0.47	0.32	-1.42	16	10	-62
DTC-275 (A)	Mini-Surg	0.32	5.6	0.19	101%	0.12	0.06	-0.32	0.46	0.27	-1.03	17	12	-30
DTC-289 (B)	Mini-Surg	0.34	5.5	0.28	100%	0.12	0.05	-0.25	0.43	0.19	-0.85	15	4	-41
DTC-278 (A)	Full Surg	0.16	4.2	0.07	59%	0.32	0.29	[c]	0.49	0.47	[c]	28	23	[c]
DTC-290 (A)	Full Surg	0.17	3.9	0.16	56%	0.31	0.24	[c]	0.47	0.42	[c]	29	19	[c]
DTC-276 (B)	Full Surg	0.16	3.8	0.20	105%	0.32	0.28	-0.22	0.49	0.46	-0.13	32	19	-63
CTC-151 (A)	CTC Full Surg	0.47	5.2	0.26	88%	0.37	0.34	-0.13	0.64	0.62	-0.09	20	14	-24
CTC-158 (A)	CTC Full Surg	0.38	5.2	0.62	104%	0.35	0.22	-0.21	0.69	0.60	-0.14	25	11	-22
n-C_{15}														
DTC-280 (A)	Full Surg	0.16	4.0	0.08	35%	0.32	0.26	[c]	0.49	0.44	[c]	30	21	[c]
DTC-279 (B)	Mini-Surg	0.32	5.6	0.17	89%	0.09	0.04	-0.28	0.43	0.23	-1.21	14	7	-44
n-C_{16}														
DTC-282 (A)	Mini-Surg	0.35	5.5	0.09	47%	0.15	0.08	[c]	0.53	0.31	[c]		9	[c]
DTC-291 (B)	Mini-Surg	0.32	5.7	0.26	94%	0.12	0.05	-0.26	0.44	0.21	-0.89	14	5	-36
DTC-281 (B)	Full Surg	0.16	3.8	0.16	88%	0.30	0.26	-0.23	0.47	0.45	-0.09	31	20	-66
DTC-292 (B)	Full Surg	0.16	4.0	0.25	88%	0.30	0.23	-0.28	0.46	0.42	-0.15	31	16	-62
DTC-298 (B)	Low NOx Surg	0.08	3.6	0.14	76%	0.29	0.26	-0.17	0.31	0.32	0.06	23	16	-49
CTC-152 (B)	CTC Full Surg	0.40	3.9	0.26	87%	0.27	0.22	-0.17	0.48	0.48	0.00	18	12	-24
CTC-156 (B)	CTC Full Surg	0.43	4.8	0.48	82%	0.36	0.25	-0.24	0.67	0.59	-0.16	24	12	-24

Notes

[a] Total base ROG surrogate in ppmC.

[b] Ratio of the measured initial alkane to initial concentration calculated based on amount of pure compound injected.

[c] Could not be reliably determined because the amount of test alkane is uncertain. The measured initial amount was less than 55% of the calculated amount injected.

discussed below, there is no significant difference between the observed/expected ratios for n-C_{12} and n-$C_{14,}$ which suggests that we are probably achieving nearly 100% gas-phase injection for these compounds. However, the ratios for n-C_{15} and n-C_{16} are somewhat lower, indicating that ~90% injection for n-C_{15} and ~85% injection for n-C_{16} is more likely to be the case. This uncertainty is considered to be small compared to the other uncertainties in the experiments.

However, for n-C_{14} runs DTC-278 and 290, for n-C_{15} run DTC-280w, and for n-C_{16} run DTC-282, the observed/expected n-alkane ratio was in the 50-55% range, significantly lower than for the other experiments. This suggests that either there is a problem in the n-alkane injection or in the measurement of the gas-phase n-alkane concentration for these experiments. Modeling these experiments suggested that the actual injected gas-phase concentrations of the n-alkane may be closer to the calculated injected amounts than the gas-phase concentrations determined by the GC analyses. Therefore, the actual initial gas-phase n-alkane concentrations are considered to be too uncertain for these experiments to be used for mechanism evaluation. However the data from these experiments are shown for completeness.

Results of The Reactivity Experiments and Mechanism Evaluations

Summaries of the conditions and results of the incremental reactivity experiments are given in Table 3, and Appendix B gives time series plots for the relevant measurements used for mechanism evaluation. The results indicate that in all cases the addition of the n-alkane caused a decrease in the rate of ozone formation and NO oxidation in the initial stages of the experiments, and a significant decrease in the rates of consumption of m-xylene, indicating a decrease in the integrated OH radical levels. This radical inhibition is attributed to the formation of alkyl nitrates in the OH + C_{12+} n-alkane reactions, as discussed in the previous section. As discussed in detail elsewhere (Carter et al, 1993a; 1995a,b; Carter, 1995), this radical inhibition causes a reduction in the rates of the ozone forming reactions of all the VOCs present in the system, causing a net decrease in the rates of NO oxidation and O_3 formation. This inhibition has less of an effect on the final ozone [and thus d(O_3-NO)] yields in the lower NO_x experiments, as indicated by the results of the lower NO_x/ROG full surrogate experiments where the maximum or near-maximum ozone formation potential has been achieved.

The figures in Appendix B also show results of model simulations of the experiments which were sufficiently well characterized for modeling, using two mechanisms for the C_{12+} n-alkanes. The first, shown as the solid lines on the figures, is calculated using the current standard mechanism derived using the extrapolated organic nitrate yields derived by Carter and Atkinson (1989b). The second, shown as the dashed lines on the figures, was derived by assuming 20% higher nitrate yields for the C_{12+} n-alkanes, i.e.,

20% greater radical inhibition in the reactions of these compounds. Note that both mechanisms give the same predictions for the base case experiments, because these do not contain C_{12+} alkanes. On the other hand, the model with the higher nitrate yields predicts consistently greater inhibition by the C_{12+} alkane on the d(O_3-NO) and IntOH levels. These results are discussed in more detail below for the specific types of experiments.

Mini-Surrogate Experiments. Figures B-1 through B-9 show the experimental and model simulation results for the mini-surrogate experiments. Note that the base case experiment was carried out at a relatively low ROG/NO_x ratio, and after an induction period the d(O_3-NO) formation occurred at essentially a constant rate during the experiment until the irradiation was terminated after 6 hours. The effects of the C_{12+} n-alkane addition were similar for all alkanes studied. In all cases, the alkane addition slowed down the rates of NO oxidation, O_3 formation, and m-xylene consumption. This indicated negative d(O_3-NO) and IntOH reactivities, which became increasingly negative with time during the experiments. Thus, under the conditions of these experiments all the C_{12+} n-alkanes studied inhibited both O_3 formation and OH radical levels.

The model tended to have a slight bias toward overprediction of the rate of d(O_3-NO) formation in the simulations of the base case mini-surrogate experiments, though it gave reasonably good fits to the base case m-xylene consumption rates and IntOH levels. However, the standard model correctly predicted this inhibition by the C_{12+} n-alkanes on d(O_3-NO) and IntOH in these experiments, and, at least for n-C_{12}, fit the observed final d(O_3-NO) and IntOH incremental reactivities to within their experimental uncertainties. (The model performance for the individual runs and VOCs will be discussed later.) This bias towards overprediction in d(O_3-NO) formation rates in the base case experiments can be removed by suitable adjustment of the uncertain parameters in the m-xylene mechanism. However, this adjustment does not cause a significant change in model predictions of d(O_3-NO) or IntOH incremental reactivities. Because of this, we do not think that the existence of this small bias in absolute d(O_3-NO) predictions causes a bias in the predictions of incremental reactivities, and thus these data still provide a useful test of model performance in this regard.

Figures B-1 through B-3 show the experimental and model simulation results of the mini-surrogate experiments with n-C_{12}. The model performs quite well in simulating the d(O_3-NO) and IntOH incremental reactivities of n-C_{12}, and also the rate of consumption of n-C_{12}, in the mini-surrogate experiments. The slight overprediction of the inhibition at t=1 and 2 hours in the experiments is probably not outside the range of uncertainty due to chamber effects or uncertainties in simulating the base case

experiments. The high nitrate yield model is also not inconsistent with the data, though the fits indicate that this can probably be considered an upper limit to the true overall nitrate yield for this compound.

Figures B-4 through B-6 show that similar results are obtained in the simulations of the n-C_{14} experiments, though the quality of fits to the n-C_{14} consumption rates are poor in two of the three experiments. This is attributed to analytical or sampling difficulties, as indicated by the inconsistent results among experiments, and probably does not indicate problems with the model. Unlike n-C_{12}, there appears to be a slight bias in the standard model for underpredicting the magnitude of the d(O_3-NO) inhibition effect, while the high nitrate yield model fits the data with somewhat less bias.

Figure B-7 shows the experimental and model simulation results for the single n-C_{15} mini-surrogate experiment. The results are similar to the simulations of the n-C_{14} experiments, though in this case most of the alkane measurements are reasonably consistent with model predictions. As with n-C_{14}, the data are fit somewhat better by the mechanism assuming higher nitrate yields than the standard mechanism.

Figure B-8 shows the results for the one n-C_{16} mini-surrogate run which is considered sufficiently well characterized for modeling. The n-C_{16} measurements are too scattered to provide a useful test for model performance. The results are slightly different than those with n-C_{14} and n-C_{15} in that the standard model performs better in simulating the d(O_3-NO) reactivities than the model with the higher nitrate yield. The results of the other n-C_{16} mini-surrogate experiment are qualitatively similar (Figure B-9), but the run could not be modeled because of the uncertainty in the amount of added n-C_{16}.

Full Surrogate Experiments (Higher NO_x). Figures B-10 through B-18 show the experimental and (where applicable) model simulation results for the full surrogate experiments at the higher NO_x levels. In addition to using a different mixture for the base ROG surrogate, these runs had somewhat higher ROG/NO_x ratios than the mini-surrogate experiments. Because of this, the formation of O_3 [and thus also d(O_3-NO)] leveled off around the end of the experiments and nearly achieved a maximum value. This indicates that the experiment is approaching, though not quite achieving, NO_x-limited conditions (Carter et al, 1995b). Although the addition of the n-alkanes had about the same effect on IntOH in these experiments as in the mini-surrogate runs, the effect on d(O_3-NO) was much less. This is consistent with previous reactivity data we obtained for n-octane (Carter et al. 1995b), which had negative d(O_3-NO) reactivities in experiments with the mini-surrogate but small positive effects on d(O_3-NO) in runs with the more realistic full surrogate. In the case of these n-C_{12+} alkanes, the reactivities are still negative when the full surrogate is used, though much less so.

This large surrogate effect is attributed to the fact that the net effect of an alkane on O_3 formation is due to two opposing factors, whose balance differs depending on the ROG surrogate employed. As discussed by Carter et al (1993b. 1995a), the d(O_3-NO) reactivity of a VOC can be broken into two components, their "direct" and "indirect" reactivities. The direct reactivity of a VOC is the O_3 formation (or NO to NO_2 conversions) caused directly by the reactions of the radicals formed in the photooxidation of the VOC and its reacting products. The indirect reactivity of a VOC reflects the effect of the VOC's reactions on the O_3 formed (or NO to NO_2 conversions) from the reactions of the base ROG surrogate. For example, if the compound's reactions tend to inhibit radical levels, it would have a negative indirect reactivity because the presence of the compound causes less of the base ROG components to react and convert NO to NO_2. Thus, the higher alkanes, whose reactions inhibit radical levels (as indicated by their negative IntOH reactivities) have negative indirect reactivities. On the other hand, the reactions of the higher alkanes form a relatively large number of peroxy radicals which convert NO to NO_2, and because of this they are observed to have relatively high, positive, direct reactivities (Carter et al, 1993a, 1995a,b). The indirect reactivity effect appears to be more important than the direct effect in the mini-surrogate experiments, resulting in negative overall incremental reactivities in that system. The opposing effects are apparently more evenly balanced in the experiments using the full surrogate, resulting in a very small net effect on d(O_3-NO). This is consistent with results observed previously for n-octane (Carter et al, 1995a).

Figures B-10 through B-12 show results of the three full surrogate runs with n-C_{12}. The model tends to give a better fit to the results of the base case run than is the case with the mini-surrogate, though there is still a slight overprediction of the initial NO oxidation and O_3 formation rates. The model correctly predicted that the n-C_{12} addition has a relatively small effect on d(O_3-NO), but a relatively large inhibiting effect on IntOH. The large error bars in the measured d(O_3-NO) incremental reactivities reflect the fact that the differences between the test and base case experiments are almost within measurement variability, and for the most part the model simulations were within these error bars. However, there may be a slight bias in the standard model toward overpredicting d(O_3-NO) reactivities in these experiments, and this bias is somewhat less if the higher nitrate yields are assumed. In two of the three experiments the model somewhat underpredicted the magnitude of the IntOH reactivities, but this was not significantly improved by assuming the higher nitrate yields. We did not examine the effects of assuming yet higher nitrate yields since predictions of such models would be inconsistent with the results of the mini-surrogate experiments, discussed above.

Figures B-13 through B-15 show the results of the three full surrogate experiments with n-C_{14}. The results of the simulation of the one experiment sufficiently well characterized for model testing (DTC-

276 on Figure B-13), are consistent with those for the n-C_{12} experiments; the standard model slightly overpredicted the d(O_3-NO) incremental reactivities, and slightly underpredicted the relatively large negative effect on IntOH. Increasing the assumed nitrate yield by ~20% improved the fits to the d(O_3-NO) reactivities but did not significantly affect the model performance for IntOH. The results of the other two experiments (Figures B-14 and B-15), which could not be modeled because of uncertainties in the initial n-C_{14} concentrations, are qualitatively consistent with the results of run DTC-276.

Figure B-16 shows results of the one full surrogate experiment with n-C_{15}. Unfortunately, that experiment could not be modeled because of uncertainty in the amount of n-C_{15} added. However, the results are qualitatively consistent with the comparable runs with the other compounds.

Figures B-17 and B-18 show results of the higher NO_x full surrogate experiments with n-C_{16}. The results are similar to those for the useable n-C_{14} experiment, discussed above. In particular, the standard model overpredicted the d(O_3-NO) and IntOH reactivities somewhat, while the ~20% higher nitrate model performed somewhat better for d(O_3-NO) but not for IntOH.

Low NO_x Full Surrogate Experiments. A limited number of full surrogate experiments, one each for n-C_{12} and n-C_{16}, were carried out to assess the effects of changing NO_x levels on predictions of alkane reactivity. The experimental and model simulation results are shown on Figures B-19 and B-20, respectively. Ozone reached a maximum concentration after about 4 hours of irradiation, and the addition of the n-alkane did not significantly affect this maximum. In both cases, the model slightly overpredicted the initial NO oxidation and O_3 formation rates of the base case experiment, while slightly underpredicting the final O_3 yields. However, the model gave good simulations to the effects of the alkane additions on d(O_3-NO) in both these experiments, and to the effect of the alkane on IntOH in the n-C_{12} run. The model slightly underpredicted the magnitudes of the negative IntOH reactivities in the n-C_{16} experiment, but the discrepancy is smaller than in the simulations of the n-C_{16} full surrogate experiments with the higher NO_x levels (Figure B-20). Thus, changing the NO_x levels does not significantly affect the model performance in simulating the experimental data.

Xenon Arc Experiments. The experiments in the CTC chamber with the xenon arc light source all employed the full surrogate with relatively high NO_x levels. The results of these experiments are shown on Figures B-21 through B-26. Like the mini-surrogate experiments in the DTC, these experiments did not achieve their full ozone formation potential, since O_3 [and d(O_3-NO)] was still increasing when the experiments were terminated at the end of 6 hours. This indicates that, unlike the higher NO_x full

surrogates in the DTC, these experiments never approached NO_x-limited conditions. This is because somewhat different reactant concentrations were employed in the base case experiments, as well as the fact that the CTC has somewhat lower overall light intensity than the DTC. However, the observed n-alkane incremental reactivities in these experiments were similar to the full surrogate incremental reactivities in the DTC chamber in that relatively small effects of the n-alkane on $d(O_3\text{-NO})$ were observed despite relatively large effects on IntOH.

Figures B-21 through B-26 show that the model gave good simulations of the results of most of the base case experiments in this chamber, in contrast to the simulations of the DTC runs where it tended to have a slight bias towards overprediction NO oxidation and O_3 formation rates. The model also gave good fits to both the $d(O_3\text{-NO})$ and the IntOH incremental reactivities. In the case of n-C_{12}, the standard model gives good fits to the data in both experiments. The model with the ~20% higher nitrate formation also gives good fits to the IntOH reactivities, but tends to be slightly biased towards overpredicting the inhibition effect on $d(O_3\text{-NO})$. In the case of n-C_{16}, the higher nitrate yield model gives reasonably good fits to the incremental reactivities, while the standard model tends to slightly underpredict the inhibitory effects on $d(O_3\text{-NO})$ and IntOH. The reactivity modeling results for the n-C_{14} experiments tend to be somewhat intermediate between those for n-C_{12} and n-C_{16}; in one run the data are fit somewhat better by the higher nitrate model, while in the other the data tend to fall between the two.

ATMOSPHERIC REACTIVITY CALCULATIONS

Incremental reactivities of VOCs have been shown to be highly dependent on environmental conditions, so reactivities measured in environmental chamber experiments cannot necessarily be assumed to be exactly the same as those under atmospheric conditions (Carter and Atkinson, 1989a; Carter et al, 1995b). The only method available to obtain quantitative estimates of incremental reactivities of VOCs in ambient air pollution episodes is to conduct airshed model simulations of the episodes. Since these simulations cannot be any more reliable than the chemical mechanisms used, the major objective of this program was to assess the reliability of the C_{12+} n-alkane mechanism for use in such simulations. This was discussed in the previous sections. In this section, we discuss the results of model simulations of the alkanes' incremental reactivities in a variety of model scenarios representing ozone exceedence episodes in various areas in the United States (Baugues, 1990), and compare the results to incremental reactivities calculated for ethane and for the base ROG, i.e., the mixture representing total ROG emissions from all sources. Because most of the data tend to indicate that the actual reactivities of these C_{12+} n-alkanes may be somewhere between those calculated by the standard mechanism and the version assuming ~20% higher alkyl nitrate yields, atmospheric reactivity calculations were carried out using both these mechanisms.

Scenarios Used for Reactivity Assessment

The set of airshed scenarios employed to assess the alkanes' reactivities for this study is the same as those used for calculating the MIR and other reactivity scales, which were also used in our previous assessment of acetone reactivity (Carter, 1994a; Carter et al, 1993a). The objective is to use a set of scenarios which represents, as much as possible, a comprehensive distribution of the environmental conditions where unacceptable levels of ozone are formed. Although a set of scenarios has not been developed for the specific purpose of VOC reactivity assessment, the EPA developed an extensive set of scenarios for conducting analyses of effects of ROG and NO_x controls on ozone formation using the EKMA modeling approach (Gipson et al., 1981; Gipson and Freas, 1983; EPA, 1984; Gery et al., 1987; Baugues, 1990). The EKMA approach involves use of single-cell box models to simulate how ozone formation in one day episodes is affected by changes in ROG and NO_x inputs. Although single-cell models cannot represent realistic pollution episodes in great detail, they can represent dynamic injection of pollutants, time-varying changes of inversion heights with entrainment of pollutants from aloft as the inversion height increases throughout the day, and time-varying photolysis rates, temperatures, and humidities (Gipson and Freas, 1981; EPA, 1984; Gipson, 1984; Hogo et al., 1988). Thus, they can be

used to simulate a wide range of the chemical conditions which affect ozone formation from ROG and NO_x. These are the same as those affecting VOC reactivity. Therefore, at least to the extent they are suitable for their intended purpose, an appropriate set of EKMA scenarios should also be suitable for assessing methods to develop reactivity scales encompassing a wide range of conditions.

Base Case Scenarios

The set of EKMA scenarios used in this study were developed by the United States EPA for assessing how various ROG and NO_x control strategies would affect ozone nonattainment in various areas of the country (Baugues, 1990). The characteristics of these scenarios and the methods used to derive their input data are described in more detail elsewhere (Baugues, 1990; Carter, 1993). Briefly, 39 urban areas in the United States were selected based on geographical representativeness of ozone nonattainment areas and data availability, and a representative high ozone episode was selected for each. The initial NMOC and NO_x concentrations, the aloft O_3 concentrations, and the mixing height inputs were based on measurement data for the various areas, the hourly emissions in the scenarios were obtained from the National Acid Precipitation Assessment Program emissions inventory (Baugues, 1990), and biogenic emissions were also included. Table 4 gives a summary of the urban areas represented and other selected characteristics of the scenarios.

Several changes to the scenario inputs were made based on discussions with the California ARB staff and others (Carter, 1993). Two percent of the initial NO_x and 0.1% of the emitted NO_x in all the scenarios was assumed to be in the form of HONO. The photolysis rates were calculated using solar light intensities and spectra calculated by Jeffries (1991) for 640 meters, the approximate mid-point of the mixed layer during daylight hours. The composition of the NMOCs entrained from aloft was based on the analysis of Jeffries et al (1989). The composition of the initial and emitted reactive organics were derived as discussed below. Complete listings of the input data for the scenarios are given elsewhere (Carter, 1993).

This set of 39 EKMA scenarios are referred to as "base case" to distinguish them from the scenarios derived from them by adjusting NO_x inputs to yield standard conditions of NO_x availability as discussed below. No claim is made as to the accuracy of these scenarios in representing any real episode, but they are a result of an effort to represent, as accurately as possible given the available data and the limitations of the formulation of the EKMA model, the range of conditions occurring in urban areas throughout the United States. When developing general reactivity scales it is more important that the

Table 4. Summary of conditions of base case scenarios used for atmospheric reactivity assessment.

City, State	Calc. Max O_3 (ppb)	ROG /NO_x	NO_x /NO_x^{MOR}	Final Height (km)	Init.+Emit Base ROG (mmol m^{-2})	Aloft O_3 (ppb)
Atlanta, GA	174	7.3	0.7	2.1	12	63
Austin, TX	171	9.3	0.5	2.1	11	85
Baltimore, MD	304	5.2	1.1	1.2	17	84
Baton Rouge, LA	235	6.8	1.0	1.0	11	62
Birmingham, AL	233	6.9	0.6	1.8	13	81
Boston, MA	191	6.5	0.6	2.6	14	105
Charlotte, NC	142	7.8	0.3	3.0	7	92
Chicago, IL	273	11.6	0.5	1.4	25	40
Cincinnati, OH	192	6.4	0.8	2.8	17	70
Cleveland, OH	239	6.6	1.0	1.7	16	89
Dallas, TX	192	4.7	1.3	2.3	18	75
Denver, CO	195	6.3	1.2	3.4	29	57
Detroit, MI	229	6.8	0.8	1.8	17	68
El Paso, TX	177	6.6	1.1	2.0	12	65
Hartford, CT	166	8.4	0.5	2.3	11	78
Houston, TX	291	6.1	1.0	1.7	25	65
Indianapolis, IN	201	6.6	0.9	1.7	12	52
Jacksonville, FL	152	7.6	0.7	1.5	8	40
Kansas City, MO	151	7.1	0.6	2.2	9	65
Lake Charles, LA	282	7.4	0.7	0.5	7	40
Los Angeles, CA	546	7.6	1.0	0.5	23	100
Louisville, KY	203	5.5	0.9	2.5	14	75
Memphis, TN	218	6.8	0.7	1.8	15	58
Miami, FL	131	9.6	0.4	2.7	9	57
Nashville, TN	163	8.1	0.5	1.6	7	50
New York, NY	350	8.1	0.8	1.5	39	103
Philadelphia, PA	230	6.2	1.0	1.8	19	53
Phoenix, AZ	258	7.6	1.0	3.3	40	60
Portland, OR	161	6.5	0.7	1.6	6	66
Richmond, VA	225	6.2	0.8	1.9	16	64
Sacramento, CA	194	6.6	0.9	1.1	7	60
St Louis, MO	301	6.1	1.1	1.6	26	82
Salt Lake City, UT	179	8.5	0.6	2.2	11	85
San Antonio, TX	126	3.9	1.1	2.3	6	60
San Diego, CA	186	7.1	1.0	0.9	8	90
San Francisco, CA	222	4.8	1.8	0.7	25	70
Tampa, FL	217	4.4	1.1	1.0	8	68
Tulsa, OK	216	5.3	0.9	1.8	15	70
Washington, DC	268	5.3	0.9	1.4	13	99

scenarios employed represent a realistic distribution of chemical conditions than accurately representing the details of any one particular episode.

The Base ROG mixture is the mixture of reactive organic gases used to represent the chemical composition of the initial and emitted anthropogenic reactive organic gases from all sources in the scenarios. Consistent with the approach used in the original EPA scenarios, the same mixture was used for all scenarios. The speciation for this mixture was derived by Croes (1991) based on an analysis of the EPA database (Jeffries et al. 1989) for the hydrocarbons and the 1987 Southern California Air Quality Study (SCAQS) database for the oxygenates (Croes et al., 1994; Lurmann et al., 1992). This mixture consists of 52% (by carbon) alkanes, 15% alkenes, 27% aromatics, 1% formaldehyde, 2% higher aldehydes, 1% ketones, and 2% acetylene. The detailed composition of this mixture is given elsewhere (Carter, 1993).

Adjusted NO_x scenarios

Incremental reactivities in the base case scenarios would be expected to vary widely, since incremental reactivities depend on the ROG/NO_x ratio, and that ratio varies widely among the base case scenarios. To obtain reactivity scales for specified NO_x conditions, separate sets of scenarios, designated MIR (for maximum incremental reactivity), MOR (for maximum ozone reactivity), and Equal Benefit Incremental Reactivity (EBIR) were developed (Carter, 1984). In the MIR scenarios, the NO_x inputs were adjusted so the base ROG mixture (and most other VOCs) have their highest incremental reactivity. This is representative of the highest NO_x conditions of relevance to VOC reactivity assessment because at higher NO_x levels O_3 yields become significantly suppressed, but is also the condition where O_3 is most sensitive to VOC emissions. In the MOR scenarios, the NO_x inputs were adjusted to yield the highest ozone concentration. In the EBIR scenarios, the NO_x inputs were adjusted so that the relative effects of NO_x reductions and total ROG reductions on peak ozone levels were equal. This represents the lowest NO_x condition of relevance for VOC reactivity assessment, because O_3 formation becomes more sensitive to NO_x emissions than VOC emissions at lower NO_x levels. The changes in the base case ROG/NO_x ratios which yielded the MOR scenarios are given in Table 4. As discussed by Carter (1994a) the MIR and EBIR ROG/NO_x ratios are respectively ~1.5 and ~0.7 times those for the MOR scenarios in all cases.

NO_x Conditions in the Base Case Scenarios

The variability of ROG/NO_x ratios in the base case scenarios suggests a variability of reactivity characteristics in the base case scenarios. However, as discussed previously (Carter, 1994a), the ROG/NO_x ratio is also variable in the MIR or MOR scenarios, despite the fact that the NO_x inputs in these

scenarios were adjusted to yield a specified reactivity characteristic. Thus, the ROG/NO_x ratio, by itself, is not necessarily a good predictor of reactivity characteristics of a particular scenario. The NO_x/NO_x^{MOR} ratio is a much better predictor of this, with values greater than 1 indicating relatively high NO_x conditions where ozone formation is more sensitive to VOCs, and values less than 1 indicating NO_x-limited conditions. NO_x/NO_x^{MOR} ratios less than 0.7 represent conditions where NO_x control is a more effective ozone control strategy than ROG control (Carter, 1994a). Note that more than half of the base case scenarios represent NO_x-limited conditions, and ~25% of them represent conditions where NO_x control is more beneficial than VOC control. A relatively small number of scenarios represent MIR or near MIR conditions. However, as discussed elsewhere (Carter, 1994a), this set of scenarios is based on near-worst-case conditions for ozone formation in each of the airsheds. Had scenarios representing less-than-worst-case conditions been included, one might expect a larger number of MIR or near MIR scenarios. This is because NO_x is consumed more slowly on days with lower light intensity or temperature, and thus the scenario is less likely to become NO_x-limited.

Incremental and Relative Reactivities

The incremental reactivity of a VOC in an airshed scenario is the change in ozone caused by adding the VOC to the emissions, divided by the amount of VOC added, calculated for sufficiently small amounts of added VOC that the incremental reactivity is independent of the amount added. The procedure used to calculate incremental reactivities in a scenario was discussed in detail elsewhere (Carter, 1993, 1994a,b). The incremental reactivities depend on how the amount of VOC added is quantified. In this work, the added VOC was quantified on a mass basis, since this is how VOCs are regulated. In addition, the incremental reactivities also depend on how ozone impacts are quantified (Carter, 1994a). In this work, two different ozone quantifications were used, resulting in two different incremental reactivities being calculated for a VOC in a scenario. These are discussed below.

The "Ozone Yield" incremental reactivities measure the effect of the VOC on the total amount of ozone formed in the scenario at the time of its maximum concentration. In this work, this is quantified as grams O_3 formed per gram VOC added. This gives the same ratios of incremental reactivities as reactivities calculated from peak ozone concentrations, but is preferred because it permits magnitudes of reactivities in scenarios with differing dilutions to be compared on the same basis. Most previous recent studies of incremental reactivity (Dodge, 1984; Carter and Atkinson, 1987, 1989a, Chang and Rudy, 1990; Jeffries and Crouse, 1991) have all been based on ozone yield or peak ozone concentration reactivities.

The ozone yield incremental reactivities do not necessarily measure the effect of the VOC on exposure of unacceptable levels of ozone because it does not measure how long high levels of ozone are present. A quantification which reflects this is integrated ozone over the standard, which is defined as the sum of the hourly ozone concentrations for the hours when ozone exceeds the standard in the base case scenarios (Carter 1994a). In the previous work (Carter, 1994a), we used the California ozone standard of 90 ppb, but in this work we will use the national standard of 0.12 ppm. Reactivities relative to this quantification of ozone are referred to by the abbreviation "IntO_3>0.12" reactivities.

Relative reactivities are ratios of incremental reactivities to incremental reactivities of some standard VOC or mixture. Since these are the quantities which usually are the most relevant to control strategy applications, the results in this work will be given in terms of relative reactivities. In our previous work (Carter 1991, 1994a), we used the incremental reactivity of the base ROG mixture, i.e., the mixture representing ROG pollutants from all sources, as the standard to define relative reactivities. To be consistent with the terminology in the previous work, if the term "relative reactivity" is used without qualifier it refers to incremental reactivities relative to the base ROG mixture. However, because of the tendency within the EPA to consider ethane as the standard to define exempt vs controlled VOCs, we will also give reactivity ratios where ethane is used as the standard.

Reactivity Scales

A reactivity scale is a set of incremental or relative reactivities for a particular scenario or group of scenarios. Two types of reactivity scales will be discussed here, "base case" scales and adjusted NO_x scales. Base case scales are simply the set of incremental or relative reactivities in the 39 base case scenarios. Two sets of base case scales are derived — those based ozone yield reactivities and those based on IntO_3>0.12 reactivities. In the previous work (Carter, 1991, 1994a) we derived various multi-scenario scales from the individual base case scales by averaging or other procedures, to evaluate alternative approaches for developing single reactivity scales for applications requiring single scales. However, the decision of whether to exempt a VOC should not be made based on relative reactivities of a single scale, but on a knowledge of the range of relative reactivities for a variety of conditions. Thus in this work we present the distribution of base case relative reactivities for the 39 individual scenarios rather than developing aggregated or optimum scales which represent the distribution by single numbers.

The adjusted NO_x incremental reactivity scales refer to the MIR (maximum incremental reactivity), MOIR (maximum ozone incremental reactivity), or the EBIR (Equal Benefit Incremental Reactivity) scales. These consist of averages of ozone yield incremental reactivities MIR, MOR or EBIR scenarios,

respectively. Relative reactivities in these scales are ratios of incremental reactivities in these scales. Reactivities in the MIR scale are of interest because the California Air Resources Board utilized a MIR scale to calculate reactivity adjustment factors in its clean fuels/low emissions vehicle regulations (CARB, 1993). The justification for using this scale in applications requiring a single scale (such as the CARB vehicle regulations) is that it reflects conditions where ozone is most sensitive to changes in VOC emissions, and complements NO_x control, which is most effective for reducing ozone under conditions where the MIR scale is least applicable (Carter, 1994a). The MOIR scale is preferred by many as an alternative for such applications because it reflects conditions which are most favorable for ozone, and is more representative of the distribution of conditions in the base case scenarios (Carter 1994a). Most other alternative reactivity scales which might be appropriate for assessing VOC control strategies (i.e., excluding scales representing highly NO_x-limited conditions where ozone is more sensitive to NO_x than VOCs) tend to fall in the range defined by the MIR and MOIR scales. Since the EBIR scale represents lower NO_x conditions where O_3 is less sensitive to VOCs, its use in applications requiring a single scale has not been considered. However, it is useful for assessing how reactivities depend on NO_x conditions.

Note that the MIR, MOIR and base case scales derived in this work are somewhat different from those calculated previously (Carter, 1994a; Carter et al, 1993a) because an updated chemical mechanism was used. The updates to the mechanism were discussed in the previous section.

Calculated Relative Reactivities of Ethane and the n-Alkanes

Table 5 lists the relative reactivities of ethane and representative C_{10+} n-alkanes calculated for the adjusted NO_x (MIR, MOIR, and EBIR) reactivity scales and for the various base case scenarios, and Figure 2 compares the average, maximum, and minimum relative reactivities of the various compounds in the base case scenarios. Both ozone yield and $IntO_3$>0.12 relative reactivities are shown. The codes "N-C12a", "N-C14a" and "N-C16a" refer to the compounds represented using the mechanism with the ~20% higher alkyl nitrate yields. Note that relative reactivities are reactivities relative to the average reactivities for all emitted VOCs, and that all these compounds are less reactive than average. The distribution of reactivities of these C_{12+} n-alkanes relative to ethane are shown on Figures 3-6, where Figure 3 compares the minimum, average, and maximum C_{12+} n-alkane / ethane ratios for the various scenarios, O_3 quantification methods, and mechanisms, and Figures 4-6 show the distribution plots for the various types of scenarios.

Table 5. Summary of results of relative reactivity calculations for ethane and several representative C$_{8+}$ n-alkanes. (The suffix "a" means the reactivities were cacluated using the high nitrate yield mechanism.)

SCENARIO	OZONE YIELD RELATIVE REACTIVITIES								
or SCALE	**ETHANE**	**N-C8**	**N-C10**	**N-C12**	**N-C14**	**N-C16**	**N-C12a**	**N-C14a**	**N-C16a**
MIR	0.08	0.22	0.17	0.15	0.13	0.12	0.13	0.11	0.10
MIOR	0.15	0.41	0.34	0.29	0.26	0.23	0.26	0.23	0.21
EBIR	0.19	0.41	0.31	0.27	0.24	0.22	0.21	0.19	0.18
Base Case									
Average	0.17	0.40	0.31	0.26	0.23	0.22	0.21	0.19	0.18
Maximum	0.27	0.55	0.47	0.42	0.37	0.34	0.39	0.34	0.33
Minimum	0.05	0.04	-0.07	-0.08	-0.06	-0.04	-0.21	-0.22	-0.15
ATL GA	0.17	0.38	0.28	0.24	0.22	0.20	0.18	0.17	0.16
AUS TX	0.19	0.33	0.21	0.16	0.14	0.15	0.06	0.07	0.07
BAL MD	0.15	0.47	0.39	0.34	0.29	0.28	0.30	0.29	0.27
BAT LA	0.15	0.36	0.26	0.21	0.18	0.16	0.16	0.13	0.11
BIR AL	0.23	0.51	0.42	0.36	0.34	0.32	0.31	0.30	0.28
BOS MA	0.20	0.54	0.44	0.39	0.34	0.32	0.35	0.31	0.29
CHA NC	0.21	0.28	0.17	0.14	0.15	0.15	0.04	0.05	0.06
CHI IL	0.27	0.23	0.04	-0.03	-0.02	0.01	-0.13	-0.22	-0.11
CIN OH	0.19	0.52	0.44	0.39	0.36	0.33	0.37	0.34	0.33
CLE OH	0.15	0.39	0.31	0.27	0.23	0.22	0.24	0.21	0.17
DAL TX	0.12	0.30	0.24	0.20	0.17	0.16	0.17	0.15	0.13
DEN CO	0.11	0.28	0.21	0.17	0.15	0.14	0.13	0.11	0.10
DET MI	0.20	0.55	0.47	0.42	0.37	0.34	0.39	0.34	0.32
ELP TX	0.11	0.25	0.18	0.15	0.13	0.13	0.10	0.08	0.08
HAR CT	0.21	0.41	0.32	0.29	0.25	0.25	0.22	0.22	0.21
HOU TX	0.18	0.52	0.43	0.37	0.32	0.29	0.35	0.31	0.28
IND IN	0.16	0.38	0.31	0.26	0.23	0.22	0.22	0.20	0.19
JAC FL	0.16	0.27	0.17	0.14	0.12	0.12	0.06	0.06	0.06
KAN MO	0.20	0.50	0.42	0.39	0.35	0.33	0.36	0.33	0.32
LAK LA	0.22	0.46	0.31	0.24	0.21	0.20	0.20	0.16	0.12
LOS CA	0.15	0.41	0.33	0.27	0.22	0.19	0.21	0.17	0.15
LOU KY	0.19	0.51	0.41	0.35	0.31	0.28	0.33	0.29	0.26
MEM TN	0.20	0.53	0.44	0.38	0.34	0.32	0.38	0.32	0.29
MIA FL	0.18	0.04	-0.07	-0.08	-0.06	-0.04	-0.21	-0.19	-0.15
NAS TN	0.23	0.43	0.31	0.27	0.26	0.24	0.22	0.19	0.18
NEW NY	0.17	0.54	0.34	0.26	0.21	0.23	0.20	0.16	0.17
PHI PA	0.17	0.48	0.38	0.34	0.30	0.27	0.30	0.28	0.26
PHO AZ	0.16	0.43	0.35	0.30	0.28	0.27	0.26	0.24	0.23
POR OR	0.18	0.40	0.30	0.26	0.23	0.21	0.21	0.18	0.17
RIC VA	0.18	0.52	0.44	0.39	0.35	0.33	0.38	0.34	0.31
SAC CA	0.17	0.40	0.32	0.28	0.24	0.22	0.25	0.21	0.20
SAI MO	0.14	0.41	0.33	0.28	0.25	0.23	0.25	0.23	0.20
SAL UT	0.19	0.38	0.29	0.26	0.25	0.24	0.21	0.19	0.19
SAN TX	0.13	0.31	0.24	0.20	0.18	0.17	0.16	0.15	0.13
SDO CA	0.12	0.26	0.16	0.13	0.10	0.09	0.04	0.06	0.05
SFO CA	0.05	0.16	0.13	0.10	0.09	0.08	0.08	0.06	0.06
TAM FL	0.13	0.36	0.28	0.24	0.20	0.18	0.20	0.17	0.16
TUL OK	0.18	0.53	0.44	0.38	0.35	0.31	0.37	0.33	0.30
WAS DC	0.19	0.55	0.46	0.40	0.37	0.32	0.38	0.34	0.31

Table 5 (continued)

SCENARIO	INTO$_3$ > 0.12 RELATIVE REACTIVITIES								
or SCALE	**ETHANE**	**N-C8**	**N-C10**	**N-C12**	**N-C14**	**N-C16**	**N-C12a**	**N-C14a**	**N-C16a**
MIR	0.07	0.20	0.16	0.14	0.12	0.11	0.11	0.09	0.08
MIOR	0.10	0.26	0.20	0.16	0.14	0.12	0.12	0.10	0.09
EBIR	0.12	0.25	0.15	0.12	0.10	0.08	0.04	0.03	0.02
Base Case									
Average	0.12	0.24	0.16	0.12	0.10	0.09	0.06	0.04	0.04
Maximum	0.19	0.34	0.26	0.22	0.20	0.18	0.18	0.15	0.15
Minimum	0.05	0.01	-0.11	-0.13	-0.14	-0.13	-0.28	-0.34	-0.27
ATL GA	0.12	0.25	0.16	0.13	0.11	0.10	0.05	0.04	0.04
AUS TX	0.14	0.23	0.09	0.04	0.02	0.03	-0.07	-0.07	-0.07
BAL MD	0.09	0.25	0.20	0.16	0.13	0.12	0.12	0.11	0.10
BAT LA	0.10	0.23	0.13	0.09	0.07	0.05	0.03	0.01	0.00
BIR AL	0.13	0.25	0.16	0.11	0.10	0.09	0.04	0.03	0.02
BOS MA	0.12	0.32	0.24	0.20	0.17	0.15	0.14	0.11	0.11
CHA NC	0.16	0.18	0.06	0.03	0.03	0.03	-0.11	-0.09	-0.08
CHI IL	0.17	0.14	-0.06	-0.13	-0.14	-0.13	-0.28	-0.34	-0.27
CIN OH	0.12	0.32	0.24	0.21	0.19	0.17	0.17	0.15	0.14
CLE OH	0.09	0.23	0.16	0.13	0.11	0.10	0.08	0.07	0.06
DAL TX	0.09	0.23	0.17	0.14	0.12	0.10	0.10	0.08	0.07
DEN CO	0.07	0.19	0.13	0.10	0.08	0.07	0.05	0.04	0.03
DET MI	0.13	0.33	0.26	0.22	0.19	0.18	0.18	0.15	0.14
ELP TX	0.08	0.16	0.10	0.08	0.06	0.06	0.03	0.01	0.01
HAR CT	0.15	0.25	0.15	0.12	0.10	0.09	0.03	0.04	0.03
HOU TX	0.11	0.29	0.22	0.18	0.15	0.13	0.13	0.11	0.10
IND IN	0.11	0.23	0.16	0.12	0.11	0.10	0.07	0.06	0.05
JAC FL	0.14	0.20	0.09	0.07	0.05	0.06	-0.02	-0.02	-0.02
KAN MO	0.14	0.33	0.25	0.22	0.20	0.18	0.18	0.15	0.15
LAK LA	0.13	0.19	0.04	-0.02	-0.04	-0.04	-0.12	-0.14	-0.16
LOS CA	0.08	0.21	0.14	0.10	0.07	0.05	0.05	0.02	0.00
LOU KY	0.13	0.34	0.25	0.20	0.18	0.16	0.16	0.13	0.12
MEM TN	0.13	0.32	0.23	0.19	0.16	0.15	0.14	0.11	0.09
MIA FL	0.17	0.01	-0.11	-0.12	-0.11	-0.08	-0.27	-0.24	-0.20
NAS TN	0.19	0.22	0.10	0.07	0.07	0.06	-0.03	-0.04	-0.03
NEW NY	0.09	0.30	0.18	0.14	0.10	0.09	0.06	0.04	0.04
PHI PA	0.11	0.30	0.22	0.19	0.16	0.15	0.14	0.13	0.11
PHO AZ	0.09	0.23	0.16	0.13	0.11	0.11	0.08	0.07	0.06
POR OR	0.14	0.30	0.20	0.16	0.14	0.12	0.09	0.07	0.07
RIC VA	0.11	0.31	0.24	0.20	0.18	0.16	0.17	0.14	0.13
SAC CA	0.12	0.24	0.16	0.13	0.11	0.10	0.08	0.06	0.06
SAI MO	0.08	0.23	0.17	0.13	0.12	0.10	0.10	0.08	0.06
SAL UT	0.12	0.20	0.12	0.09	0.08	0.08	0.02	0.01	0.02
SAN TX	0.12	0.28	0.21	0.18	0.16	0.14	0.13	0.12	0.11
SDO CA	0.09	0.21	0.12	0.09	0.07	0.05	0.01	0.01	0.01
SFO CA	0.05	0.15	0.11	0.08	0.08	0.06	0.05	0.04	0.04
TAM FL	0.09	0.23	0.16	0.13	0.11	0.09	0.08	0.07	0.06
TUL OK	0.11	0.32	0.25	0.20	0.18	0.17	0.17	0.15	0.14
WAS DC	0.11	0.30	0.22	0.18	0.16	0.14	0.14	0.11	0.10

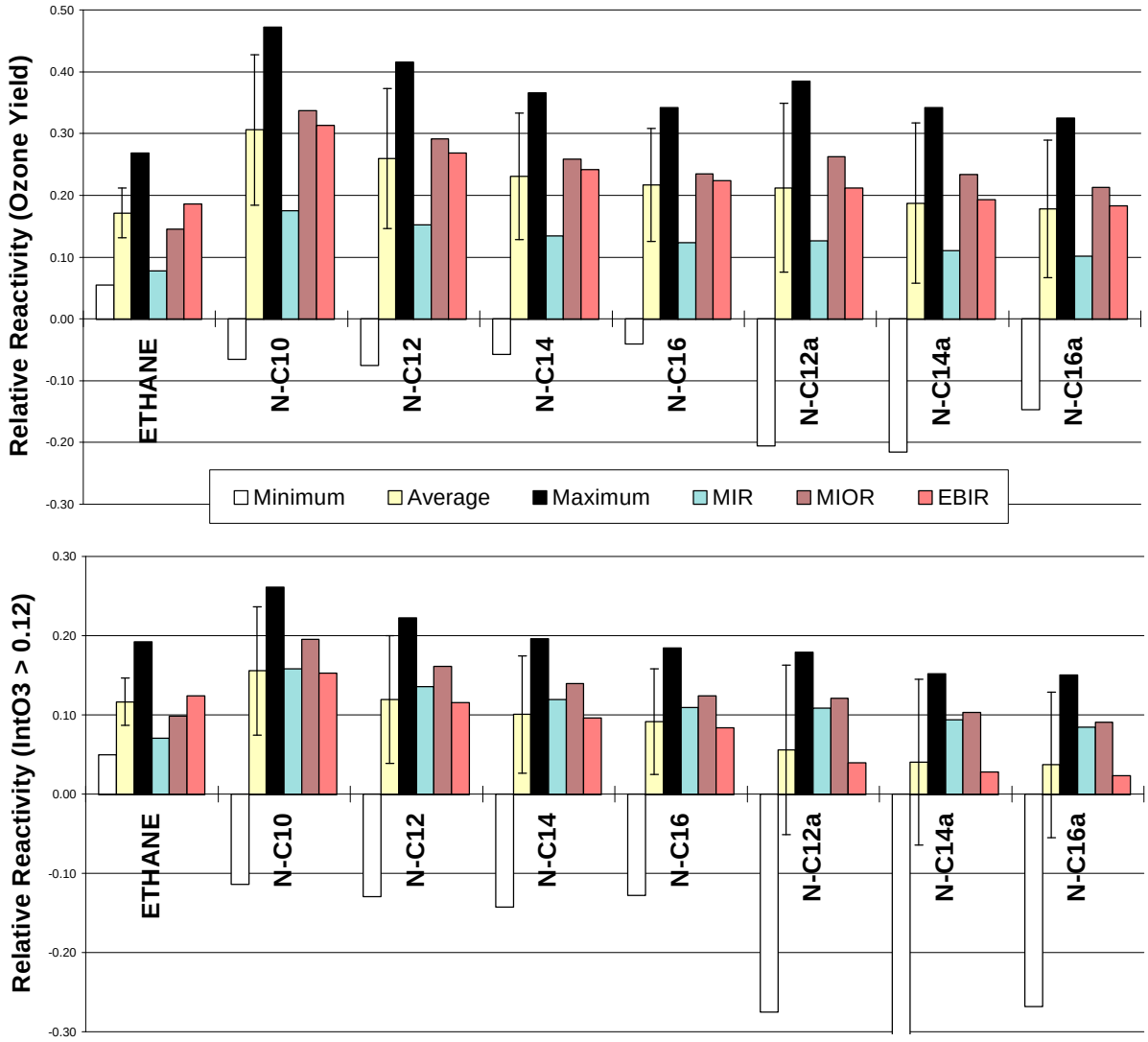

Figure 2. Comparisons of base case minimum, average and maximum, and MIR, MOIR, and EBIR relative reactivities for the representative C10+ n-alkanes. (The suffix "a" means the reactivities were cacluated using the high nitrate yield mechanism.)

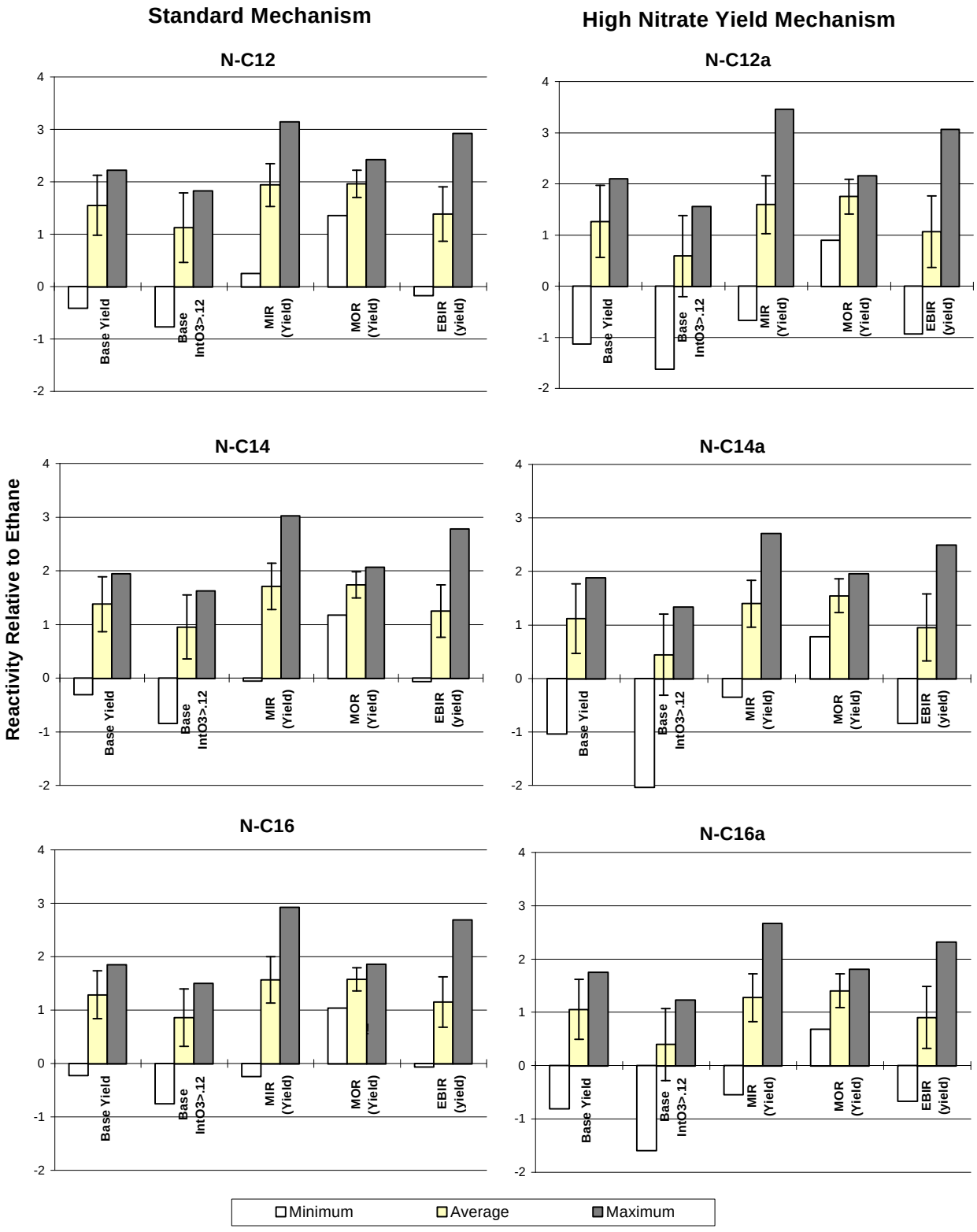

Figure 3. Comparisons of minimum, average, and maximum C_{12+} n-alkane / ethane reactivity ratios for various mechanisms, types of scenarios, and ozone quantification methods.

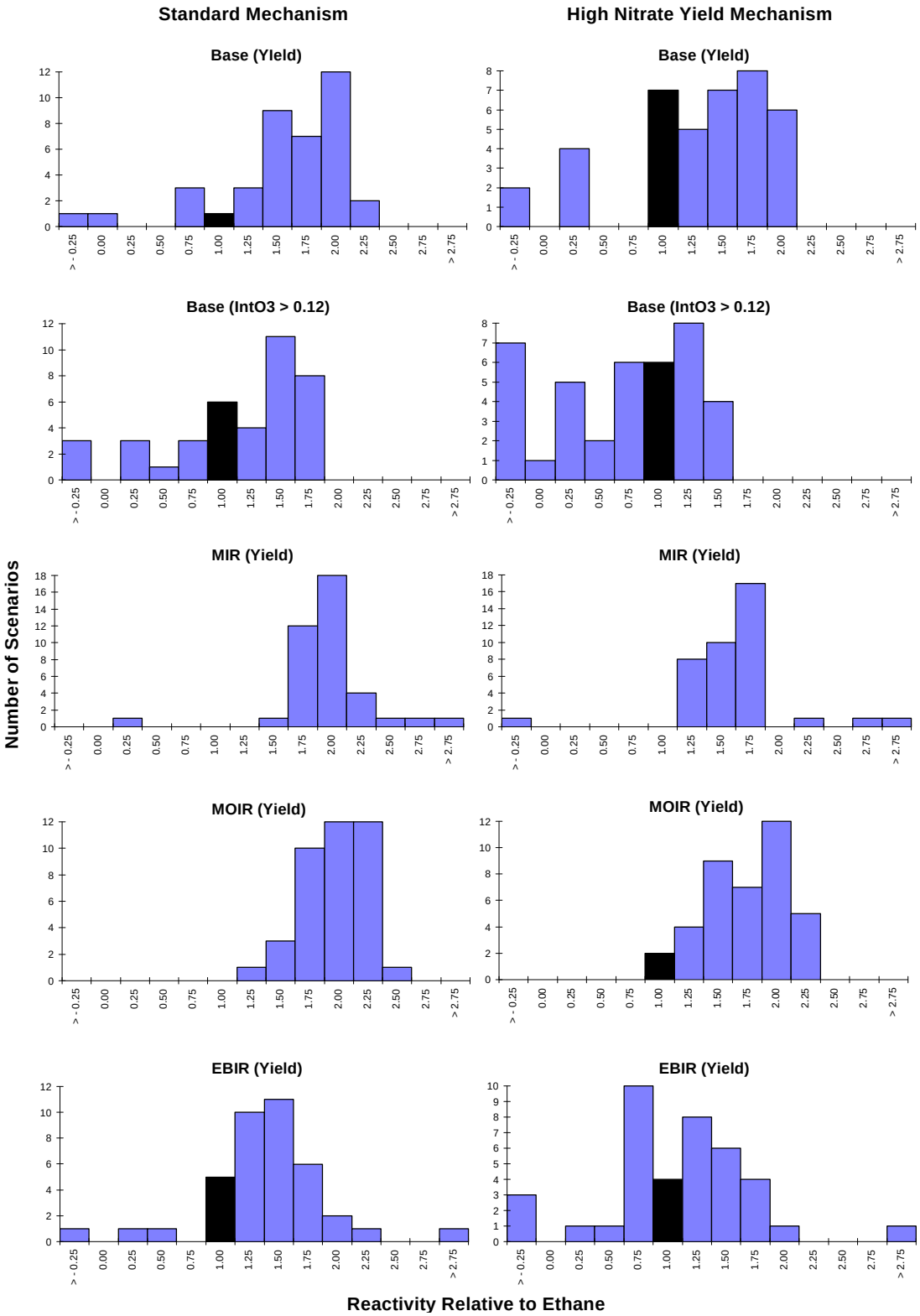

Figure 4. Distribution plots of n-dodecane / ethane reactivity ratios for various mechanisms, types of scenarios, and ozone quantification methods.

.

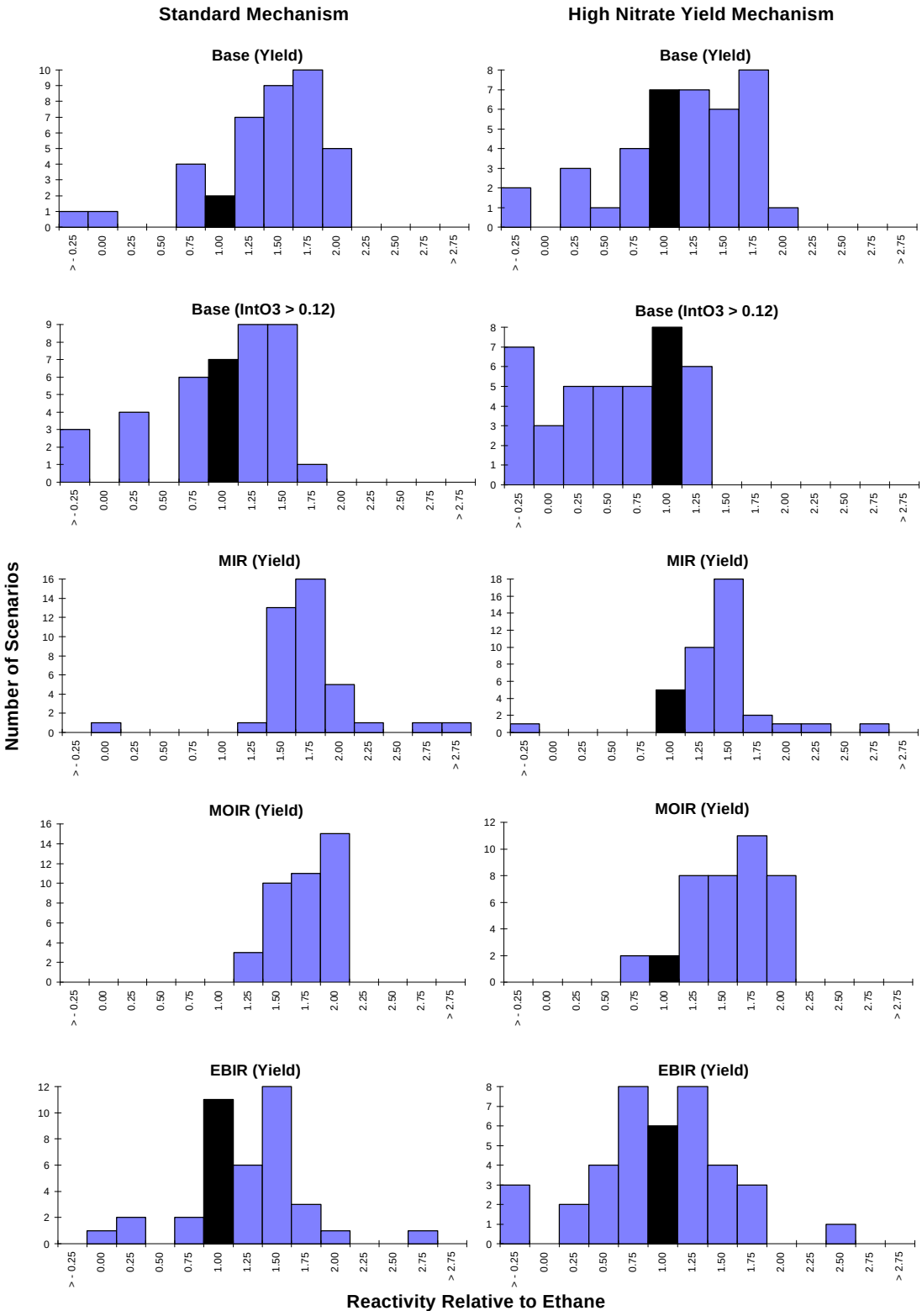

Figure 5. Distribution plots of n-tetradecane / ethane reactivity ratios for various mechanisms, types of scenarios, and ozone quantification methods.

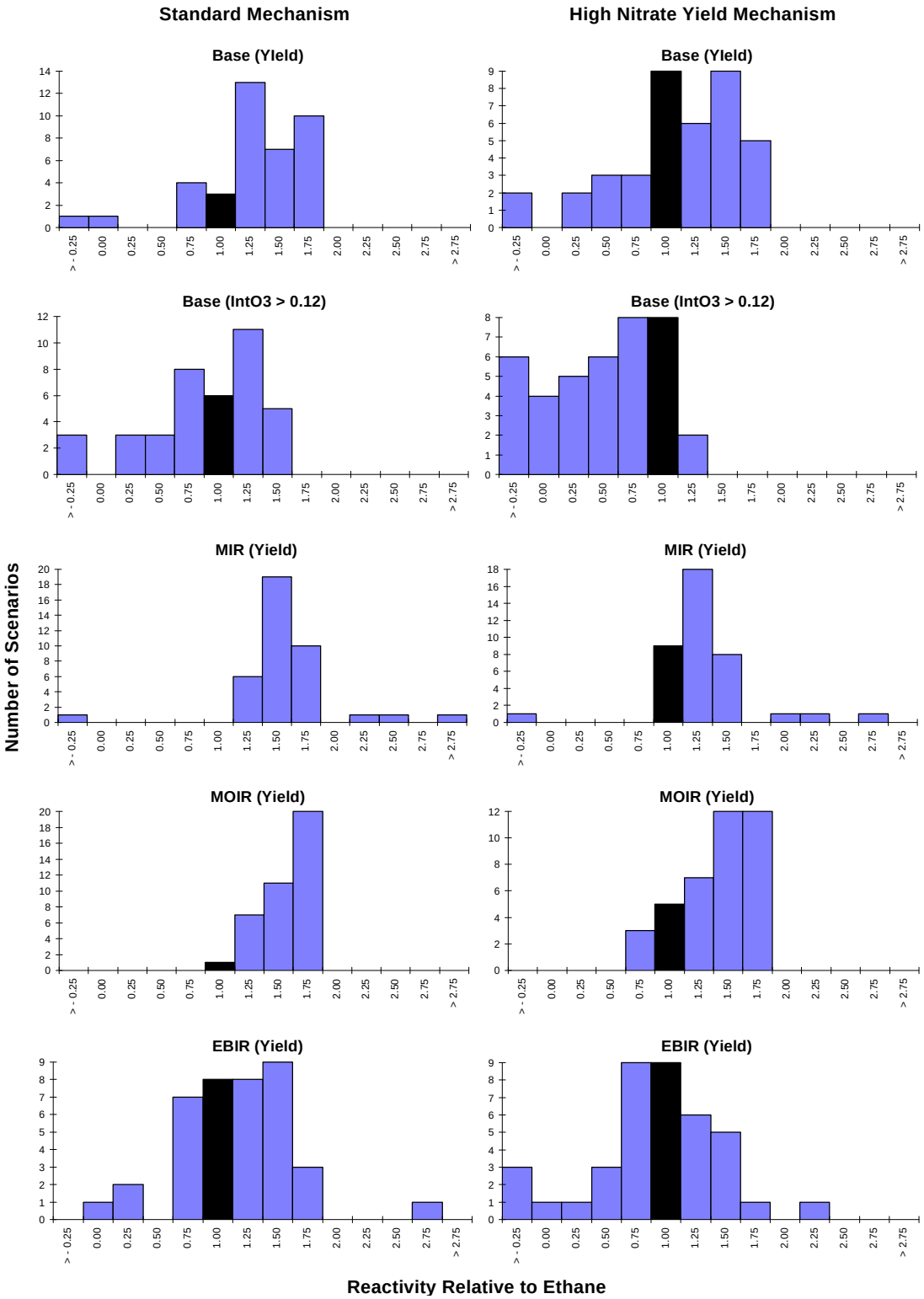

Figure 6. Distribution plots of n-hexadecane / ethane reactivity ratios for various mechanisms, types of scenarios, and ozone quantification methods.

These results show that the C_{12+} n-alkane relative reactivities are highly dependent on scenario conditions. This variability cannot be attributed to variability in NO_x conditions alone since, as can be seen from Figures 3-5, relatively wide distributions of n-alkane / ethane reactivity ratios are observed in both the MIR and EBIR adjusted NO_x scenarios. Interestingly, the variability is much less in the moderate NO_x MOR scenarios than it is under both higher (MIR) or lower (EBIR) NO_x conditions. Also, unlike most VOCs, the trend in relative reactivities is not monotonic as NO_x conditions change; the C_{12+} n-alkane / ethane reactivity ratios tend to be higher in the MIR and EBIR scenarios than under MOR conditions, except for a few scenarios where negative MIR or EBIR reactivities were observed. Note that the scenarios where the C_{12+} alkane reactivities were negative under MIR conditions were not the same as those where they had negative EBIR reactivities.

The fact that the C_{12+} n-alkane relative reactivities are highly variable and do not change monotonically with NO_x conditions can be explained by considering the different factors affecting their reactivities. As indicated above, the higher alkanes have a large positive effect on O_3 formation in that they form a relatively large number of peroxy radicals which convert NO to NO_2. This positive impact is important under all NO_x conditions, though the efficiency of O_3 formation from NO to NO_2 conversions tends to decrease as NO_x levels decrease (Carter and Atkinson, 1989a). This positive effect is counteracted by the radical inhibition and NO_x removal processes caused by the nitrate formation reaction. Under high NO_x MIR conditions, it is the radical inhibition factor which is dominant, and the variability of overall reactivity from scenario to scenario is due to the variability of the relative importance of the radical inhibition vs direct NO to NO_2 conversion effects. The NO_x removal effect of the nitrate formation reaction is unimportant. However, under low NO_x EBIR conditions, the NO_x removal factor becomes much more important than the radical inhibition factor, and thus the variability is due to the varying balance between this factor and the direct NO to NO_2 conversions. Under moderate NO_x MOR conditions, all three of these factors are important, and the apparent net effect of all these factors being operative is that the overall variability in the relative reactivity is less.

Another interesting general result is that the C_{10+} n-alkane relative reactivities are lower when O_3 impacts are quantified by integrated O_3 than they are when O_3 impacts are quantified by O_3 yields. For example, the standard mechanism calculates that the average ozone yield reactivities relative to ethane in the base case scenarios are 1.6, 1.4, and 1.3 for n-C_{12}, n-C_{14}, and n-C_{16}, respectively, while the average $IntO_3$>0.12 reactivity ratios are respectively 1.1, 1.0, and 0.9 for the same compounds, scenarios, and mechanisms. The difference is even greater for the high nitrate mechanisms, where the average base case ozone yield reactivities relative to ethane for those three compounds are respectively 1.3, 1.1, and 1.1,

while the corresponding $IntO_3$>0.12 reactivity ratios are 0.6, 0.4, and 0.4. This can be attributed to the fact that the radical inhibition effects of the alkane mechanisms slow down the rate of ozone formation, and thus decrease the total time period when O_3 concentrations are greater than the standard.

In terms of comparing the individual n-alkane compounds, the calculations indicate that, as expected, the ozone impact decreases monotonically as the size of the compound increases. In the case of n-C_{12}, the standard mechanism performs well in simulating the chamber data, and thus it is likely that the standard mechanism will give a good estimate of its atmospheric reactivity. This compound is calculated to be somewhat more reactive than ethane in ~85% of the scenarios when O_3 is quantified by peak yields, and in ~70% of the scenarios when O_3 is quantified by $IntO_3$ > 0.12. For C_{14+} n-alkanes, the chamber data suggest that the reactivities are probably between those calculated using the standard mechanism and that assuming the ~20% increased nitrate yields. In the case of n-C_{16}, the standard mechanism predicts that the MIR and MOIR reactivities are ~50% higher than those of ethane, though on the average their reactivities are about the same as ethane in the $IntO_3$ > 0.12 scales. The high nitrate mechanism for n-C_{16} predicts comparable or lower reactivities than ethane in most of the base case scales, though still ~30-40% higher reactivities in the MIR and MOIR scales.

CONCLUSIONS

The decision whether it is appropriate to regulate a compound as an ozone precursor requires a qualitative assessment of its ozone impacts under a variety of environmental conditions. This requires developing and experimentally validating a chemical mechanism for the compound's relevant atmospheric reactions, which can then be used in airshed models to predict its atmospheric reactivity. Although we have previously estimated the ozone impacts of the higher n-alkanes as part of a paper study on the atmospheric ozone impacts of representative aluminum cold rolling lubricant constituents (Carter and Venkataraman, 1995), these estimates were uncertain because of the lack of sufficient data to evaluate the chemical mechanisms used. The objective of this study was to provide the data needed to evaluate these mechanisms for the higher n-alkanes, and thus improve the reliability of the atmospheric reactivity estimates for these compounds. We believe this program succeeded in addressing this objective.

The alkane mechanisms which we developed previously (Carter, 1990) based on estimation techniques derived by Carter and Atkinson (1985, 1989b) were found to perform quite well in simulating experiments containing n-dodecane, which is consistent with its good performance in comparable experiments for n-octane in previous work (Carter et al, 1993a, 1995b). This indicates that our existing alkane mechanism, which was used in the previous assessment of Carter and Venkataraman (1995) probably gives reasonably reliable estimates of atmospheric reactivities of $C_{\leq 12}$ n-alkanes. For the higher n-alkanes, for which the data are somewhat more uncertain because of experimental difficulties in handling and analyzing these relatively low volatility compounds, it is possible that the existing mechanism may be slightly biased towards overestimating their atmospheric ozone impacts (or underestimating their inhibition of radicals and NO_x). An adjusted mechanism, assuming ~20% higher alkyl nitrate yields, tends to have the opposite bias. This means that probable atmospheric ozone impacts of the C_{14+} n-alkanes are probably somewhere between the predictions of the previous mechanism and the adjusted mechanism assuming higher alkyl nitrate yields. Thus, the two mechanisms together can indicate the range of probable impacts of these compounds.

The calculated relative atmospheric ozone impacts for the higher n-alkanes were found to be highly variable, even in the scenarios where NO_x inputs were adjusted to yield comparable conditions of NO_x availability. In some scenarios the higher n-alkanes actually inhibited ozone formation, and thus had negative incremental reactivity. These scenarios with negative reactivities occurred at both high and low

NO_x levels, though not in scenarios where NO_x levels were optimum for peak ozone formation. However, in most scenarios the C_{12+} n-alkanes had positive ozone impacts, and in extreme cases the ozone yield reactivities were as high as ~40% of the average reactivity of all reactive VOC emissions or ~3 times the reactivity of ethane. The average ozone yield relative reactivities were slightly larger than those for ethane, though, for C_{12} and larger n-alkanes, there was significant overlap in their standard deviations. Overall, we would conclude that in a majority of conditions these C_{12+} n-alkanes probably are slightly more reactive in terms of their effects on maximum ozone yields than is ethane, though, in view of the large variability, it is unclear whether this difference should be considered to be significant.

Another factor to consider is that the relative reactivities of the higher n-alkanes are lower if they are derived from effects on integrated ozone over the standard than if they are derived from effects on peak ozone yields. By this quantification, the C_{12+} n-alkanes have lower reactivities than ethane in a majority of the base case scenarios, and no case was found where they were more than ~25% of the reactivity of the average of all emissions, or more than ~1.8 times the reactivity of ethane. Thus, if the integrated ozone impact quantification is used, then we would conclude that these C_{12+} n-alkanes have comparable or slightly lower reactivities than ethane.

REFERENCES

Atkinson, R. and W. P. L. Carter (1984): "Kinetics and Mechanisms of the Gas-Phase Reactions of Ozone with Organic Compounds under Atmospheric Conditions," Chem. Rev. 1984, 437-470.

Atkinson, R. (1987): "A Structure-Activity Relationship for the Estimation of Rate Constants for the Gas-Phase Reactions of OH Radicals with Organic Compounds," Int. J. Chem. Kinet., 19, 799-828.

Atkinson, R. (1989): "Kinetics and Mechanisms of the Gas-Phase Reactions of the Hydroxyl Radical with Organic Compounds," J. Phys. Chem. Ref. Data, Monograph no 1.

Atkinson, R. (1990): "Gas-Phase Tropospheric Chemistry of Organic Compounds: A Review," Atmos. Environ., 24A, 1-24.

Atkinson, R. (1991): "Kinetics and Mechanisms of the Gas-Phase Reactions of the NO_3 Radical with Organic Compounds," J. Phys. Chem. Ref. Data, 20, 459-507.

Atkinson, R., D. L. Baulch, R. A. Cox, R. F. Hampson, Jr., J. A. Kerr, M. J. Rossi, and J. Troe (1996): "Evaluated Kinetic, Photochemical and Heterogenious Data for Atmospheric Chemistry: Supplement V., IUPAC Subcommittee on Gas Kinetic Data Evaluation for Atmospheric Chemistry," J. Phys. Chem. Ref. Data, in press.

Baugues, K. (1990): "Preliminary Planning Information for Updating the Ozone Regulatory Impact Analysis Version of EKMA," Draft Document, Source Receptor Analysis Branch, Technical Support Division, U. S. Environmental Protection Agency, Research Triangle Park, NC, January.

CARB (1993): "Proposed Regulations for Low-Emission Vehicles and Clean Fuels — Staff Report and Technical Support Document," California Air Resources Board, Sacramento, CA, August 13, 1990. See also Appendix VIII of "California Exhaust Emission Standards and Test Procedures for 1988 and Subsequent Model Passenger Cars, Light Duty Trucks and Medium Duty Vehicles," as last amended September 22, 1993. Incorporated by reference in Section 1960.1 (k) of Title 13, California Code of Regulations.

Calvert, J. G., and J. N. Pitts, Jr. (1966): Photochemistry, John Wiley and Sons, New York.

Carter, W. P. L. (1987): "An Experimental and Modeling Study of the Photochemical Reactivity of Heatset Printing Oils," Report #2 on U. S. EPA Cooperative Agreement No. CR810214-01

Carter, W. P. L., and R. Atkinson (1985): "Atmospheric Chemistry of Alkanes", J. Atmos. Chem., 3, 377-405, 1985.

Carter, W. P. L. (1990): "A Detailed Mechanism for the Gas-Phase Atmospheric Reactions of Organic Compounds," Atmos. Environ., 24A, 481-518.

Carter, W. P. L. (1991): "Development of Ozone Reactivity Scales for Volatile Organic Compounds", EPA-600/3-91/050, August.

Carter, W. P. L. (1993): "Development and Application of an Up-To-Date Photochemical Mechanism for Airshed Modeling and Reactivity Assessment," Draft final report for California Air Resources Board Contract No. A934-094, April 26.

Carter, W. P. L. (1994a): "Development of Ozone Reactivity Scales for Volatile Organic Compounds," J. Air & Waste Manage. Assoc., 44, 881-899.

Carter, W. P. L. (1994b): "Calculation of Reactivity Scales Using an Updated Carbon Bond IV Mechanism," Draft Report Prepared for Systems Applications International Under Funding from the Auto/Oil Air Quality Improvement Research Program, April 12.

Carter, W. P. L. (1995): "Computer Modeling of Environmental Chamber Measurements of Maximum Incremental Reactivities of Volatile Organic Compounds," Atmos. Environ., 29, 2513-2517.

Carter, W. P. L. and R. Atkinson (1987): "An Experimental Study of Incremental Hydrocarbon Reactivity," Environ. Sci. Technol., 21, 670-679

Carter, W. P. L. and R. Atkinson (1989a): "A Computer Modeling Study of Incremental Hydrocarbon Reactivity", Environ. Sci. Technol., 23, 864.

Carter, W. P. L. and R. Atkinson (1989b): "Alkyl Nitrate Formation from the Atmospheric Photooxidation of Alkanes; a Revised Estimation Method," J. Atm. Chem. 8, 165-173.

Carter, W. P. L., and F. W. Lurmann (1990): "Evaluation of the RADM Gas-Phase Chemical Mechanism," Final Report, EPA-600/3-90-001.

Carter, W. P. L. and F. W. Lurmann (1991): "Evaluation of a Detailed Gas-Phase Atmospheric Reaction Mechanism using Environmental Chamber Data," Atm. Environ. 25A, 2771-2806.

Carter, W. P. L, D. Luo, I. L. Malkina, and J. A. Pierce (1993a): "An Experimental and Modeling Study of the Photochemical Ozone Reactivity of Acetone," Final Report to Chemical Manufacturers Association Contract No. KET-ACE-CRC-2.0. December 10.

Carter, W. P. L., J. A. Pierce, I. L. Malkina, D. Luo and W. D. Long (1993b): "Environmental Chamber Studies of Maximum Incremental Reactivities of Volatile Organic Compounds," Report to Coordinating Research Council, Project No. ME-9, California Air Resources Board Contract No. A032-0692; South Coast Air Quality Management District Contract No. C91323, United States Environmental Protection Agency Cooperative Agreement No. CR-814396-01-0, University Corporation for Atmospheric Research Contract No. 59166, and Dow Corning Corporation. April 1.

Carter, W. P. L., J. A. Pierce, D. Luo, and I. L. Malkina (1995a): "Environmental Chamber Study of Maximum Incremental Reactivities of Volatile Organic Compounds," Atmos. Environ. 29, 2499-2511.

Carter, W. P. L., D. Luo, I. L. Malkina, and J. A. Pierce (1995b): "Environmental Chamber Studies of Atmospheric Reactivities of Volatile Organic Compounds. Effects of Varying ROG Surrogate and NO_x," Final report to Coordinating Research Council, Inc., Project ME-9, California Air Resources Board, Contract A032-0692, and South Coast Air Quality Management District, Contract C91323. March 24.

Carter, W. P. L., D. Luo, I. L. Malkina, and J. A. Pierce (1995c): "Environmental Chamber Studies of Atmospheric Reactivities of Volatile Organic Compounds. Effects of Varying Chamber and Light Source," Final report to National Renewable Energy Laboratory, Contract XZ-2-12075, Coordinating Research Council, Inc., Project M-9, California Air Resources Board, Contract A032-0692, and South Coast Air Quality Management District, Contract C91323, March 26.

Carter, W. P. L., D. Luo, I. L. Malkina, and D. Fitz (1995d): "The University of California, Riverside Environmental Chamber Data Base for Evaluating Oxidant Mechanism. Indoor Chamber Experiments through 1993," Report submitted to the U. S. Environmental Protection Agency, EPA/AREAL, Research Triangle Park, NC., March 20..

Carter, W. P. L. and C. Venkataraman (1995): "Atmospheric Ozone Formation Potential of Common Aluminum Rolling Lubricant Constituents," Report to Alcoa Aluminum Co., April 9, 1995.

Chang, T. Y. and S. J. Rudy (1990): "Ozone-Forming Potential of Organic Emissions from Alternative-Fueled Vehicles," Atmos. Environ., 24A, 2421-2430.

Croes, B. E., Technical Support Division, California Air Resources Board, personal communication (1991).

Croes, B. E., et al. (1994): "Southern California Air Quality Study Data Archive," Research Division, California Air Resources Board.

Dodge, M. C. (1984): "Combined effects of organic reactivity and NMHC/NOx ratio on photochemical oxidant formation -- a modeling study," Atmos. Environ., 18, 1657.

EPA (1984): "Guideline for Using the Carbon Bond Mechanism in City-Specific EKMA," EPA-450/4-84-005, February.

Gery, M. W., R. D. Edmond and G. Z. Whitten (1987): "Tropospheric Ultraviolet Radiation. Assessment of Existing Data and Effects on Ozone Formation," Final Report, EPA-600/3-87-047, October.

Jeffries, H. E. and R. Crouse (1991): "Scientific and Technical Issues Related to the Application of Incremental Reactivity. Part II: Explaining Mechanism Differences," Report prepared for Western States Petroleum Association, Glendale, CA, October.

Gipson, G. L. and W. P. Freas (1983): "Use of City-Specific EKMA in the Ozone RIA," U. S. Environmental Protection Agency, July.

Gipson, G. L., W. P. Freas, R. A. Kelly and E. L. Meyer, "Guideline for Use of City-Specific EKMA in Preparing Ozone SIPs, EPA-450/4-80-027, March, 1981.

Gipson, G. L. (1984): "Users Manual for OZIPM-2: Ozone Isopleth Plotting Package With Optional Mechanism/Version 2," EPA-450/4-84-024, August.

Hogo, H. and M. W. Gery (1988): "Guidelines for Using OZIPM-4 with CBM-IV or Optional Mechanisms. Volume 1. Description of the Ozone Isopleth Plotting Package Version 4", Final Report for EPA Contract No. 68-02-4136, Atmospheric Sciences Research Laboratory, Research Triangle Park, NC. January.

Jeffries, H. E., K. G. Sexton, J. R. Arnold, and T. L. Kale (1989): "Validation Testing of New Mechanisms with Outdoor Chamber Data. Volume 2: Analysis of VOC Data for the CB4 and CAL Photochemical Mechanisms," Final Report, EPA-600/3-89-010b.

Jeffries, H. E. (1991): "UNC Solar Radiation Models," unpublished draft report for EPA Cooperative Agreements CR813107, CR813964 and CR815779". Undated.

Johnson, G. M. (1983): "Factors Affecting Oxidant Formation in Sydney Air," in "The Urban Atmosphere -- Sydney, a Case Study." Eds. J. N. Carras and G. M. Johnson (CSIRO, Melbourne), pp. 393-408.

Lurmann, F. W. and H. H. Main (1992): "Analysis of the Ambient VOC Data Collected in the Southern California Air Quality Study," Final Report to California Air Resources Board Contract No. A832-130, February.

Pitts, J. N., Jr., E. Sanhueza, R. Atkinson, W. P. L. Carter, A. M. Winer, G. W. Harris, and C. N. Plum (1984): "An Investigation of the Dark Formation of Nitrous Acid in Environmental Chambers," Int. J. Chem. Kinet., 16, 919-939.

Tuazon, E. C., R. Atkinson, C. N. Plum, A. M. Winer, and J. N. Pitts, Jr. (1983): "The Reaction of Gas-Phase N_2O_5 with Water Vapor," Geophys. Res. Lett. 10, 953-956.

Zafonte, L., P. L. Rieger, and J. R. Holmes (1977): "Nitrogen Dioxide Photolysis in the Los Angeles Atmosphere," Environ. Sci. Technol. 11, 483-487.

APPENDIX A
LISTING OF THE CHEMICAL MECHANISM

The chemical mechanism used in the environmental chamber and atmospheric model simulations discussed in this report is given in Tables A-1 through A-4. Table A-1 lists the species used in the mechanism, Table A-2 gives the reactions and rate constants, Table A-3 gives the parameters used to calculate the rates of the photolysis reactions, and Table A-4 gives the values and derivations of the chamber-dependent parameters used when modeling the environmental chamber experiments. Footnotes to Table A-2 indicate the format used for the reaction listing.

Table A-1. List of species in the chemical mechanism used in the model simulations for this study.

Name	Description
Constant Species.	
O2	Oxygen
M	Air
H2O	Water
Active Inorganic Species.	
O3	Ozone
NO	Nitric Oxide
NO2	Nitrogen Dioxide
NO3	Nitrate Radical
N2O5	Nitrogen Pentoxide
HONO	Nitrous Acid
HNO3	Nitric Acid
HNO4	Peroxynitric Acid
HO2H	Hydrogen Peroxide
Active Radical Species and Operators.	
HO2.	Hydroperoxide Radicals
RO2.	Operator to Calculate Total Organic Peroxy Radicals
RCO3.	Operator to Calculate Total Acetyl Peroxy Radicals
Active Reactive Organic Product Species.	
CO	Carbon Monoxide
HCHO	Formaldehyde

Table A-1, (continued)

Name	Description
CCHO	Acetaldehyde
RCHO	Lumped C3+ Aldehydes
ACET	Acetone
MEK	Lumped Ketones
PHEN	Phenol
CRES	Cresols
BALD	Aromatic aldehydes (e.g., benzaldehyde)
GLY	Glyoxal
MGLY	Methyl Glyoxal
AFG1	Reactive Aromatic Fragmentation Products from benzene and naphthalene
AFG2	Other Reactive Aromatic Fragmentation Products
AFG3	Aromatic Fragmentation Products used in adjusted m-xylene mechanism
RNO3	Organic Nitrates
NPHE	Nitrophenols
ISOPROD	Lumped isoprene product species
PAN	Peroxy Acetyl Nitrate
PPN	Peroxy Propionyl Nitrate
GPAN	PAN Analogue formed from Glyoxal
PBZN	PAN Analogues formed from Aromatic Aldehydes
-OOH	Operator Representing Hydroperoxy Groups
Non-Reacting Species	
CO2	Carbon Dioxide
-C	"Lost Carbon"
-N	"Lost Nitrogen"
H2	Hydrogen
Steady State Species and Operators.	
HO.	Hydroxyl Radicals
O	Ground State Oxygen Atoms
O*1D2	Excited Oxygen Atoms
RO2-R.	Peroxy Radical Operator representing NO to NO_2 conversion with HO_2 formation.
RO2-N.	Peroxy Radical Operator representing NO consumption with organic nitrate formation.
RO2-NP.	Peroxy Radical Operator representing NO consumption with nitrophenol formation
R2O2.	Peroxy Radical Operator representing NO to NO_2 conversion.
CCO-O2.	Peroxy Acetyl Radicals
C2CO-O2.	Peroxy Propionyl Radicals
HCOCO-O2.	Peroxyacyl Radical formed from Glyoxal
BZ-CO-O2.	Peroxyacyl Radical formed from Aromatic Aldehydes
HOCOO.	Intermediate formed in Formaldehyde + HO_2 reaction
BZ-O.	Phenoxy Radicals
BZ(NO2)-O.	Nitratophenoxy Radicals
HOCOO.	Radical Intermediate formed in the HO_2 + Formaldehyde system.

Table A-1, (continued)

Name	Description
(HCHO2)	Excited Criegee biradicals formed from $=CH_2$ groups
(CCHO2)	Excited Criegee biradicals formed from $=CHCH_3$ groups
(RCHO2)	Excited Criegee biradicals formed from =CHR groups, where R not CH_3
(C(C)CO2)	Excited Criegee biradicals formed from $=C(CH_3)_2$ groups
(C(R)CO2)	Excited Criegee biradicals formed from $=C(CH_3)R$ or CR_2 groups
(BZCHO2)	Excited Criegee biradicals formed from styrenes
Hydrocarbon species represented explicitly	
CH4	Methane (EKMA simulations only)
ETHANE	Ethane (Ethane reactivity simulations only)
N-C4	n-Butane (Chamber simulations only)
N-C6	n-Hexane (Chamber simulations only)
N-C8	n-Octane (Chamber simulations only)
ETHE	Ethene
ISOP	Isoprene (EKMA Simulations only)
APIN	α-Pinene (EKMA Simulations only)
UNKN	Unknown biogenics. (EKMA Simulations only)
PROPENE	Propene (Chamber simulations only)
T-2-BUTE	trans-2-Butene (Chamber simulations only)
TOLUENE	Toluene (Chamber simulations only)
M-XYLENE	m-Xylene (Chamber simulations only)
C_{12+} n-alkanes (standard mechanism)	
N-C12	n-Dodecane (standard mechanism)
N-C14	n-Tetradecane (standard mechanism)
N-C15	n-Pentadecane (standard mechanism)
n-C16	n-Hexadecane (standard mechanism)
C_{12+} n-alkanes (high nitrate yield mechanism)	
N-C12a	n-Dodecane (high nitrate yield mechanism)
N-C14a	n-Tetradecane (high nitrate yield mechanism)
N-C15a	n-Pentadecane (high nitrate yield mechanism)
n-C16a	n-Hexadecane (high nitrate yield mechanism)
Lumped species used to represent the Base ROG mixture in the EKMA model simulations.	
ALK1	Alkanes and other saturated compounds with $k_{OH} < 10^4$ ppm^{-1} min^{-1}.
ALK2	Alkanes and other saturated compounds with $k_{OH} \geq 10^4$ ppm^{-1} min^{-1}.
ARO1	Aromatics with $k_{OH} < 2x10^4$ ppm^{-1} min^{-1}.
ARO2	Aromatics with $k_{OH} \geq 2x10^4$ ppm^{-1} min^{-1}.
OLE2	Alkenes (other than ethene) with $k_{OH} < 7x10^4$ ppm^{-1} min^{-1}.
OLE3	Alkenes with $k_{OH} \geq 7x10^4$ ppm^{-1} min^{-1}.

Table A-2. List of reactions in the chemical mechanism used in the model simulations for this study.

Rxn. Label	Kinetic Parameters [a] k(300)	A	Ea	B	Reactions [b]
Inorganic Reactions					
1	(Phot. Set = NO2)				NO2 + HV = NO + O
2	6.00E-34	6.00E-34	0.00	-2.30	O + O2 + M = O3 + M
3A	9.69E-12	6.50E-12	-0.24	0.00	O + NO2 = NO + O2
3B	1.55E-12	(Falloff Kinetics)			O + NO2 = NO3 + M
	k0 =	9.00E-32	0.00	-2.00	
	kINF =	2.20E-11	0.00	0.00	
		F= 0.60	n= 1.00		
4	1.88E-14	2.00E-12	2.78	0.00	O3 + NO = NO2 + O2
5	3.36E-17	1.40E-13	4.97	0.00	O3 + NO2 = O2 + NO3
6	2.80E-11	1.70E-11	-0.30	0.00	NO + NO3 = 2 NO2
7	1.92E-38	3.30E-39	-1.05	0.00	NO + NO + O2 = 2 NO2
8	1.26E-12	(Falloff Kinetics)			NO2 + NO3 = N2O5
	k0 =	2.20E-30	0.00	-4.30	
	kINF =	1.50E-12	0.00	-0.50	
		F= 0.60	n= 1.00		
9	5.53E+10	9.09E+26	22.26	0.00	N2O5 + #RCON8 = NO2 + NO3
10	1.00E-21	(No T Dependence)			N2O5 + H2O = 2 HNO3
11	4.17E-16	2.50E-14	2.44	0.00	NO2 + NO3 = NO + NO2 + O2
12A	(Phot. Set = NO3NO)				NO3 + HV = NO + O2
12B	(Phot. Set = NO3NO2)				NO3 + HV = NO2 + O
13A	(Phot. Set = O3O3P)				O3 + HV = O + O2
13B	(Phot. Set = O3O1D)				O3 + HV = O*1D2 + O2
14	2.20E-10	(No T Dependence)			O*1D2 + H2O = 2 HO.
15	2.92E-11	1.92E-11	-0.25	0.00	O*1D2 + M = O + M
16	4.81E-12	(Falloff Kinetics)			HO. + NO = HONO
	k0 =	7.00E-31	0.00	-2.60	
	kINF =	1.50E-11	0.00	-0.50	
		F= 0.60	n= 1.00		
17	(Phot. Set = HONO)				HONO + HV = HO. + NO
18	1.13E-11	(Falloff Kinetics)			HO. + NO2 = HNO3
	k0 =	2.60E-30	0.00	-3.20	
	kINF =	2.40E-11	0.00	-1.30	
		F= 0.60	n= 1.00		
19	1.03E-13	6.45E-15	-1.65	0.00	HO. + HNO3 = H2O + NO3
21	2.40E-13	(No T Dependence)			HO. + CO = HO2. + CO2
22	6.95E-14	1.60E-12	1.87	0.00	HO. + O3 = HO2. + O2
23	8.28E-12	3.70E-12	-0.48	0.00	HO2. + NO = HO. + NO2
24	1.37E-12	(Falloff Kinetics)			HO2. + NO2 = HNO4
	k0 =	1.80E-31	0.00	-3.20	
	kINF =	4.70E-12	0.00	-1.40	
		F= 0.60	n= 1.00		
25	7.92E+10	4.76E+26	21.66	0.00	HNO4 + #RCON24 = HO2. + NO2
27	4.61E-12	1.30E-12	-0.75	0.00	HNO4 + HO. = H2O + NO2 + O2
28	2.08E-15	1.10E-14	0.99	0.00	HO2. + O3 = HO. + 2 O2
29A	1.73E-12	2.20E-13	-1.23	0.00	HO2. + HO2. = HO2H + O2
29B	5.00E-32	1.90E-33	-1.95	0.00	HO2. + HO2. + M = HO2H + O2
29C	3.72E-30	3.10E-34	-5.60	0.00	HO2. + HO2. + H2O = HO2H + O2 + H2O
29D	2.65E-30	6.60E-35	-6.32	0.00	HO2. + HO2. + H2O = HO2H + O2 + H2O
30A	1.73E-12	2.20E-13	-1.23	0.00	NO3 + HO2. = HNO3 + O2
30B	5.00E-32	1.90E-33	-1.95	0.00	NO3 + HO2. + M = HNO3 + O2
30C	3.72E-30	3.10E-34	-5.60	0.00	NO3 + HO2. + H2O = HNO3 + O2 + H2O
30D	2.65E-30	6.60E-35	-6.32	0.00	NO3 + HO2. + H2O = HNO3 + O2 + H2O
31	(Phot. Set = H2O2)				HO2H + HV = 2 HO.
32	1.70E-12	3.30E-12	0.40	0.00	HO2H + HO. = HO2. + H2O
33	9.90E-11	4.60E-11	-0.46	0.00	HO. + HO2. = H2O + O2
Peroxy Radical Operators					
B1	7.68E-12	4.20E-12	-0.36	0.00	RO2. + NO = NO
B2	2.25E-11	(Falloff Kinetics)			RCO3. + NO = NO
	k0 =	5.65E-28	0.00	-7.10	
	kINF =	2.64E-11	0.00	-0.90	
		F= 0.27	n= 1.00		
B4	1.04E-11	(Falloff Kinetics)			RCO3. + NO2 = NO2
	k0 =	2.57E-28	0.00	-7.10	
	kINF =	1.20E-11	0.00	-0.90	
		F= 0.30	n= 1.00		
B5	4.90E-12	3.40E-13	-1.59	0.00	RO2. + HO2. = HO2. + RO2-HO2-PROD
B6	4.90E-12	3.40E-13	-1.59	0.00	RCO3. + HO2. = HO2. + RO2-HO2-PROD
B8	1.00E-15	(No T Dependence)			RO2. + RO2. = RO2-RO2-PROD
B9	1.09E-11	1.86E-12	-1.05	0.00	RO2. + RCO3. = RO2-RO2-PROD

Table A-2 (continued)

Rxn. Label	Kinetic Parameters [a] k(300)	A	Ea	B	Reactions [b]
B10	1.64E-11	2.80E-12	-1.05	0.00	RCO3. + RCO3. = RO2-RO2-PROD
B11	(Same k as for RO2.)				RO2-R. + NO = NO2 + HO2.
B12	(Same k as for RO2.)				RO2-R. + HO2. = -OOH
B13	(Same k as for RO2.)				RO2-R. + RO2. = RO2. + 0.5 HO2.
B14	(Same k as for RO2.)				RO2-R. + RCO3. = RCO3. + 0.5 HO2.
B19	(Same k as for RO2.)				RO2-N. + NO = RNO3
B20	(Same k as for RO2.)				RO2-N. + HO2. = -OOH + MEK + 1.5 -C
B21	(Same k as for RO2.)				RO2-N. + RO2. = RO2. + 0.5 HO2. + MEK + 1.5 -C
B22	(Same k as for RO2.)				RO2-N. + RCO3. = RCO3. + 0.5 HO2. + MEK + 1.5 -C
B15	(Same k as for RO2.)				R2O2. + NO = NO2
B16	(Same k as for RO2.)				R2O2. + HO2. =
B17	(Same k as for RO2.)				R2O2. + RO2. = RO2.
B18	(Same k as for RO2.)				R2O2. + RCO3. = RCO3.
B23	(Same k as for RO2.)				RO2-XN. + NO = -N
B24	(Same k as for RO2.)				RO2-XN. + HO2. = -OOH
B25	(Same k as for RO2.)				RO2-XN. + RO2. = RO2. + 0.5 HO2.
B26	(Same k as for RO2.)				RO2-XN. + RCO3. = RCO3. + HO2.
G2	(Same k as for RO2.)				RO2-NP. + NO = NPHE
G3	(Same k as for RO2.)				RO2-NP. + HO2. = -OOH + 6 -C
G4	(Same k as for RO2.)				RO2-NP. + RO2. = RO2. + 0.5 HO2. + 6 -C
G5	(Same k as for RO2.)				RO2-NP. + RCO3. = RCO3. + HO2. + 6 -C
Excited Criegee Biradicals					
RZ1	(fast)				(HCHO2) = 0.7 HCOOH + 0.12 "HO. + HO2. + CO" + 0.18 "H2 + CO2"
RZ2	(fast)				(CCHO2) = 0.25 CCOOH + 0.15 "CH4 + CO2" + 0.6 HO. + 0.3 "CCO-O2. + RCO3." + 0.3 "RO2-R. + HCHO + CO + RO2."
RZ3	(fast)				(RCHO2) = 0.25 CCOOH + 0.15 CO2 + 0.6 HO. + 0.3 "C2CO-O2. + RCO3." + 0.3 "RO2-R. + CCHO + CO + RO2." + 0.55 -C
RZ4	(fast)				(C(C)CO2) = HO. + R2O2. + HCHO + CCO-O2. + RCO3. + RO2.
RZ5	(fast)				(C(R)CO2) = HO. + CCO-O2. + CCHO + R2O2. + RCO3. + RO2.
RZ6	(fast)				(CYCCO2) = 0.3 "HO. + C2CO-O2. + R2O2. + RCO3. + RO2." + 0.3 RCHO + 4.2 -C
RZ8	(fast)				(BZCHO2) = 0.5 "BZ-O. + R2O2. + CO + HO."
ISZ1	(fast)				(C:CC(C)O2) = HO. + R2O2. + HCHO + C2CO-O2. + RO2. + RCO3.
ISZ2	(fast)				(C:C(C)CHO2) = 0.75 RCHO + 0.25 ISOPROD + 0.5 -C
MAZ1	(fast)				(C2(O2)CHO) = HO. + R2O2. + HCHO + HCOCO-O2. + RO2. + RCO3.
M1Z1	(fast)				(HOCCHO2) = 0.6 HO. + 0.3 "CCO-O2. + RCO3." + 0.3 "RO2-R. + HCHO + CO + RO2." + 0.8 -C
M2Z1	(fast)				(HCOCHO2) = 0.12 "HO2. + 2 CO + HO." + 0.74 -C + 0.51 "CO2 + HCHO"
M2Z2	(fast)				(C2(O2)COH) = HO. + MGLY + HO2. + R2O2. + RO2.
Organic Product Species					
B7	(Phot. Set = CO2H)				-OOH + HV = HO2. + HO.
B7A	1.81E-12	1.18E-12	-0.25	0.00	HO. + -OOH = HO.
B7B	3.71E-12	1.79E-12	-0.44	0.00	HO. + -OOH = RO2-R. + RO2.
C1	(Phot. Set = HCHONEWR)				HCHO + HV = 2 HO2. + CO
C2	(Phot. Set = HCHONEWM)				HCHO + HV = H2 + CO
C3	9.76E-12	1.13E-12	-1.29	2.00	HCHO + HO. = HO2. + CO + H2O
C4	7.79E-14	9.70E-15	-1.24	0.00	HCHO + HO2. = HOCOO.
C4A	1.77E+02	2.40E+12	13.91	0.00	HOCOO. = HO2. + HCHO
C4B	(Same k as for RO2.)				HOCOO. + NO = -C + NO2 + HO2.
C9	6.38E-16	2.80E-12	5.00	0.00	HCHO + NO3 = HNO3 + HO2. + CO
C10	1.57E-11	5.55E-12	-0.62	0.00	CCHO + HO. = CCO-O2. + H2O + RCO3.
C11A	(Phot. Set = CCHOR)				CCHO + HV = CO + HO2. + HCHO + RO2-R. + RO2.
C12	2.84E-15	1.40E-12	3.70	0.00	CCHO + NO3 = HNO3 + CCO-O2. + RCO3.
C25	1.97E-11	8.50E-12	-0.50	0.00	RCHO + HO. = C2CO-O2. + RCO3.
C26	(Phot. Set = RCHO)				RCHO + HV = CCHO + RO2-R. + RO2. + CO + HO2.
C27	2.84E-15	1.40E-12	3.70	0.00	NO3 + RCHO = HNO3 + C2CO-O2. + RCO3.
C38	2.23E-13	4.81E-13	0.46	2.00	ACET + HO. = R2O2. + HCHO + CCO-O2. + RCO3. + RO2.

Table A-2 (continued)

Rxn. Label	Kinetic Parameters [a] k(300)	A	Ea	B	Reactions [b]
C39	(Phot. Set = ACET-93C)				ACET + HV = CCO-O2. + HCHO + RO2-R. + RCO3. + RO2.
C44	1.16E-12	2.92E-13	-0.82	2.00	MEK + HO. = H2O + 0.5 "CCHO + HCHO + CCO-O2. + C2CO-O2." + RCO3. + 1.5 "R2O2. + RO2."
C57	(Phot. Set = KETONE)				MEK + HV + #0.1 = CCO-O2. + CCHO + RO2-R. + RCO3. + RO2.
C95	2.07E-12	2.19E-11	1.41	0.00	RNO3 + HO. = NO2 + 0.155 MEK + 1.05 RCHO + 0.48 CCHO + 0.16 HCHO + 0.11 -C + 1.39 "R2O2. + RO2."
C58A	(Phot. Set = GLYOXAL1)				GLY + HV = 0.8 HO2. + 0.45 HCHO + 1.55 CO
C58B	(Phot. Set = GLYOXAL2)				GLY + HV + #0.029 = 0.13 HCHO + 1.87 CO
C59	1.14E-11 (No T Dependence)				GLY + HO. = 0.6 HO2. + 1.2 CO + 0.4 "HCOCO-O2. + RCO3."
C60	(Same k as for CCHO)				GLY + NO3 = HNO3 + 0.6 HO2. + 1.2 CO + 0.4 "HCOCO-O2. + RCO3."
C68A	(Phot. Set = MEGLYOX1)				MGLY + HV = HO2. + CO + CCO-O2. + RCO3.
C68B	(Phot. Set = MEGLYOX2)				MGLY + HV + 0.107 = HO2. + CO + CCO-O2. + RCO3.
C69	1.72E-11 (No T Dependence)				MGLY + HO. = CO + CCO-O2. + RCO3.
C70	(Same k as for CCHO)				MGLY + NO3 = HNO3 + CO + CCO-O2. + RCO3.
G7	1.14E-11 (No T Dependence)				HO. + AFG1 = HCOCO-O2. + RCO3.
G8	(Phot. Set = ACROLEIN)				AFG1 + HV + #0.029 = HO2. + HCOCO-O2. + RCO3.
U2OH	1.72E-11 (No T Dependence)				HO. + AFG2 = C2CO-O2. + RCO3.
U2HV	(Phot. Set = ACROLEIN)				AFG2 + HV = HO2. + CO + CCO-O2. + RCO3.
G46	2.63E-11 (No T Dependence)				HO. + PHEN = 0.15 RO2-NP. + 0.85 RO2-R. + 0.2 GLY + 4.7 -C + RO2.
G51	3.60E-12 (No T Dependence)				NO3 + PHEN = HNO3 + BZ-O.
G52	4.20E-11 (No T Dependence)				HO. + CRES = 0.15 RO2-NP. + 0.85 RO2-R. + 0.2 MGLY + 5.5 -C + RO2.
G57	2.10E-11 (No T Dependence)				NO3 + CRES = HNO3 + BZ-O. + -C
G30	1.29E-11 (No T Dependence)				BALD + HO. = BZ-CO-O2. + RCO3.
G31	(Phot. Set = BZCHO)				BALD + HV + #0.05 = 7 -C
G32	2.61E-15	1.40E-12	3.75	0.00	BALD + NO3 = HNO3 + BZ-CO-O2.
G58	3.60E-12 (No T Dependence)				NPHE + NO3 = HNO3 + BZ(NO2)-O.
G59	(Same k as for BZ-O.)				BZ(NO2)-O. + NO2 = 2 -N + 6 -C
G60	(Same k as for RO2.)				BZ(NO2)-O. + HO2. = NPHE
G61	(Same k as for BZ-O.)				BZ(NO2)-O. = NPHE
C13	(Same k as for RCO3.)				CCO-O2. + NO = CO2 + NO2 + HCHO + RO2-R. + RO2.
C14	(Same k as for RCO3.)				CCO-O2. + NO2 = PAN
C15	(Same k as for RCO3.)				CCO-O2. + HO2. = -OOH + CO2 + HCHO
C16	(Same k as for RCO3.)				CCO-O2. + RO2. = RO2. + 0.5 HO2. + CO2 + HCHO
C17	(Same k as for RCO3.)				CCO-O2. + RCO3. = RCO3. + HO2. + CO2 + HCHO
C18	6.50E-04 (Falloff Kinetics)				PAN = CCO-O2. + NO2 + RCO3.
	k0 =	4.90E-03	23.97	0.00	
	kINF =	4.00E+16	27.08	0.00	
		F= 0.30	n= 1.00		
C28	(Same k as for RCO3.)				C2CO-O2. + NO = CCHO + RO2-R. + CO2 + NO2 + RO2.
C29	8.40E-12 (No T Dependence)				C2CO-O2. + NO2 = PPN
C30	(Same k as for RCO3.)				C2CO-O2. + HO2. = -OOH + CCHO + CO2
C31	(Same k as for RCO3.)				C2CO-O2. + RO2. = RO2. + 0.5 HO2. + CCHO + CO2
C32	(Same k as for RCO3.)				C2CO-O2. + RCO3. = RCO3. + HO2. + CCHO + CO2
C33	6.78E-04	1.60E+17	27.97	0.00	PPN = C2CO-O2. + NO2 + RCO3.
C62	(Same k as for RCO3.)				HCOCO-O2. + NO = NO2 + CO2 + CO + HO2.
C63	(Same k as for RCO3.)				HCOCO-O2. + NO2 = GPAN
C65	(Same k as for RCO3.)				HCOCO-O2. + HO2. = -OOH + CO2 + CO
C66	(Same k as for RCO3.)				HCOCO-O2. + RO2. = RO2. + 0.5 HO2. + CO2 + CO
C67	(Same k as for RCO3.)				HCOCO-O2. + RCO3. = RCO3. + HO2. + CO2 + CO
C64	(Same k as for PAN)				GPAN = HCOCO-O2. + NO2 + RCO3.
G33	(Same k as for RCO3.)				BZ-CO-O2. + NO = BZ-O. + CO2 + NO2 + R2O2. + RO2.
G43	3.53E-11	1.30E-11	-0.60	0.00	BZ-O. + NO2 = NPHE
G44	(Same k as for RO2.)				BZ-O. + HO2. = PHEN
G45	1.00E-03 (No T Dependence)				BZ-O. = PHEN
G34	8.40E-12 (No T Dependence)				BZ-CO-O2. + NO2 = PBZN
G36	(Same k as for RCO3.)				BZ-CO-O2. + HO2. = -OOH + CO2 + PHEN
G37	(Same k as for RCO3.)				BZ-CO-O2. + RO2. = RO2. + 0.5 HO2. + CO2 + PHEN

Table A-2 (continued)

Rxn. Label	Kinetic Parameters [a] k(300)	A	Ea	B	Reactions [b]
G38	(Same k as for RCO3.)				BZ-CO-O2. + RCO3. = RCO3. + HO2. + CO2 + PHEN
G35	2.17E-04	1.60E+15	25.90	0.00	PBZN = BZ-CO-O2. + NO2 + RCO3.
IPOH	3.36E-11	(No T Dependence)			ISOPROD + HO. = 0.293 CO + 0.252 CCHO + 0.126 HCHO + 0.041 GLY + 0.021 RCHO + 0.168 MGLY + 0.314 MEK + 0.503 RO2-R. + 0.21 CCO-O2. + 0.288 C2CO-O2. + 0.21 R2O2. + 0.713 RO2. + 0.498 RCO3. + -0.112 -C
IPO3	7.11E-18	(No T Dependence)			ISOPROD + O3 = 0.02 CCHO + 0.04 HCHO + 0.01 GLY + 0.84 MGLY + 0.09 MEK + 0.66 (HCHO2) + 0.09 (HCOCHO2) + 0.18 (HOCCHO2) + 0.06 (C2(O2)CHO) + 0.01 (C2(O2)COH) + -0.39 -C
IPHV	(Phot. Set = ACROLEIN)				ISOPROD + HV + 0.0036 = 0.333 CO + 0.067 CCHO + 0.9 HCHO + 0.033 MEK + 0.333 HO2. + 0.7 RO2-R. + 0.267 CCO-O2. + 0.7 C2CO-O2. + 0.7 RO2. + 0.967 RCO3. + -0.133 -C
IPN3	1.00E-15	(No T Dependence)			ISOPROD + NO3 = 0.643 CO + 0.282 HCHO + 0.85 RNO3 + 0.357 RCHO + 0.925 HO2. + 0.075 C2CO-O2. + 0.075 R2O2. + 0.925 RO2. + 0.075 RCO3. + 0.075 HNO3 + -2.471 -C
Hydrocarbon Species Represented Explicitly					
	2.56E-12	1.36E-12	-0.38	2.00	N-C4 + HO. = 0.076 RO2-N. + 0.924 RO2-R. + 0.397 R2O2. + 0.001 HCHO + 0.571 CCHO + 0.14 RCHO + 0.533 MEK + -0.076 -C + 1.397 RO2.
	5.63E-12	1.35E-11	0.52	0.00	N-C6 + HO. = 0.185 RO2-N. + 0.815 RO2-R. + 0.738 R2O2. + 0.02 CCHO + 0.105 RCHO + 1.134 MEK + 0.186 -C + 1.738 RO2.
	8.76E-12	3.15E-11	0.76	0.00	N-C8 + HO. = 0.333 RO2-N. + 0.667 RO2-R. + 0.706 R2O2. + 0.002 RCHO + 1.333 MEK + 0.998 -C + 1.706 RO2.
	8.43E-12	1.96E-12	-0.87	0.00	ETHENE + HO. = RO2-R. + RO2. + 1.56 HCHO + 0.22 CCHO
	1.68E-18	9.14E-15	5.13	0.00	ETHENE + O3 = HCHO + (HCHO2)
	2.18E-16	4.39E-13	4.53	2.00	ETHENE + NO3 = R2O2. + RO2. + 2 HCHO + NO2
	7.42E-13	1.04E-11	1.57	0.00	ETHENE + O = RO2-R. + HO2. + RO2. + HCHO + CO
	2.60E-11	4.85E-12	-1.00	0.00	PROPENE + HO. = RO2-R. + RO2. + HCHO + CCHO
	1.05E-17	5.51E-15	3.73	0.00	PROPENE + O3 = 0.6 HCHO + 0.4 CCHO + 0.4 (HCHO2) + 0.6 (CCHO2)
	9.74E-15	4.59E-13	2.30	0.00	PROPENE + NO3 = R2O2. + RO2. + HCHO + CCHO + NO2
	4.01E-12	1.18E-11	0.64	0.00	PROPENE + O = 0.4 HO2. + 0.5 RCHO + 0.5 MEK + -0.5 -C
	6.30E-11	1.01E-11	-1.09	0.00	T-2-BUTE + HO. = RO2-R. + RO2. + 2 CCHO
	1.95E-16	6.64E-15	2.10	0.00	T-2-BUTE + O3 = CCHO + (CCHO2)
	3.92E-13	1.10E-13	-0.76	2.00	T-2-BUTE + NO3 = R2O2. + RO2. + 2 CCHO + NO2
	2.34E-11	2.26E-11	-0.02	0.00	T-2-BUTE + O = 0.4 HO2. + 0.5 RCHO + 0.5 MEK + 0.5 -C
	9.88E-11	2.54E-11	-0.81	0.00	ISOP + HO. = 0.088 RO2-N. + 0.912 RO2-R. + 0.629 HCHO + 0.912 ISOPROD + 0.079 R2O2. + 1.079 RO2. + 0.283 -C
	1.34E-17	7.86E-15	3.80	0.00	ISOP + O3 = 0.4 HCHO + 0.6 ISOPROD + 0.55 (HCHO2) + 0.2 (C:CC(C)O2) + 0.2 (C:C(C)CHO2) + 0.05 -C
	3.60E-11	(No T Dependence)			ISOP + O = 0.75 "ISOPROD + -C "+ 0.25 "C2CO-O2. + RCO3. + 2 HCHO + RO2-R. + RO2."
	6.81E-13	3.03E-12	0.89	0.00	ISOP + NO3 = 0.8 "RCHO + RNO3 + RO2-R." + 0.2 "ISOPROD + R2O2. + NO2" + RO2. + -2.2 -C
	1.50E-19	(No T Dependence)			ISOP + NO2 = 0.8 "RCHO + RNO3 + RO2-R." + 0.2 "ISOPROD + R2O2. + NO" + RO2. + -2.2 -C
	5.31E-11	1.21E-11	-0.88	0.00	APIN + HO. = RO2-R. + RCHO + RO2. + 7 -C
	1.00E-16	9.90E-16	1.37	0.00	APIN + O3 = 0.05 HCHO + 0.2 CCHO + 0.5 RCHO + 0.61 MEK + 0.075 CO + 0.05 CCO-O2. + 0.05 C2CO-O2. + 0.1 RCO3. + 0.105 HO2. + 0.16 HO. + 0.135 RO2-R. + 0.15 R2O2. + 0.285 RO2. + 5.285 -C
	6.10E-12	1.19E-12	-0.97	0.00	APIN + NO3 = NO2 + R2O2. + RCHO + RO2. + 7 -C
	3.00E-11	(No T Dependence)			APIN + O = 0.4 HO2. + 0.5 MEK + 0.5 RCHO + 6.5 -C
	6.57E-11	(No T Dependence)			UNKN + HO. = RO2-R. + RO2. + 0.5 HCHO + RCHO + 6.5 -C
	5.85E-17	(No T Dependence)			UNKN + O3 = 0.135 RO2-R. + 0.135 HO2. + 0.075 R2O2. + 0.21 RO2. + 0.025 CCO-O2. + 0.025 C2CO-O2. + 0.05 RCO3. + 0.275 HCHO + 0.175 CCHO + 0.5 RCHO + 0.41 MEK + 0.185 CO + 5.925 -C + 0.11 HO.
	4.30E-12	(No T Dependence)			UNKN + NO3 = R2O2. + RO2. + 0.5 HCHO + RCHO + 6.5 -C + NO2

Table A-2 (continued)

Rxn. Label	Kinetic Parameters [a] k(300)	A	Ea	B	Reactions [b]
	2.90E-11	(No T Dependence)			UNKN + O = 0.4 HO2. + 0.5 RCHO + 0.5 MEK + 6.5 -C
	5.91E-12	1.81E-12	-0.70	0.00	TOLUENE + HO. = 0.085 BALD + 0.26 CRES + 0.118 GLY + 0.847 MGLY + 0.276 AFG2 + 0.74 RO2-R. + 0.26 HO2. + 0.981 -C + 0.74 RO2.
	2.36E-11	(No T Dependence)			M-XYLENE + HO. = 0.04 BALD + 0.18 CRES + 0.108 GLY + 1.554 MGLY + 0.505 AFG2 + 0.82 RO2-R. + 0.18 HO2. + 0.068 -C + 0.82 RO2.
Lumped Species used in EKMA Simulations [c]					
A1OH	5.11E+03	3.78E+03	-0.18	0.00	ALK1 + HO. = 0.911 RO2-R. + 0.074 RO2-N. + 0.005 RO2-XN. + 0.011 HO2. + 0.575 R2O2. + 1.564 RO2. + 0.065 HCHO + 0.339 CCHO + 0.196 RCHO + 0.322 ACET + 0.448 MEK + 0.024 CO + 0.025 GLY + 0.051 -C
A2OH	1.35E+04	7.57E+03	-0.35	0.00	ALK2 + HO. = 0.749 RO2-R. + 0.249 RO2-N. + 0.002 RO2-XN. + 0.891 R2O2. + 1.891 RO2. + 0.029 HCHO + 0.048 CCHO + 0.288 RCHO + 0.028 ACET + 1.105 MEK + 0.043 CO + 0.018 CO2 + 1.268 -C
B1OH	8.67E+03	(No T Dependence)			ARO1 + HO. = 0.742 RO2-R. + 0.258 HO2. + 0.742 RO2. + 0.015 PHEN + 0.244 CRES + 0.08 BALD + 0.124 GLY + 0.681 MGLY + 0.11 AFG1 + 0.244 AFG2 + 1.857 -C
B2OH	4.76E+04	1.77E+04	-0.59	0.00	ARO2 + HO. = 0.82 RO2-R. + 0.18 HO2. + 0.82 RO2. + 0.18 CRES + 0.036 BALD + 0.068 GLY + 1.02 MGLY + 0.532 AFG2 + 2.588 -C
O2OH	4.69E+04	3.28E+03	-1.59	0.00	OLE2 + HO. = 0.858 RO2-R. + 0.142 RO2-N. + RO2. + 0.858 HCHO + 0.252 CCHO + 0.606 RCHO + 1.267 -C
O2O3	1.59E-02	2.10E+00	2.91	0.00	OLE2 + O3 = 0.6 HCHO + 0.635 RCHO + 0.981 -C + 0.4 (HCHO2) + 0.529 (CCHO2) + 0.071 (RCHO2)
O2N3	1.72E+01	2.94E+02	1.69	0.00	OLE2 + NO3 = R2O2. + RO2. + HCHO + 0.294 CCHO + 0.706 RCHO + 1.451 -C + NO2
O2OA	6.07E+03	6.67E+03	0.06	0.00	OLE2 + O = 0.4 HO2. + 0.5 RCHO + 0.5 MEK + 1.657 -C
O3OH	9.21E+04	6.71E+03	-1.56	0.00	OLE3 + HO. = 0.861 RO2-R. + 0.139 RO2-N. + RO2. + 0.24 HCHO + 0.661 CCHO + 0.506 RCHO + 0.113 ACET + 0.086 MEK + 0.057 BALD + 0.848 -C
O3O3	2.51E-01	2.61E+00	1.40	0.00	OLE3 + O3 = 0.203 HCHO + 0.358 CCHO + 0.309 RCHO + 0.061 MEK + 0.027 BALD + 0.976 -C + 0.076 (HCHO2) + 0.409 (CCHO2) + 0.279 (RCHO2) + 0.158 (C(C)CO2 + 0.039 (C(R)CO2 + 0.04 (BZCHO2)
O3N3	1.58E+03	4.71E+02	-0.72	0.00	OLE3 + NO3 = R2O2. + RO2. + 0.278 HCHO + 0.767 CCHO + 0.588 RCHO + 0.131 ACET + 0.1 MEK + 0.066 BALD + 0.871 -C + NO2
O3OA	3.72E+04	1.28E+04	-0.64	0.00	OLE3 + O = 0.4 HO2. + 0.5 RCHO + 0.5 MEK + 2.205 -C
C_{12+} n-alkanes (standard mechanism)					
	1.43E-11	3.02E-11	0.45	0.00	N-C12 + HO. = 0.42 RO2-N. + 0.58 RO2-R. + 0.644 R2O2. + 0.001 RCHO + 1.223 MEK + 5.004 -C + 1.644 RO2.
	1.67E-11	3.64E-11	0.47	0.00	N-C14 + HO. = 0.431 RO2-N. + 0.569 RO2-R. + 0.634 R2O2. + 0.001 RCHO + 1.202 MEK + 7.033 -C + 1.634 RO2.
	1.81E-11	3.92E-11	0.46	0.00	N-C15 + HO. = 0.434 RO2-N. + 0.566 RO2-R. + 0.631 R2O2. + 0.001 RCHO + 1.196 MEK + 8.044 -C + 1.631 RO2.
	1.95E-11	4.21E-11	0.46	0.00	N-C16 + HO. = 0.437 RO2-N. + 0.563 RO2-R. + 0.628 R2O2. + 0.001 RCHO + 1.19 MEK + 9.052 -C + 1.628 RO2.
C_{12+} n-alkanes (high nitrate yield mechanism)					
	1.43E-11	3.02E-11	0.45	0.00	N-C12a + HO. = 0.504 RO2-N. + 0.495 RO2-R. + 0.644 R2O2. + 0.001 RCHO + 1.223 MEK + 4.583 -C + 1.644 RO2.
	1.67E-11	3.64E-11	0.47	0.00	N-C14a + HO. = 0.517 RO2-N. + 0.483 RO2-R. + 0.634 R2O2. + 0.001 RCHO + 1.202 MEK + 6.602 -C + 1.634 RO2.

Table A-2 (continued)

Rxn. Label	Kinetic Parameters [a] k(300)	A	Ea	B	Reactions [b]
	1.81E-11	3.92E-11	0.46	0.00	N-C15a + HO. = 0.521 RO2-N. + 0.479 RO2-R. + 0.631 R2O2. + 0.001 RCHO + 1.196 MEK + 7.61 -C + 1.631 RO2.
	1.95E-11	4.21E-11	0.46	0.00	N-C16a + HO. = 0.524 RO2-N. + 0.476 RO2-R. + 0.628 R2O2. + 0.001 RCHO + 1.19 MEK + 8.615 -C + 1.628 RO2.
Reactions used to Represent Chamber-Dependent Processes [d]					
O3W	(varied)	(No T Dependence)			O3 =
N25I	(varied)	(No T Dependence)			N2O5 = 2 NOX-WALL
N25S	(varied)	(No T Dependence)			N2O5 + H2O = 2 NOX-WALL
NO2W	(varied)	(No T Dependence)			NO2 = (yHONO) HONO + (1-yHONO) NOX-WALL
XSHC	(varied)	(No T Dependence)			HO. = HO2.
RSI	(Phot. Set = NO2)				HV + #RS/K1 = HO.
ONO2	(Phot. Set = NO2)				HV + #E-NO2/K1 = NO2 + #-1 NOX-WALL

[a] Except as noted, expression for rate constant is $k = A\ e^{Ea/RT}\ (T/300)^{B}$. Rate constants and A factor are in ppm, min units. Units of Ea is kcal $mole^{-1}$. "Phot Set" means this is a photolysis reaction, with the absorption coefficients and quantum yields given in Table A-3. In addition, if "#(number)" or "#(parameter)" is given as a reactant, then the value of that number or parameter is multiplied by the result in the "rate constant expression" columns to obtain the rate constant used. Furthermore, "#RCONnn" as a reactant means that the rate constant for the reaction is obtained by multiplying the rate constant given by that for reaction "nn". Thus, the rate constant given is actually an equilibrium constant.
[b] Format of reaction listing same as used in documentation of the detailed mechanism (Carter 1990).
[c] Rate constants and product yield parameters based on the mixture of species in the base ROG mixture which are being represented.
[d] See Table A-4 for the values of the parameters used for the specific chambers modeled in this study.

Table A-3. Absorption cross sections and quantum yields for photolysis reactions.

WL (nm)	Abs (cm^2)	QY	WL (nm)	Abs (cm^2)	QY	WL (nm)	Abs (cm^2)	QY	WL (nm)	Abs (cm^2)	QY	WL (nm)	Abs (cm^2)	QY
Photolysis File = NO2														
250.0	2.83E-20	1.000	255.0	1.45E-20	1.000	260.0	1.90E-20	1.000	265.0	2.05E-20	1.000	270.0	3.13E-20	1.000
275.0	4.02E-20	1.000	280.0	5.54E-20	1.000	285.0	6.99E-20	1.000	290.0	8.18E-20	0.999	295.0	9.67E-20	0.998
300.0	1.17E-19	0.997	305.0	1.66E-19	0.996	310.0	1.76E-19	0.995	315.0	2.25E-19	0.994	320.0	2.54E-19	0.993
325.0	2.79E-19	0.992	330.0	2.99E-19	0.991	335.0	3.45E-19	0.990	340.0	3.88E-19	0.989	345.0	4.07E-19	0.988
350.0	4.10E-19	0.987	355.0	5.13E-19	0.986	360.0	4.51E-19	0.984	365.0	5.78E-19	0.983	370.0	5.42E-19	0.981
375.0	5.35E-19	0.979	380.0	5.99E-19	0.975	381.0	5.98E-19	0.974	382.0	5.97E-19	0.973	383.0	5.96E-19	0.972
384.0	5.95E-19	0.971	385.0	5.94E-19	0.969	386.0	5.95E-19	0.967	387.0	5.96E-19	0.966	388.0	5.98E-19	0.964
389.0	5.99E-19	0.962	390.0	6.00E-19	0.960	391.0	5.98E-19	0.959	392.0	5.96E-19	0.957	393.0	5.93E-19	0.953
394.0	5.91E-19	0.950	395.0	5.89E-19	0.942	396.0	6.06E-19	0.922	397.0	6.24E-19	0.870	398.0	6.41E-19	0.820
399.0	6.59E-19	0.760	400.0	6.76E-19	0.695	401.0	6.67E-19	0.635	402.0	6.58E-19	0.560	403.0	6.50E-19	0.485
404.0	6.41E-19	0.425	405.0	6.32E-19	0.350	406.0	6.21E-19	0.290	407.0	6.10E-19	0.225	408.0	5.99E-19	0.185
409.0	5.88E-19	0.153	410.0	5.77E-19	0.130	411.0	5.88E-19	0.110	412.0	5.98E-19	0.094	413.0	6.09E-19	0.083
414.0	6.19E-19	0.070	415.0	6.30E-19	0.059	416.0	6.29E-19	0.048	417.0	6.27E-19	0.039	418.0	6.26E-19	0.030
419.0	6.24E-19	0.023	420.0	6.23E-19	0.018	421.0	6.18E-19	0.012	422.0	6.14E-19	0.008	423.0	6.09E-19	0.004
424.0	6.05E-19	0.000	425.0	6.00E-19	0.000									
Photolysis File = NO3NO														
585.0	2.77E-18	0.000	590.0	5.14E-18	0.250	595.0	4.08E-18	0.400	600.0	2.83E-18	0.250	605.0	3.45E-18	0.200
610.0	1.48E-18	0.200	615.0	1.96E-18	0.100	620.0	3.58E-18	0.100	625.0	9.25E-18	0.050	630.0	5.66E-18	0.050
635.0	1.45E-18	0.030	640.0	1.11E-18	0.000									
Photolysis File = NO3NO2														
400.0	0.00E+00	1.000	405.0	3.00E-20	1.000	410.0	4.00E-20	1.000	415.0	5.00E-20	1.000	420.0	8.00E-20	1.000
425.0	1.00E-19	1.000	430.0	1.30E-19	1.000	435.0	1.80E-19	1.000	440.0	1.90E-19	1.000	445.0	2.20E-19	1.000
450.0	2.80E-19	1.000	455.0	3.30E-19	1.000	460.0	3.70E-19	1.000	465.0	4.30E-19	1.000	470.0	5.10E-19	1.000
475.0	6.00E-19	1.000	480.0	6.40E-19	1.000	485.0	6.90E-19	1.000	490.0	8.80E-19	1.000	495.0	9.50E-19	1.000
500.0	1.01E-18	1.000	505.0	1.10E-18	1.000	510.0	1.32E-18	1.000	515.0	1.40E-18	1.000	520.0	1.45E-18	1.000
525.0	1.48E-18	1.000	530.0	1.94E-18	1.000	535.0	2.04E-18	1.000	540.0	1.81E-18	1.000	545.0	1.81E-18	1.000
550.0	2.36E-18	1.000	555.0	2.68E-18	1.000	560.0	3.07E-18	1.000	565.0	2.53E-18	1.000	570.0	2.54E-18	1.000
575.0	2.74E-18	1.000	580.0	3.05E-18	1.000	585.0	2.77E-18	1.000	590.0	5.14E-18	0.750	595.0	4.08E-18	0.600
600.0	2.83E-18	0.550	605.0	3.45E-18	0.400	610.0	1.45E-18	0.300	615.0	1.96E-18	0.250	620.0	3.58E-18	0.200
625.0	9.25E-18	0.150	630.0	5.66E-18	0.050	635.0	1.45E-18	0.000						
Photolysis File = O3O3P														
280.0	3.97E-18	0.100	281.0	3.60E-18	0.100	282.0	3.24E-18	0.100	283.0	3.01E-18	0.100	284.0	2.73E-18	0.100
285.0	2.44E-18	0.100	286.0	2.21E-18	0.100	287.0	2.01E-18	0.100	288.0	1.76E-18	0.100	289.0	1.58E-18	0.100
290.0	1.41E-18	0.100	291.0	1.26E-18	0.100	292.0	1.10E-18	0.100	293.0	9.89E-19	0.100	294.0	8.59E-19	0.100
295.0	7.70E-19	0.100	296.0	6.67E-19	0.100	297.0	5.84E-19	0.100	298.0	5.07E-19	0.100	299.0	4.52E-19	0.100
300.0	3.92E-19	0.100	301.0	3.42E-19	0.100	302.0	3.06E-19	0.100	303.0	2.60E-19	0.100	304.0	2.37E-19	0.100
305.0	2.01E-19	0.112	306.0	1.79E-19	0.149	307.0	1.56E-19	0.197	308.0	1.38E-19	0.259	309.0	1.25E-19	0.339
310.0	1.02E-19	0.437	311.0	9.17E-20	0.546	312.0	7.88E-20	0.652	313.0	6.77E-20	0.743	314.0	6.35E-20	0.816
315.0	5.10E-20	0.872	316.0	4.61E-20	0.916	317.0	4.17E-20	0.949	318.0	3.72E-20	0.976	319.0	2.69E-20	0.997
320.0	3.23E-20	1.000	330.0	6.70E-21	1.000	340.0	1.70E-21	1.000	350.0	4.00E-22	1.000	355.0	0.00E+00	1.000
400.0	0.00E+00	1.000	450.0	1.60E-22	1.000	500.0	1.34E-21	1.000	550.0	3.32E-21	1.000	600.0	5.06E-21	1.000
650.0	2.45E-21	1.000	700.0	8.70E-22	1.000	750.0	3.20E-22	1.000	800.0	1.60E-22	1.000	900.0	0.00E+00	1.000
Photolysis File = O3O1D														
280.0	3.97E-18	0.900	281.0	3.60E-18	0.900	282.0	3.24E-18	0.900	283.0	3.01E-18	0.900	284.0	2.73E-18	0.900
285.0	2.44E-18	0.900	286.0	2.21E-18	0.900	287.0	2.01E-18	0.900	288.0	1.76E-18	0.900	289.0	1.58E-18	0.900
290.0	1.41E-18	0.900	291.0	1.26E-18	0.900	292.0	1.10E-18	0.900	293.0	9.89E-19	0.900	294.0	8.59E-19	0.900
295.0	7.70E-19	0.900	296.0	6.67E-19	0.900	297.0	5.84E-19	0.900	298.0	5.07E-19	0.900	299.0	4.52E-19	0.900
300.0	3.92E-19	0.900	301.0	3.42E-19	0.900	302.0	3.06E-19	0.900	303.0	2.60E-19	0.900	304.0	2.37E-19	0.900
305.0	2.01E-19	0.888	306.0	1.79E-19	0.851	307.0	1.56E-19	0.803	308.0	1.38E-19	0.741	309.0	1.25E-19	0.661
310.0	1.02E-19	0.563	311.0	9.17E-20	0.454	312.0	7.88E-20	0.348	313.0	6.77E-20	0.257	314.0	6.35E-20	0.184
315.0	5.10E-20	0.128	316.0	4.61E-20	0.084	317.0	4.17E-20	0.051	318.0	3.72E-20	0.024	319.0	2.69E-20	0.003
320.0	3.23E-20	0.000												
Photolysis File = HONO														
311.0	0.00E+00	1.000	312.0	2.00E-21	1.000	313.0	4.20E-21	1.000	314.0	4.60E-21	1.000	315.0	4.20E-21	1.000
316.0	3.00E-21	1.000	317.0	4.60E-21	1.000	318.0	3.60E-20	1.000	319.0	6.10E-20	1.000	320.0	2.10E-20	1.000
321.0	4.27E-20	1.000	322.0	4.01E-20	1.000	323.0	3.93E-20	1.000	324.0	4.01E-20	1.000	325.0	4.04E-20	1.000
326.0	3.13E-20	1.000	327.0	4.12E-20	1.000	328.0	7.55E-20	1.000	329.0	6.64E-20	1.000	330.0	7.29E-20	1.000
331.0	8.70E-20	1.000	332.0	1.38E-19	1.000	333.0	5.91E-20	1.000	334.0	5.91E-20	1.000	335.0	6.45E-20	1.000
336.0	5.91E-20	1.000	337.0	4.58E-20	1.000	338.0	1.91E-19	1.000	339.0	1.63E-19	1.000	340.0	1.05E-19	1.000
341.0	8.70E-20	1.000	342.0	3.35E-19	1.000	343.0	2.01E-19	1.000	344.0	1.02E-19	1.000	345.0	8.54E-20	1.000
346.0	8.32E-20	1.000	347.0	8.20E-20	1.000	348.0	7.49E-20	1.000	349.0	7.13E-20	1.000	350.0	6.83E-20	1.000
351.0	1.74E-19	1.000	352.0	1.14E-19	1.000	353.0	3.71E-19	1.000	354.0	4.96E-19	1.000	355.0	2.46E-19	1.000
356.0	1.19E-19	1.000	357.0	9.35E-20	1.000	358.0	7.78E-20	1.000	359.0	7.29E-20	1.000	360.0	6.83E-20	1.000
361.0	6.90E-20	1.000	362.0	7.32E-20	1.000	363.0	9.00E-20	1.000	364.0	1.21E-19	1.000	365.0	1.33E-19	1.000
366.0	2.13E-19	1.000	367.0	3.52E-19	1.000	368.0	4.50E-19	1.000	369.0	2.93E-19	1.000	370.0	1.19E-19	1.000
371.0	9.46E-20	1.000	372.0	8.85E-20	1.000	373.0	7.44E-20	1.000	374.0	4.77E-20	1.000	375.0	2.70E-20	1.000
376.0	1.90E-20	1.000	377.0	1.50E-20	1.000	378.0	1.90E-20	1.000	379.0	5.80E-20	1.000	380.0	7.78E-20	1.000
381.0	1.14E-19	1.000	382.0	1.40E-19	1.000	383.0	1.72E-19	1.000	384.0	1.99E-19	1.000	385.0	1.90E-19	1.000
386.0	1.19E-19	1.000	387.0	5.65E-20	1.000	388.0	3.20E-20	1.000	389.0	1.90E-20	1.000	390.0	1.20E-20	1.000
391.0	5.00E-21	1.000	392.0	0.00E+00	1.000									
Photolysis File = H2O2														
250.0	8.30E-20	1.000	255.0	6.70E-20	1.000	260.0	5.20E-20	1.000	265.0	4.20E-20	1.000	270.0	3.20E-20	1.000
275.0	2.50E-20	1.000	280.0	2.00E-20	1.000	285.0	1.50E-20	1.000	290.0	1.13E-20	1.000	295.0	8.70E-21	1.000
300.0	6.60E-21	1.000	305.0	4.90E-21	1.000	310.0	3.70E-21	1.000	315.0	2.80E-21	1.000	320.0	2.00E-21	1.000
325.0	1.50E-21	1.000	330.0	1.20E-21	1.000	335.0	9.00E-22	1.000	340.0	7.00E-22	1.000	345.0	5.00E-22	1.000
350.0	3.00E-22	1.000	355.0	0.00E+00	1.000									

Table 3. (continued)

WL (nm)	Abs (cm^2)	QY	WL (nm)	Abs (cm^2)	QY	WL (nm)	Abs (cm^2)	QY	WL (nm)	Abs (cm^2)	QY	WL (nm)	Abs (cm^2)	QY
Photolysis File = CO2H														
210.0	3.75E-19	1.000	220.0	2.20E-19	1.000	230.0	1.38E-19	1.000	240.0	8.80E-20	1.000	250.0	5.80E-20	1.000
260.0	3.80E-20	1.000	270.0	2.50E-20	1.000	280.0	1.50E-20	1.000	290.0	9.00E-21	1.000	300.0	5.80E-21	1.000
310.0	3.40E-21	1.000	320.0	1.90E-21	1.000	330.0	1.10E-21	1.000	340.0	6.00E-22	1.000	350.0	4.00E-22	1.000
360.0	0.00E+00	1.000												
Photolysis File = HCHONEWR														
280.0	2.49E-20	0.590	280.5	1.42E-20	0.596	281.0	1.51E-20	0.602	281.5	1.32E-20	0.608	282.0	9.73E-21	0.614
282.5	6.76E-21	0.620	283.0	5.82E-21	0.626	283.5	9.10E-21	0.632	284.0	3.71E-20	0.638	284.5	4.81E-20	0.644
285.0	3.95E-20	0.650	285.5	2.87E-20	0.656	286.0	2.24E-20	0.662	286.5	1.74E-20	0.668	287.0	1.13E-20	0.674
287.5	1.10E-20	0.680	288.0	2.62E-20	0.686	288.5	4.00E-20	0.692	289.0	3.55E-20	0.698	289.5	2.12E-20	0.704
290.0	1.07E-20	0.710	290.5	1.35E-20	0.713	291.0	1.99E-20	0.717	291.5	1.56E-20	0.721	292.0	8.65E-21	0.724
292.5	5.90E-21	0.727	293.0	1.11E-20	0.731	293.5	6.26E-20	0.735	294.0	7.40E-20	0.738	294.5	5.36E-20	0.741
295.0	4.17E-20	0.745	295.5	3.51E-20	0.749	296.0	2.70E-20	0.752	296.5	1.75E-20	0.755	297.0	1.16E-20	0.759
297.5	1.51E-20	0.763	298.0	3.69E-20	0.766	298.5	4.40E-20	0.769	299.0	3.44E-20	0.773	299.5	2.02E-20	0.776
300.0	1.06E-20	0.780	300.4	7.01E-21	0.780	300.6	8.63E-21	0.779	300.8	1.47E-20	0.779	301.0	2.01E-20	0.779
301.2	2.17E-20	0.779	301.4	1.96E-20	0.779	301.6	1.54E-20	0.778	301.8	1.26E-20	0.778	302.0	1.03E-20	0.778
302.2	8.53E-21	0.778	302.4	7.13E-21	0.778	302.6	6.61E-21	0.777	302.8	1.44E-20	0.777	303.0	3.18E-20	0.777
303.2	3.81E-20	0.777	303.4	5.57E-20	0.777	303.6	6.91E-20	0.776	303.8	6.58E-20	0.776	304.0	6.96E-20	0.776
304.2	5.79E-20	0.776	304.4	5.24E-20	0.776	304.6	4.30E-20	0.775	304.8	3.28E-20	0.775	305.0	3.60E-20	0.775
305.2	5.12E-20	0.775	305.4	4.77E-20	0.775	305.6	4.43E-20	0.774	305.8	4.60E-20	0.774	306.0	4.01E-20	0.774
306.2	3.28E-20	0.774	306.4	2.66E-20	0.774	306.6	2.42E-20	0.773	306.8	1.95E-20	0.773	307.0	1.58E-20	0.773
307.2	1.37E-20	0.773	307.4	1.19E-20	0.773	307.6	1.01E-20	0.772	307.8	9.01E-21	0.772	308.0	8.84E-21	0.772
308.2	2.08E-20	0.772	308.4	2.39E-20	0.772	308.6	3.08E-20	0.771	308.8	3.39E-20	0.771	309.0	3.18E-20	0.771
309.2	3.06E-20	0.771	309.4	2.84E-20	0.771	309.6	2.46E-20	0.770	309.8	1.95E-20	0.770	310.0	1.57E-20	0.770
310.2	1.26E-20	0.767	310.4	9.26E-21	0.764	310.6	7.71E-21	0.761	310.8	6.05E-21	0.758	311.0	5.13E-21	0.755
311.2	4.82E-21	0.752	311.4	4.54E-21	0.749	311.6	6.81E-21	0.746	311.8	1.04E-20	0.743	312.0	1.43E-20	0.740
312.2	1.47E-20	0.737	312.4	1.35E-20	0.734	312.6	1.13E-20	0.731	312.8	9.86E-21	0.728	313.0	7.82E-21	0.725
313.2	6.48E-21	0.722	313.4	1.07E-20	0.719	313.6	2.39E-20	0.716	313.8	3.80E-20	0.713	314.0	5.76E-20	0.710
314.2	6.14E-20	0.707	314.4	7.45E-20	0.704	314.6	5.78E-20	0.701	314.8	5.59E-20	0.698	315.0	4.91E-20	0.695
315.2	4.37E-20	0.692	315.4	3.92E-20	0.689	315.6	2.89E-20	0.686	315.8	2.82E-20	0.683	316.0	2.10E-20	0.680
316.2	1.66E-20	0.677	316.4	2.05E-20	0.674	316.6	4.38E-20	0.671	316.8	5.86E-20	0.668	317.0	6.28E-20	0.665
317.2	5.07E-20	0.662	317.4	4.33E-20	0.659	317.6	4.17E-20	0.656	317.8	3.11E-20	0.653	318.0	2.64E-20	0.650
318.2	2.24E-20	0.647	318.4	1.70E-20	0.644	318.6	1.24E-20	0.641	318.8	1.11E-20	0.638	319.0	7.70E-21	0.635
319.2	6.36E-21	0.632	319.4	5.36E-21	0.629	319.6	4.79E-21	0.626	319.8	6.48E-21	0.623	320.0	1.48E-20	0.620
320.2	1.47E-20	0.614	320.4	1.36E-20	0.608	320.6	1.69E-20	0.601	320.8	1.32E-20	0.595	321.0	1.49E-20	0.589
321.2	1.17E-20	0.583	321.4	1.15E-20	0.577	321.6	9.64E-21	0.570	321.8	7.26E-21	0.564	322.0	5.94E-21	0.558
322.2	4.13E-21	0.552	322.4	3.36E-21	0.546	322.6	2.39E-21	0.539	322.8	2.01E-21	0.533	323.0	1.76E-21	0.527
323.2	2.82E-21	0.521	323.4	4.65E-21	0.515	323.6	7.00E-21	0.508	323.8	7.80E-21	0.502	324.0	7.87E-21	0.496
324.2	6.59E-21	0.490	324.4	5.60E-21	0.484	324.6	4.66E-21	0.477	324.8	4.21E-21	0.471	325.0	7.77E-21	0.465
325.2	2.15E-20	0.459	325.4	3.75E-20	0.453	325.6	4.10E-20	0.446	325.8	6.47E-20	0.440	326.0	7.59E-20	0.434
326.2	6.51E-20	0.428	326.4	5.53E-20	0.422	326.6	5.76E-20	0.415	326.8	4.43E-20	0.409	327.0	3.44E-20	0.403
327.2	3.22E-20	0.397	327.4	2.13E-20	0.391	327.6	1.91E-20	0.384	327.8	1.42E-20	0.378	328.0	9.15E-21	0.372
328.2	6.79E-21	0.366	328.4	4.99E-21	0.360	328.6	4.77E-21	0.353	328.8	1.75E-20	0.347	329.0	3.27E-20	0.341
329.2	3.99E-20	0.335	329.4	5.13E-20	0.329	329.6	4.00E-20	0.322	329.8	3.61E-20	0.316	330.0	3.38E-20	0.310
330.2	3.08E-20	0.304	330.4	2.16E-20	0.298	330.6	2.09E-20	0.291	330.8	1.41E-20	0.285	331.0	9.95E-21	0.279
331.2	7.76E-21	0.273	331.4	6.16E-21	0.267	331.6	4.06E-21	0.260	331.8	3.03E-21	0.254	332.0	2.41E-21	0.248
332.2	1.74E-21	0.242	332.4	1.33E-21	0.236	332.6	2.70E-21	0.229	332.8	1.65E-21	0.223	333.0	1.17E-21	0.217
333.2	9.84E-22	0.211	333.4	8.52E-22	0.205	333.6	6.32E-22	0.198	333.8	5.21E-22	0.192	334.0	1.46E-21	0.186
334.2	1.80E-21	0.180	334.4	1.43E-21	0.174	334.6	1.03E-21	0.167	334.8	7.19E-22	0.161	335.0	4.84E-22	0.155
335.2	2.73E-22	0.149	335.4	1.34E-22	0.143	335.6	-1.62E-22	0.136	335.8	1.25E-22	0.130	336.0	4.47E-22	0.124
336.2	1.23E-21	0.118	336.4	2.02E-21	0.112	336.6	3.00E-21	0.105	336.8	2.40E-21	0.099	337.0	3.07E-21	0.093
337.2	2.29E-21	0.087	337.4	2.46E-21	0.081	337.6	2.92E-21	0.074	337.8	8.10E-21	0.068	338.0	1.82E-20	0.062
338.2	3.10E-20	0.056	338.4	3.24E-20	0.050	338.6	4.79E-20	0.043	338.8	5.25E-20	0.037	339.0	5.85E-20	0.031
339.2	4.33E-20	0.025	339.4	4.20E-20	0.019	339.6	3.99E-20	0.012	339.8	3.11E-20	0.006	340.0	2.72E-20	0.000
Photolysis File = HCHONEWM														
280.0	2.49E-20	0.350	280.5	1.42E-20	0.346	281.0	1.51E-20	0.341	281.5	1.32E-20	0.336	282.0	9.73E-21	0.332
282.5	6.76E-21	0.327	283.0	5.82E-21	0.323	283.5	9.10E-21	0.319	284.0	3.71E-20	0.314	284.5	4.81E-20	0.309
285.0	3.95E-20	0.305	285.5	2.87E-20	0.301	286.0	2.24E-20	0.296	286.5	1.74E-20	0.291	287.0	1.13E-20	0.287
287.5	1.10E-20	0.282	288.0	2.62E-20	0.278	288.5	4.00E-20	0.273	289.0	3.55E-20	0.269	289.5	2.12E-20	0.264
290.0	1.07E-20	0.260	290.5	1.35E-20	0.258	291.0	1.99E-20	0.256	291.5	1.56E-20	0.254	292.0	8.65E-21	0.252
292.5	5.90E-21	0.250	293.0	1.11E-20	0.248	293.5	6.26E-20	0.246	294.0	7.40E-20	0.244	294.5	5.36E-20	0.242
295.0	4.17E-20	0.240	295.5	3.51E-20	0.238	296.0	2.70E-20	0.236	296.5	1.75E-20	0.234	297.0	1.16E-20	0.232
297.5	1.51E-20	0.230	298.0	3.69E-20	0.228	298.5	4.40E-20	0.226	299.0	3.44E-20	0.224	299.5	2.02E-20	0.222
300.0	1.06E-20	0.220	300.4	7.01E-21	0.220	300.6	8.63E-21	0.221	300.8	1.47E-20	0.221	301.0	2.01E-20	0.221
301.2	2.17E-20	0.221	301.4	1.96E-20	0.221	301.6	1.54E-20	0.222	301.8	1.26E-20	0.222	302.0	1.03E-20	0.222
302.2	8.53E-21	0.222	302.4	7.13E-21	0.222	302.6	6.61E-21	0.223	302.8	1.44E-20	0.223	303.0	3.18E-20	0.223
303.2	3.81E-20	0.223	303.4	5.57E-20	0.223	303.6	6.91E-20	0.224	303.8	6.58E-20	0.224	304.0	6.96E-20	0.224
304.2	5.79E-20	0.224	304.4	5.24E-20	0.224	304.6	4.30E-20	0.225	304.8	3.28E-20	0.225	305.0	3.60E-20	0.225
305.2	5.12E-20	0.225	305.4	4.77E-20	0.225	305.6	4.43E-20	0.226	305.8	4.60E-20	0.226	306.0	4.01E-20	0.226
306.2	3.28E-20	0.226	306.4	2.66E-20	0.226	306.6	2.42E-20	0.227	306.8	1.95E-20	0.227	307.0	1.58E-20	0.227
307.2	1.37E-20	0.227	307.4	1.19E-20	0.227	307.6	1.01E-20	0.228	307.8	9.01E-21	0.228	308.0	8.84E-21	0.228
308.2	2.08E-20	0.228	308.4	2.39E-20	0.228	308.6	3.08E-20	0.229	308.8	3.39E-20	0.229	309.0	3.18E-20	0.229
309.2	3.06E-20	0.229	309.4	2.84E-20	0.229	309.6	2.46E-20	0.230	309.8	1.95E-20	0.230	310.0	1.57E-20	0.230
310.2	1.26E-20	0.233	310.4	9.26E-21	0.236	310.6	7.71E-21	0.239	310.8	6.05E-21	0.242	311.0	5.13E-21	0.245
311.2	4.82E-21	0.248	311.4	4.54E-21	0.251	311.6	6.81E-21	0.254	311.8	1.04E-20	0.257	312.0	1.43E-20	0.260
312.2	1.47E-20	0.263	312.4	1.35E-20	0.266	312.6	1.13E-20	0.269	312.8	9.86E-21	0.272	313.0	7.82E-21	0.275
313.2	6.48E-21	0.278	313.4	1.07E-20	0.281	313.6	2.39E-20	0.284	313.8	3.80E-20	0.287	314.0	5.76E-20	0.290
314.2	6.14E-20	0.293	314.4	7.45E-20	0.296	314.6	5.78E-20	0.299	314.8	5.59E-20	0.302	315.0	4.91E-20	0.305
315.2	4.37E-20	0.308	315.4	3.92E-20	0.311	315.6	2.89E-20	0.314	315.8	2.82E-20	0.317	316.0	2.10E-20	0.320
316.2	1.66E-20	0.323	316.4	2.05E-20	0.326	316.6	4.38E-20	0.329	316.8	5.86E-20	0.332	317.0	6.28E-20	0.335
317.2	5.07E-20	0.338	317.4	4.33E-20	0.341	317.6	4.17E-20	0.344	317.8	3.11E-20	0.347	318.0	2.64E-20	0.350
318.2	2.24E-20	0.353	318.4	1.70E-20	0.356	318.6	1.24E-20	0.359	318.8	1.11E-20	0.362	319.0	7.70E-21	0.365

Table 3. (continued)

WL (nm)	Abs (cm^2)	QY	WL (nm)	Abs (cm^2)	QY	WL (nm)	Abs (cm^2)	QY	WL (nm)	Abs (cm^2)	QY	WL (nm)	Abs (cm^2)	QY
319.2	6.36E-21	0.368	319.4	5.36E-21	0.371	319.6	4.79E-21	0.374	319.8	6.48E-21	0.377	320.0	1.48E-20	0.380
320.2	1.47E-20	0.386	320.4	1.36E-20	0.392	320.6	1.69E-20	0.399	320.8	1.32E-20	0.405	321.0	1.49E-20	0.411
321.2	1.17E-20	0.417	321.4	1.15E-20	0.423	321.6	9.64E-21	0.430	321.8	7.26E-21	0.436	322.0	5.94E-21	0.442
322.2	4.13E-21	0.448	322.4	3.36E-21	0.454	322.6	2.39E-21	0.461	322.8	2.01E-21	0.467	323.0	1.76E-21	0.473
323.2	2.82E-21	0.479	323.4	4.65E-21	0.485	323.6	7.00E-21	0.492	323.8	7.80E-21	0.498	324.0	7.87E-21	0.504
324.2	6.59E-21	0.510	324.4	5.60E-21	0.516	324.6	4.66E-21	0.523	324.8	4.21E-21	0.529	325.0	7.77E-21	0.535
325.2	2.15E-20	0.541	325.4	3.75E-20	0.547	325.6	4.10E-20	0.554	325.8	6.47E-20	0.560	326.0	7.59E-20	0.566
326.2	6.51E-20	0.572	326.4	5.53E-20	0.578	326.6	5.76E-20	0.585	326.8	4.43E-20	0.591	327.0	3.44E-20	0.597
327.2	3.22E-20	0.603	327.4	2.13E-20	0.609	327.6	1.91E-20	0.616	327.8	1.42E-20	0.622	328.0	9.15E-21	0.628
328.2	6.79E-21	0.634	328.4	4.99E-21	0.640	328.6	4.77E-21	0.647	328.8	1.75E-20	0.653	329.0	3.27E-20	0.659
329.2	3.99E-20	0.665	329.4	5.13E-20	0.671	329.6	4.00E-20	0.678	329.8	3.61E-20	0.684	330.0	3.38E-20	0.690
330.2	3.08E-20	0.694	330.4	2.16E-20	0.699	330.6	2.09E-20	0.703	330.8	1.41E-20	0.708	331.0	9.95E-21	0.712
331.2	7.76E-21	0.717	331.4	6.16E-21	0.721	331.6	4.06E-21	0.726	331.8	3.03E-21	0.730	332.0	2.41E-21	0.735
332.2	1.74E-21	0.739	332.4	1.33E-21	0.744	332.6	2.70E-21	0.748	332.8	1.65E-21	0.753	333.0	1.17E-21	0.757
333.2	9.84E-22	0.762	333.4	8.52E-22	0.766	333.6	6.32E-22	0.771	333.8	5.21E-22	0.775	334.0	1.46E-21	0.780
334.2	1.80E-21	0.784	334.4	1.43E-21	0.789	334.6	1.03E-21	0.793	334.8	7.19E-22	0.798	335.0	4.84E-22	0.802
335.2	2.73E-22	0.798	335.4	1.34E-22	0.794	335.6	0.00E+00	0.790	335.8	1.25E-22	0.786	336.0	4.47E-22	0.782
336.2	1.23E-21	0.778	336.4	2.02E-21	0.773	336.6	3.00E-21	0.769	336.8	2.40E-21	0.764	337.0	3.07E-21	0.759
337.2	2.29E-21	0.754	337.4	2.46E-21	0.749	337.6	2.92E-21	0.745	337.8	8.10E-21	0.740	338.0	1.82E-20	0.734
338.2	3.10E-20	0.729	338.4	3.24E-20	0.724	338.6	4.79E-20	0.719	338.8	5.25E-20	0.714	339.0	5.85E-20	0.709
339.2	4.33E-20	0.703	339.4	4.20E-20	0.698	339.6	3.99E-20	0.693	339.8	3.11E-20	0.687	340.0	2.72E-20	0.682
340.2	1.99E-20	0.676	340.4	1.76E-20	0.671	340.6	1.39E-20	0.666	340.8	1.01E-20	0.660	341.0	6.57E-21	0.655
341.2	4.83E-21	0.649	341.4	3.47E-21	0.643	341.6	2.23E-21	0.638	341.8	1.55E-21	0.632	342.0	3.70E-21	0.627
342.2	4.64E-21	0.621	342.4	1.08E-20	0.616	342.6	1.14E-20	0.610	342.8	1.79E-20	0.604	343.0	2.33E-20	0.599
343.2	1.72E-20	0.593	343.4	1.55E-20	0.588	343.6	1.46E-20	0.582	343.8	1.38E-20	0.576	344.0	1.00E-20	0.571
344.2	8.26E-21	0.565	344.4	6.32E-21	0.559	344.6	4.28E-21	0.554	344.8	3.22E-21	0.548	345.0	2.54E-21	0.542
345.2	1.60E-21	0.537	345.4	1.15E-21	0.531	345.6	8.90E-22	0.525	345.8	6.50E-22	0.520	346.0	5.09E-22	0.514
346.2	5.15E-22	0.508	346.4	3.45E-22	0.503	346.6	3.18E-22	0.497	346.8	3.56E-22	0.491	347.0	3.24E-22	0.485
347.2	3.34E-22	0.480	347.4	2.88E-22	0.474	347.6	2.84E-22	0.468	347.8	9.37E-22	0.463	348.0	9.70E-22	0.457
348.2	7.60E-22	0.451	348.4	6.24E-22	0.446	348.6	4.99E-22	0.440	348.8	4.08E-22	0.434	349.0	3.39E-22	0.428
349.2	1.64E-22	0.423	349.4	1.49E-22	0.417	349.6	8.30E-23	0.411	349.8	2.52E-23	0.406	350.0	2.57E-23	0.400
350.2	0.00E+00	0.394	350.4	5.16E-23	0.389	350.6	0.00E+00	0.383	350.8	2.16E-23	0.377	351.0	7.07E-23	0.371
351.2	3.45E-23	0.366	351.4	1.97E-22	0.360	351.6	4.80E-22	0.354	351.8	3.13E-21	0.349	352.0	6.41E-21	0.343
352.2	8.38E-21	0.337	352.4	1.55E-20	0.331	352.6	1.86E-20	0.326	352.8	1.94E-20	0.320	353.0	2.78E-20	0.314
353.2	1.96E-20	0.309	353.4	1.67E-20	0.303	353.6	1.75E-20	0.297	353.8	1.63E-20	0.291	354.0	1.36E-20	0.286
354.2	1.07E-20	0.280	354.4	9.82E-21	0.274	354.6	8.66E-21	0.269	354.8	6.44E-21	0.263	355.0	4.84E-21	0.257
355.2	3.49E-21	0.251	355.4	2.41E-21	0.246	355.6	1.74E-21	0.240	355.8	1.11E-21	0.234	356.0	7.37E-22	0.229
356.2	4.17E-22	0.223	356.4	1.95E-22	0.217	356.6	1.50E-22	0.211	356.8	8.14E-23	0.206	357.0	0.00E+00	0.200
Photolysis File = CCHOR														
260.0	2.00E-20	0.310	270.0	3.40E-20	0.390	280.0	4.50E-20	0.580	290.0	4.90E-20	0.530	295.0	4.50E-20	0.480
300.0	4.30E-20	0.430	305.0	3.40E-20	0.370	315.0	2.10E-20	0.170	320.0	1.80E-20	0.100	325.0	1.10E-20	0.040
330.0	6.90E-21	0.000												
Photolysis File = RCHO														
280.0	5.26E-20	0.960	290.0	5.77E-20	0.910	300.0	5.05E-20	0.860	310.0	3.68E-20	0.600	320.0	1.66E-20	0.360
330.0	6.49E-21	0.200	340.0	1.44E-21	0.080	345.0	0.00E+00	0.020						
Photolysis File = ACET-93C														
250.0	2.37E-20	0.760	260.0	3.66E-20	0.800	270.0	4.63E-20	0.640	280.0	5.05E-20	0.550	290.0	4.21E-20	0.300
300.0	2.78E-20	0.150	310.0	1.44E-20	0.050	320.0	4.80E-21	0.026	330.0	8.00E-22	0.017	340.0	1.00E-22	0.000
350.0	3.00E-23	0.000	360.0	0.00E+00	0.000									
Photolysis File = KETONE														
210.0	1.10E-21	1.000	220.0	1.20E-21	1.000	230.0	4.60E-21	1.000	240.0	1.30E-20	1.000	250.0	2.68E-20	1.000
260.0	4.21E-20	1.000	270.0	5.54E-20	1.000	280.0	5.92E-20	1.000	290.0	5.16E-20	1.000	300.0	3.44E-20	1.000
310.0	1.53E-20	1.000	320.0	4.60E-21	1.000	330.0	1.10E-21	1.000	340.0	0.00E+00	1.000			
Photolysis File = GLYOXAL1														
230.0	2.87E-21	1.000	235.0	2.87E-21	1.000	240.0	4.30E-21	1.000	245.0	5.73E-21	1.000	250.0	8.60E-21	1.000
255.0	1.15E-20	1.000	260.0	1.43E-20	1.000	265.0	1.86E-20	1.000	270.0	2.29E-20	1.000	275.0	2.58E-20	1.000
280.0	2.87E-20	1.000	285.0	3.30E-20	1.000	290.0	3.15E-20	1.000	295.0	3.30E-20	1.000	300.0	3.58E-20	1.000
305.0	2.72E-20	1.000	310.0	2.72E-20	1.000	312.5	2.87E-20	1.000	315.0	2.29E-20	1.000	320.0	1.43E-20	1.000
325.0	1.15E-20	1.000	327.5	1.43E-20	1.000	330.0	1.15E-20	1.000	335.0	2.87E-21	1.000	340.0	0.00E+00	1.000
Photolysis File = GLYOXAL2														
355.0	0.00E+00	1.000	360.0	2.29E-21	1.000	365.0	2.87E-21	1.000	370.0	8.03E-21	1.000	375.0	1.00E-20	1.000
380.0	1.72E-20	1.000	382.0	1.58E-20	1.000	384.0	1.49E-20	1.000	386.0	1.49E-20	1.000	388.0	2.87E-20	1.000
390.0	3.15E-20	1.000	391.0	3.24E-20	1.000	392.0	3.04E-20	1.000	393.0	2.23E-20	1.000	394.0	2.63E-20	1.000
395.0	3.04E-20	1.000	396.0	2.63E-20	1.000	397.0	2.43E-20	1.000	398.0	3.24E-20	1.000	399.0	3.04E-20	1.000
400.0	2.84E-20	1.000	401.0	3.24E-20	1.000	402.0	4.46E-20	1.000	403.0	5.27E-20	1.000	404.0	4.26E-20	1.000
405.0	3.04E-20	1.000	406.0	3.04E-20	1.000	407.0	2.84E-20	1.000	408.0	2.43E-20	1.000	409.0	2.84E-20	1.000
410.0	6.08E-20	1.000	411.0	5.07E-20	1.000	411.5	6.08E-20	1.000	412.0	4.86E-20	1.000	413.0	8.31E-20	1.000
413.5	6.48E-20	1.000	414.0	7.50E-20	1.000	414.5	8.11E-20	1.000	415.0	8.11E-20	1.000	415.5	6.89E-20	1.000
416.0	4.26E-20	1.000	417.0	4.86E-20	1.000	418.0	5.88E-20	1.000	419.0	6.69E-20	1.000	420.0	3.85E-20	1.000
421.0	5.67E-20	1.000	421.5	4.46E-20	1.000	422.0	5.27E-20	1.000	422.5	1.05E-19	1.000	423.0	8.51E-20	1.000
424.0	6.08E-20	1.000	425.0	7.29E-20	1.000	426.0	1.18E-19	1.000	426.5	1.30E-19	1.000	427.0	1.07E-19	1.000
428.0	1.66E-19	1.000	429.0	4.05E-20	1.000	430.0	5.07E-20	1.000	431.0	4.86E-20	1.000	432.0	4.05E-20	1.000
433.0	3.65E-20	1.000	434.0	4.05E-20	1.000	434.5	6.08E-20	1.000	435.0	5.07E-20	1.000	436.0	8.11E-20	1.000
436.5	1.13E-19	1.000	437.0	5.27E-20	1.000	438.0	1.01E-19	1.000	438.5	1.38E-19	1.000	439.0	7.70E-20	1.000
440.0	2.47E-19	1.000	441.0	8.11E-20	1.000	442.0	6.08E-20	1.000	443.0	7.50E-20	1.000	444.0	9.32E-20	1.000
445.0	1.13E-19	1.000	446.0	5.27E-20	1.000	447.0	2.43E-20	1.000	448.0	2.84E-20	1.000	449.0	3.85E-20	1.000
450.0	6.08E-20	1.000	451.0	1.09E-19	1.000	451.5	9.32E-20	1.000	452.0	1.22E-19	1.000	453.0	2.39E-19	1.000
454.0	1.70E-19	1.000	455.0	3.40E-19	1.000	455.5	4.05E-19	1.000	456.0	1.01E-19	1.000	457.0	1.62E-20	1.000

Table 3. (continued)

WL (nm)	Abs (cm^2)	QY	WL (nm)	Abs (cm^2)	QY	WL (nm)	Abs (cm^2)	QY	WL (nm)	Abs (cm^2)	QY	WL (nm)	Abs (cm^2)	QY
458.0	1.22E-20	1.000	458.5	1.42E-20	1.000	459.0	4.05E-21	1.000	460.0	4.05E-21	1.000	460.5	6.08E-21	1.000
461.0	2.03E-21	1.000	462.0	0.00E+00	1.000									
Photolysis File = MEGLYOX1														
220.0	2.10E-21	1.000	225.0	2.10E-21	1.000	230.0	4.21E-21	1.000	235.0	7.57E-21	1.000	240.0	9.25E-21	1.000
245.0	8.41E-21	1.000	250.0	9.25E-21	1.000	255.0	9.25E-21	1.000	260.0	9.67E-21	1.000	265.0	1.05E-20	1.000
270.0	1.26E-20	1.000	275.0	1.43E-20	1.000	280.0	1.51E-20	1.000	285.0	1.43E-20	1.000	290.0	1.47E-20	1.000
295.0	1.18E-20	1.000	300.0	1.14E-20	1.000	305.0	9.25E-21	1.000	310.0	6.31E-21	1.000	315.0	5.47E-21	1.000
320.0	3.36E-21	1.000	325.0	1.68E-21	1.000	330.0	8.41E-22	1.000	335.0	0.00E+00	1.000			
Photolysis File = MEGLYOX2														
350.0	0.00E+00	1.000	354.0	4.21E-22	1.000	358.0	1.26E-21	1.000	360.0	2.10E-21	1.000	362.0	2.10E-21	1.000
364.0	2.94E-21	1.000	366.0	3.36E-21	1.000	368.0	4.21E-21	1.000	370.0	5.47E-21	1.000	372.0	5.89E-21	1.000
374.0	7.57E-21	1.000	376.0	7.99E-21	1.000	378.0	8.83E-21	1.000	380.0	1.01E-20	1.000	382.0	1.09E-20	1.000
384.0	1.35E-20	1.000	386.0	1.51E-20	1.000	388.0	1.72E-20	1.000	390.0	2.06E-20	1.000	392.0	2.10E-20	1.000
394.0	2.31E-20	1.000	396.0	2.48E-20	1.000	398.0	2.61E-20	1.000	400.0	2.78E-20	1.000	402.0	2.99E-20	1.000
404.0	3.20E-20	1.000	406.0	3.79E-20	1.000	408.0	3.95E-20	1.000	410.0	4.33E-20	1.000	412.0	4.71E-20	1.000
414.0	4.79E-20	1.000	416.0	4.88E-20	1.000	418.0	5.05E-20	1.000	420.0	5.21E-20	1.000	422.0	5.30E-20	1.000
424.0	5.17E-20	1.000	426.0	5.30E-20	1.000	428.0	5.21E-20	1.000	430.0	5.55E-20	1.000	432.0	5.13E-20	1.000
434.0	5.68E-20	1.000	436.0	6.22E-20	1.000	438.0	6.06E-20	1.000	440.0	5.47E-20	1.000	441.0	6.14E-20	1.000
442.0	5.47E-20	1.000	443.0	5.55E-20	1.000	443.5	6.81E-20	1.000	444.0	5.97E-20	1.000	445.0	5.13E-20	1.000
446.0	4.88E-20	1.000	447.0	5.72E-20	1.000	448.0	5.47E-20	1.000	449.0	6.56E-20	1.000	450.0	5.05E-20	1.000
451.0	3.03E-20	1.000	452.0	4.29E-20	1.000	453.0	2.78E-20	1.000	454.0	2.27E-20	1.000	456.0	1.77E-20	1.000
458.0	8.41E-21	1.000	460.0	4.21E-21	1.000	464.0	1.68E-21	1.000	468.0	0.00E+00	1.000			
Photolysis File = BZCHO														
299.0	1.78E-19	1.000	304.0	7.40E-20	1.000	306.0	6.91E-20	1.000	309.0	6.41E-20	1.000	313.0	6.91E-20	1.000
314.0	6.91E-20	1.000	318.0	6.41E-20	1.000	325.0	8.39E-20	1.000	332.0	7.65E-20	1.000	338.0	8.88E-20	1.000
342.0	8.88E-20	1.000	346.0	7.89E-20	1.000	349.0	7.89E-20	1.000	354.0	9.13E-20	1.000	355.0	8.14E-20	1.000
364.0	5.67E-20	1.000	368.0	6.66E-20	1.000	369.0	8.39E-20	1.000	370.0	8.39E-20	1.000	372.0	3.45E-20	1.000
374.0	3.21E-20	1.000	376.0	2.47E-20	1.000	377.0	2.47E-20	1.000	380.0	3.58E-20	1.000	382.0	9.90E-21	1.000
386.0	0.00E+00	1.000												
Photolysis File = ACROLEIN														
250.0	1.80E-21	1.000	252.0	2.05E-21	1.000	253.0	2.20E-21	1.000	254.0	2.32E-21	1.000	255.0	2.45E-21	1.000
256.0	2.56E-21	1.000	257.0	2.65E-21	1.000	258.0	2.74E-21	1.000	259.0	2.83E-21	1.000	260.0	2.98E-21	1.000
261.0	3.24E-21	1.000	262.0	3.47E-21	1.000	263.0	3.58E-21	1.000	264.0	3.93E-21	1.000	265.0	4.67E-21	1.000
266.0	5.10E-21	1.000	267.0	5.38E-21	1.000	268.0	5.73E-21	1.000	269.0	6.13E-21	1.000	270.0	6.64E-21	1.000
271.0	7.20E-21	1.000	272.0	7.77E-21	1.000	273.0	8.37E-21	1.000	274.0	8.94E-21	1.000	275.0	9.55E-21	1.000
276.0	1.04E-20	1.000	277.0	1.12E-20	1.000	278.0	1.19E-20	1.000	279.0	1.27E-20	1.000	280.0	1.27E-20	1.000
281.0	1.26E-20	1.000	282.0	1.26E-20	1.000	283.0	1.28E-20	1.000	284.0	1.33E-20	1.000	285.0	1.38E-20	1.000
286.0	1.44E-20	1.000	287.0	1.50E-20	1.000	288.0	1.57E-20	1.000	289.0	1.63E-20	1.000	290.0	1.71E-20	1.000
291.0	1.78E-20	1.000	292.0	1.86E-20	1.000	293.0	1.95E-20	1.000	294.0	2.05E-20	1.000	295.0	2.15E-20	1.000
296.0	2.26E-20	1.000	297.0	2.37E-20	1.000	298.0	2.48E-20	1.000	299.0	2.60E-20	1.000	300.0	2.73E-20	1.000
301.0	2.85E-20	1.000	302.0	2.99E-20	1.000	303.0	3.13E-20	1.000	304.0	3.27E-20	1.000	305.0	3.39E-20	1.000
306.0	3.51E-20	1.000	307.0	3.63E-20	1.000	308.0	3.77E-20	1.000	309.0	3.91E-20	1.000	310.0	4.07E-20	1.000
311.0	4.25E-20	1.000	312.0	4.39E-20	1.000	313.0	4.44E-20	1.000	314.0	4.50E-20	1.000	315.0	4.59E-20	1.000
316.0	4.75E-20	1.000	317.0	4.90E-20	1.000	318.0	5.05E-20	1.000	319.0	5.19E-20	1.000	320.0	5.31E-20	1.000
321.0	5.43E-20	1.000	322.0	5.52E-20	1.000	323.0	5.60E-20	1.000	324.0	5.67E-20	1.000	325.0	5.67E-20	1.000
326.0	5.62E-20	1.000	327.0	5.63E-20	1.000	328.0	5.71E-20	1.000	329.0	5.76E-20	1.000	330.0	5.80E-20	1.000
331.0	5.95E-20	1.000	332.0	6.23E-20	1.000	333.0	6.39E-20	1.000	334.0	6.38E-20	1.000	335.0	6.24E-20	1.000
336.0	6.01E-20	1.000	337.0	5.79E-20	1.000	338.0	5.63E-20	1.000	339.0	5.56E-20	1.000	340.0	5.52E-20	1.000
341.0	5.54E-20	1.000	342.0	5.53E-20	1.000	343.0	5.47E-20	1.000	344.0	5.41E-20	1.000	345.0	5.40E-20	1.000
346.0	5.48E-20	1.000	347.0	5.90E-20	1.000	348.0	6.08E-20	1.000	349.0	6.00E-20	1.000	350.0	5.53E-20	1.000
351.0	5.03E-20	1.000	352.0	4.50E-20	1.000	353.0	4.03E-20	1.000	354.0	3.75E-20	1.000	355.0	3.55E-20	1.000
356.0	3.45E-20	1.000	357.0	3.46E-20	1.000	358.0	3.49E-20	1.000	359.0	3.41E-20	1.000	360.0	3.23E-20	1.000
361.0	2.95E-20	1.000	362.0	2.81E-20	1.000	363.0	2.91E-20	1.000	364.0	3.25E-20	1.000	365.0	3.54E-20	1.000
366.0	3.30E-20	1.000	367.0	2.78E-20	1.000	368.0	2.15E-20	1.000	369.0	1.59E-20	1.000	370.0	1.19E-20	1.000
371.0	8.99E-21	1.000	372.0	7.22E-21	1.000	373.0	5.86E-21	1.000	374.0	4.69E-21	1.000	375.0	3.72E-21	1.000
376.0	3.57E-21	1.000	377.0	3.55E-21	1.000	378.0	2.83E-21	1.000	379.0	1.69E-21	1.000	380.0	8.29E-24	1.000
381.0	0.00E+00	1.000												

Table A-4. Recommended values for chamber wall and contaminant effects parameters to use as a starting point when modeling runs in this data base.

Parm. [a]	Value(s)	Discussion
k(1)	DTC: 0.222 min^{-1}	Derived by fitting results of quartz tube NO_2 actinometry measurements to curve similar to that derived for other blacklight chambers by Carter et al (1995d). The results of the actinometry experiments carried out during this study were within the uncertainty range of this extrapolation.
k(1)	CTC: 0.189 min^{-1}	The change NO_2 photolysis rates over time was determined by relative NO_2 photolysis rates calculated from spectra taken during the experiments, with the spectrometer being held in a fixed position. These were placed on an absolute basis by separate experiments where the NO_2 photolysis rates were derived from measurements of low concentrations of NO, NO_2, and O_3 in steady state (Carter et al, 1995c,d). Also consistent with results of modeling Cl_2 - n-butane - air irradiations (unpublished results from this laboratory).
k(O3W)	$1.5x10^{-4}$ min^{-1}	The results of the O_3 dark decay experiments in these chambers are consistent with the recommended default of Carter et al (1995d) for Teflon bag chambers.
k(N25I) k(N25S)	$2.8\ x10^{-3}$ min^{-1}, $1.5x10^{-6}$ - k_g ppm^{-1} min^{-1}	Based on the N_2O_5 decay rate measurements in a similar chamber reported by Tuazon et al. (1983). Although we previously estimated that these ate constants were lower in the larger Teflon bag chambers (Carter and Lurmann, 1990, 1991), we now consider it more reasonable to use the same rate constants for all such chambers (Carter et al., 1995d).
k(NO2W) yHONO	$1.6x10^{-4}$ min^{-1} 0.2	Based on dark NO_2 decay and HONO formation measured in a similar chamber by Pitts et al. (1984). Assumed to be the same in all Teflon bag chambers (Carter et al, 1995d).
k(XSHC)	250 min^{-1}	This represents excess NO to NO_2 conversions caused by impurities, and mainly affects simulations of pure air or NO_x-air runs. Estimated by modeling pure air irradiations.
RS/K1	DTC: $3.27x10^6$ $e^{-7297/T}$ ppm CTC: $3.54x10^6$ $e^{-7297/T}$ ppm	Based on model simulations of n-butane - NO_x experiments. The temperature dependence is derived from simulating outdoor experiments as discussed by Carter et al. (1995d).
E-NO2/K1	0.03 ppb	Based on model simulations of pure air experiments.

[a] See Table A-2 for definition of parameters.

APPENDIX B
PLOTS OF RESULTS OF REACTIVITY EXPERIMENTS

Figures B-1 through B-26 give time series plots of selected results of the reactivity experiments carried out for this program. These include concentrations of d(O_3-NO) and m-xylene in the base case and test experiments, concentrations of the test alkane in the test experiment, and the d(O_3-NO) and IntOH incremental reactivities derived from the differences between the two. Results of model simulations are also shown for the experiments where the initial n-alkane concentrations are sufficiently well characterized for modeling. Two sets of model simulations are shown for the added C_{12+} n-alkane experiments. The first, shown as the solid lines on the figures, is calculated using the current standard mechanism derived using the extrapolated organic nitrate yields derived by Carter and Atkinson (1989b). The second, shown as the dashed lines on the figures, was derived by assuming 20% higher nitrate yields for the C_{12+} n-alkanes, i.e., 20% greater radical inhibition in the reactions of these compounds. Note that both mechanisms give the same predictions for the base case experiments, because these do not contain C_{12+} alkanes.

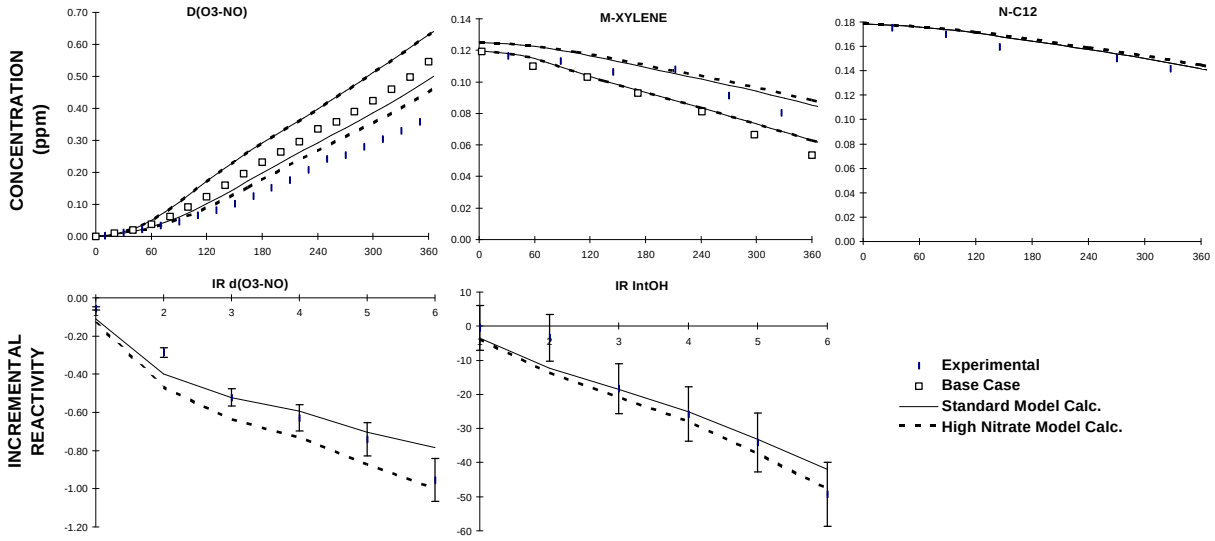

Figure B-1. Plots of selected results of the mini-surrogate + n-C_{12} experiment DTC-271.

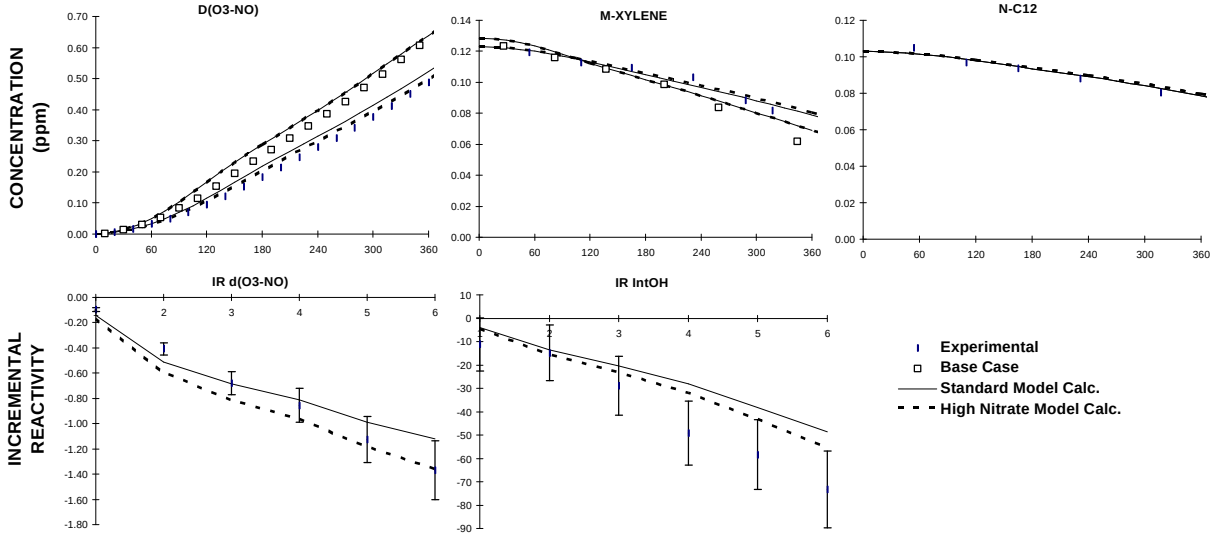

Figure B-2. Plots of selected results of the mini-surrogate + n-C_{12} experiment DTC-273.

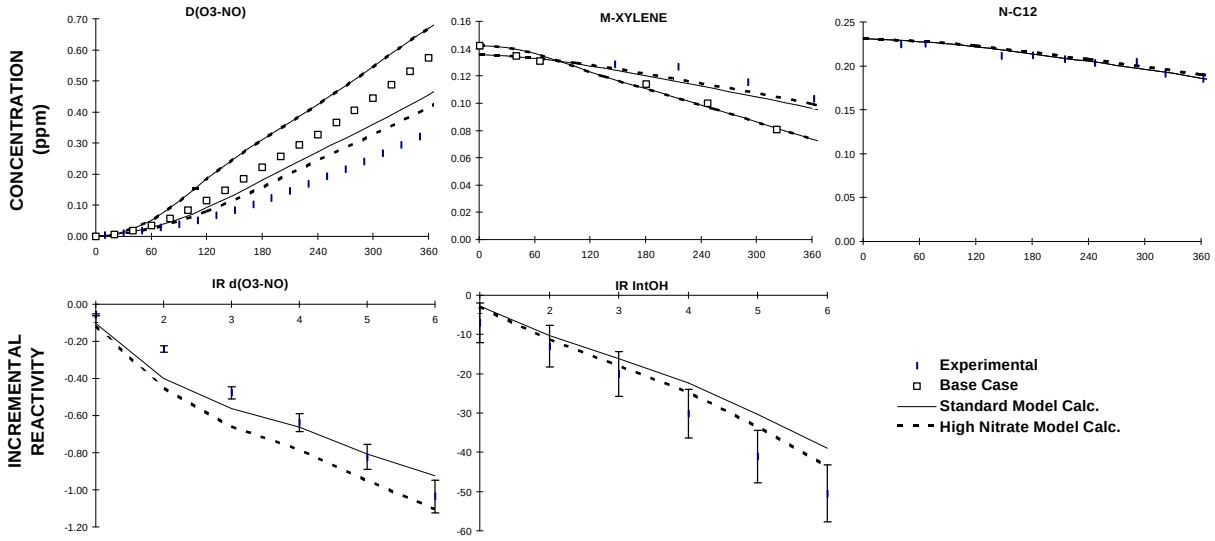

Figure B-3. Plots of selected results of the mini-surrogate + n-C_{12} experiment DTC-283.

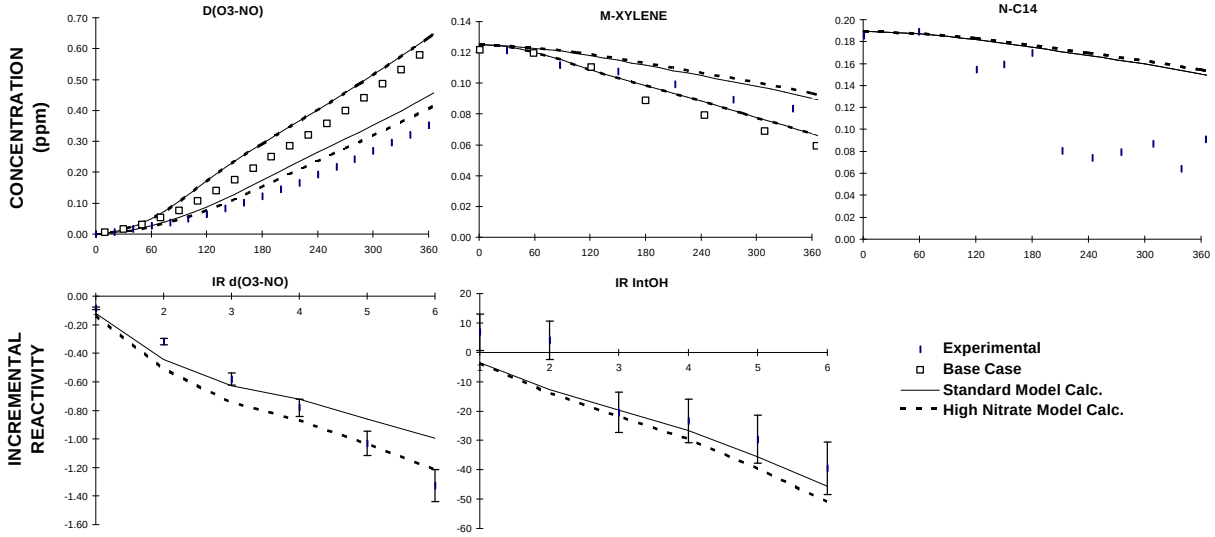

Figure B-4. Plots of selected results of the mini-surrogate + n-C_{14} experiment DTC-275.

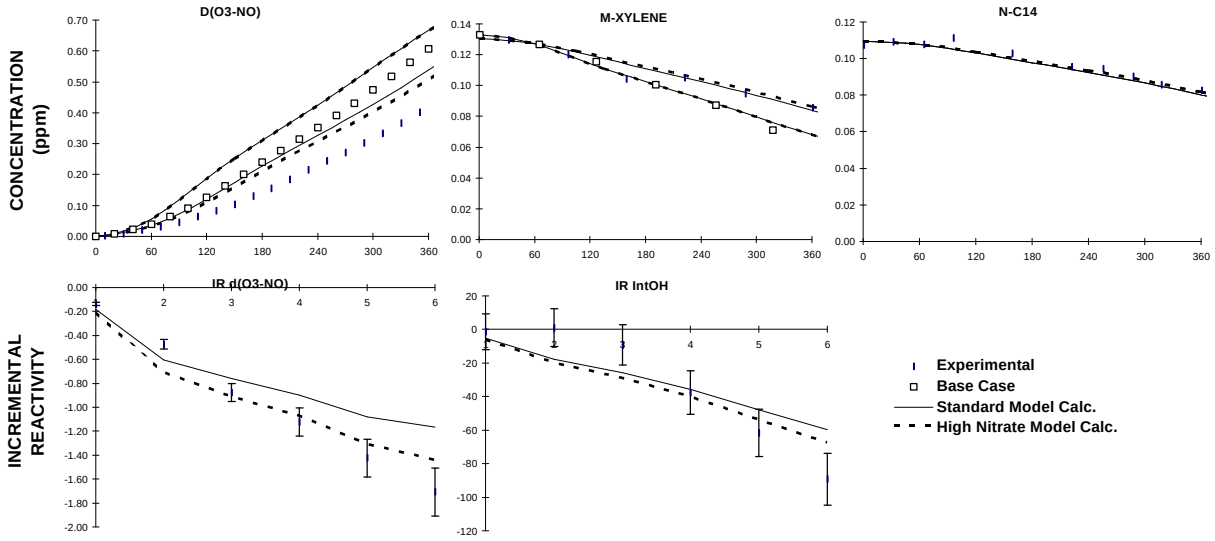

Figure B-5. Plots of selected results of the mini-surrogate + n-C_{14} experiment DTC-277.

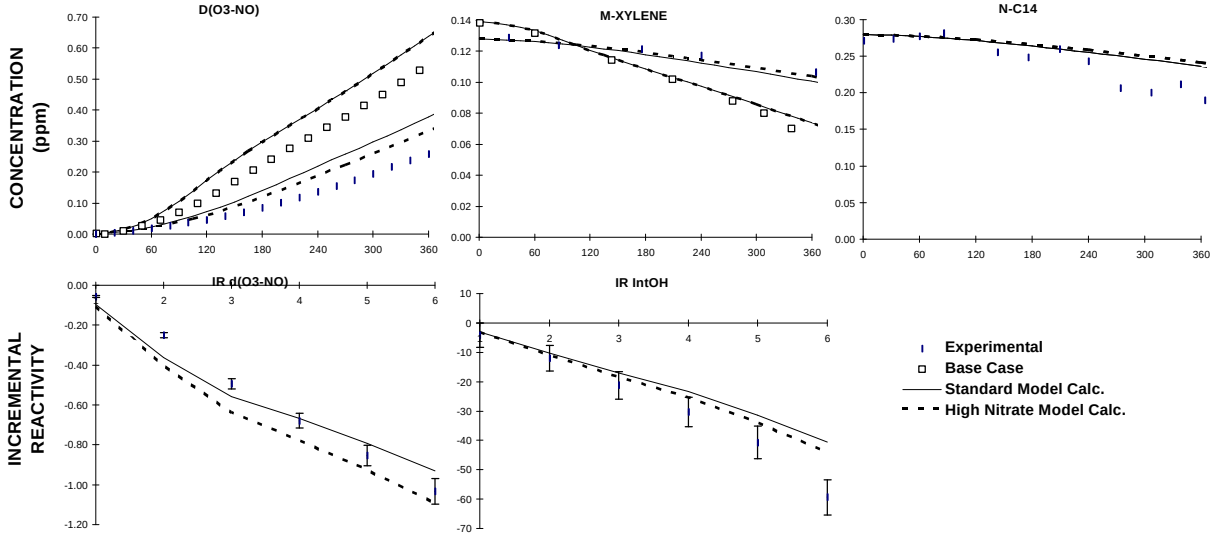

Figure B-6. Plots of selected results of the mini-surrogate + n-C_{14} experiment DTC-289.

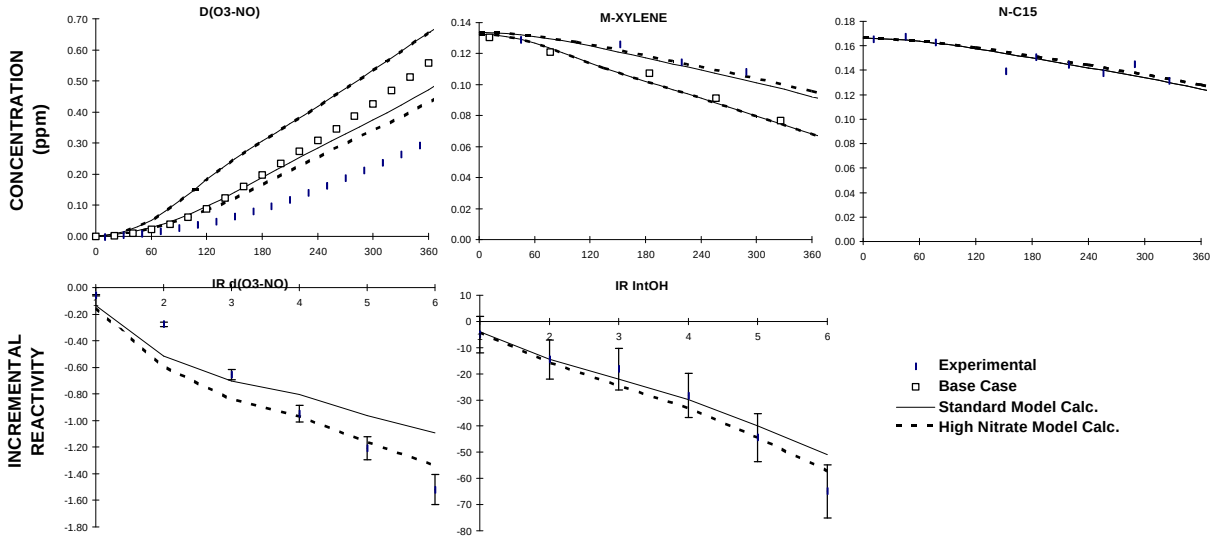

Figure B-7. Plots of selected results of the mini-surrogate + n-C_{15} experiment DTC-279.

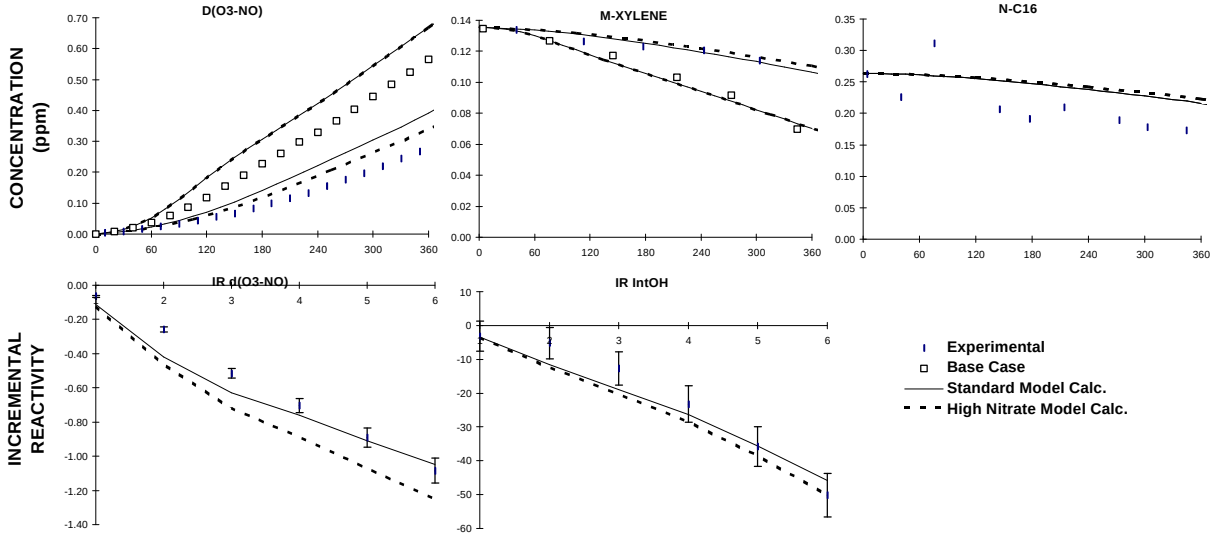

Figure B-8. Plots of selected results of the mini-surrogate + n-C_{16} experiment DTC-291.

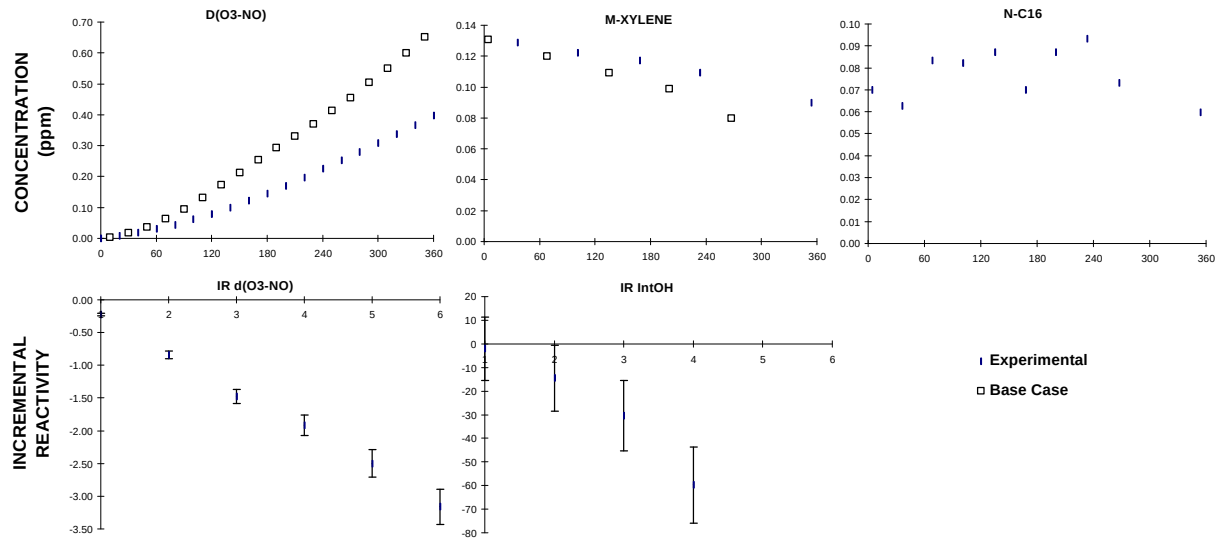

Figure B-9. Plots of selected results of the mini-surrogate + n-C_{16} experiment DTC-282. (The run was not modeled because the initial n-C_{16} was highly uncertain.)

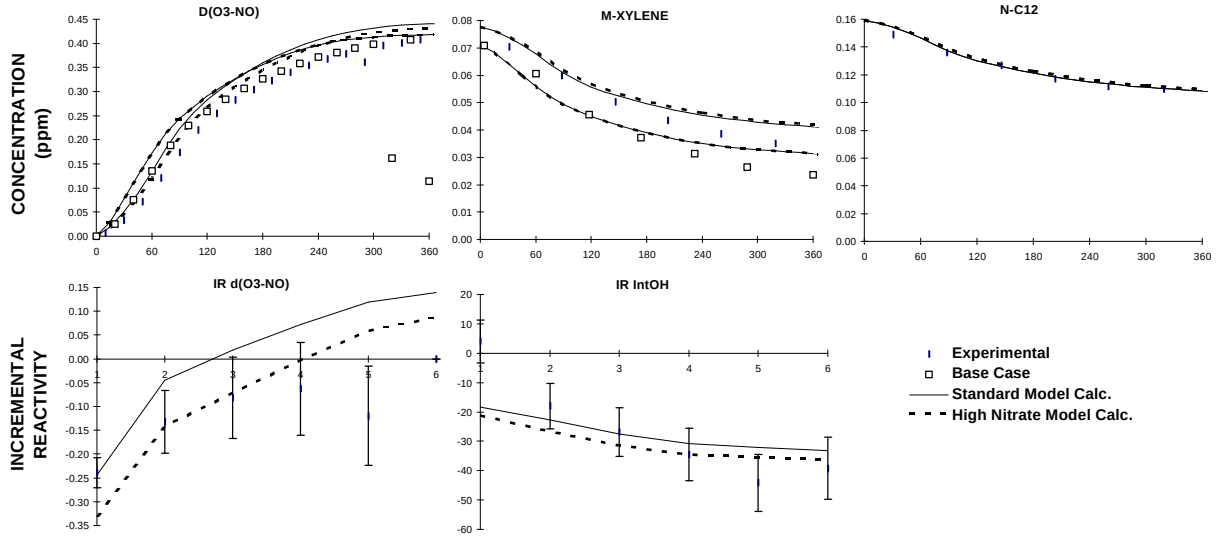

Figure B-10. Plots of selected results of the full surrogate + n-C_{12} experiment DTC-272.

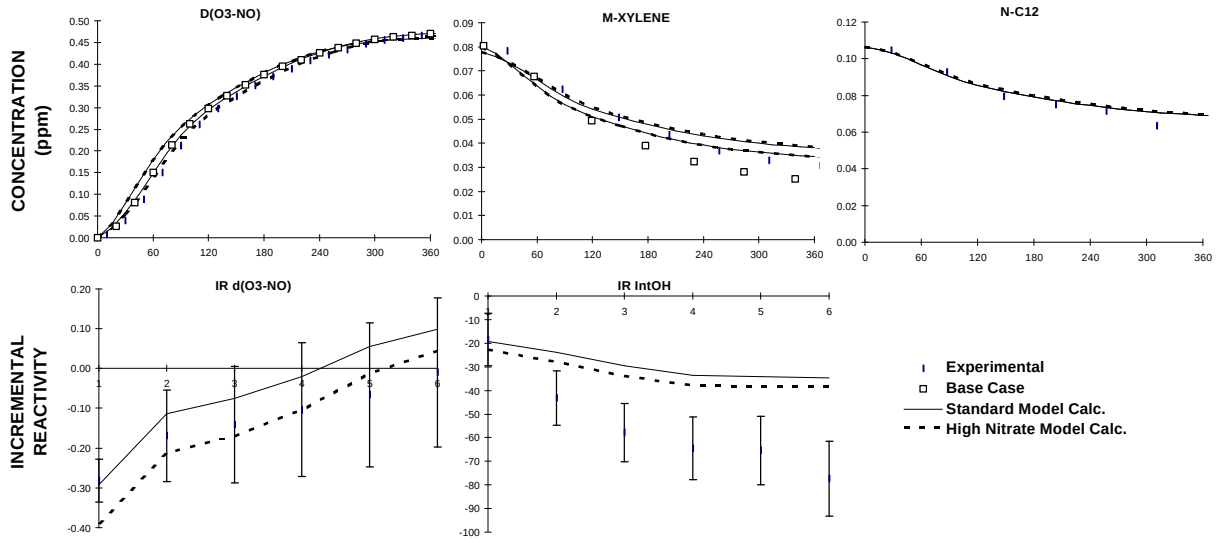

Figure B-11. Plots of selected results of the full surrogate + n-C_{12} experiment DTC-274.

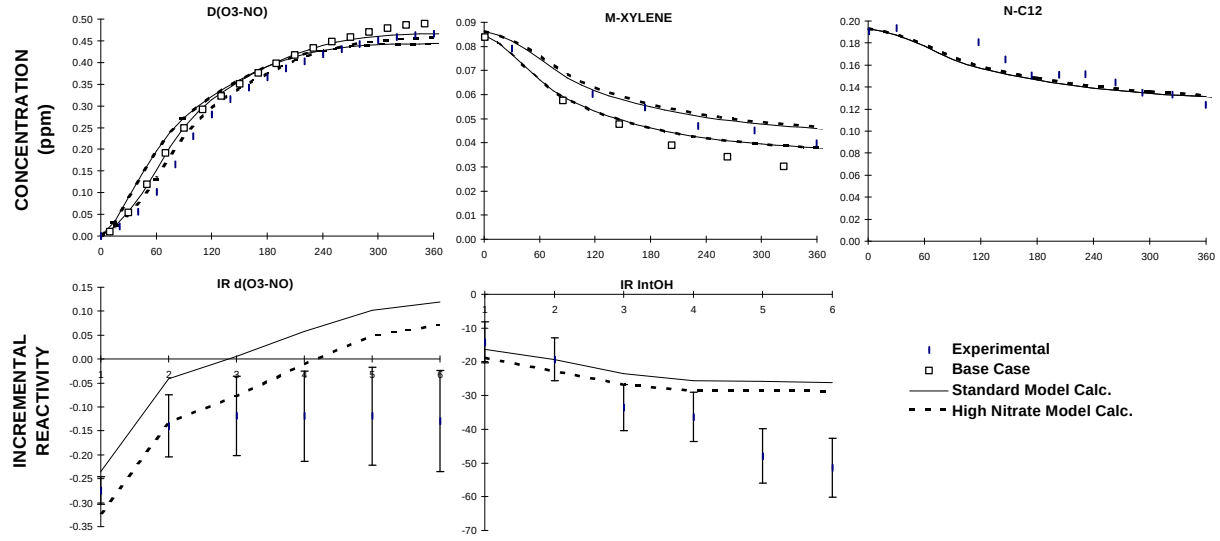

Figure B-12. Plots of selected results of the full surrogate + n-C_{12} experiment DTC-284.

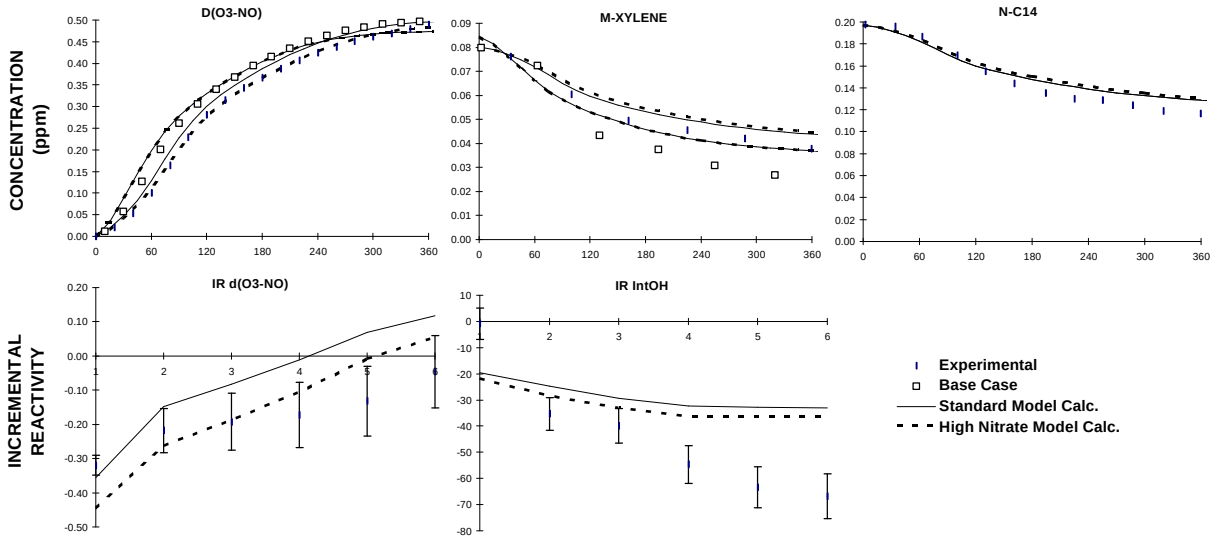

Figure B-13. Plots of selected results of the full surrogate + n-C_{14} experiment DTC-276.

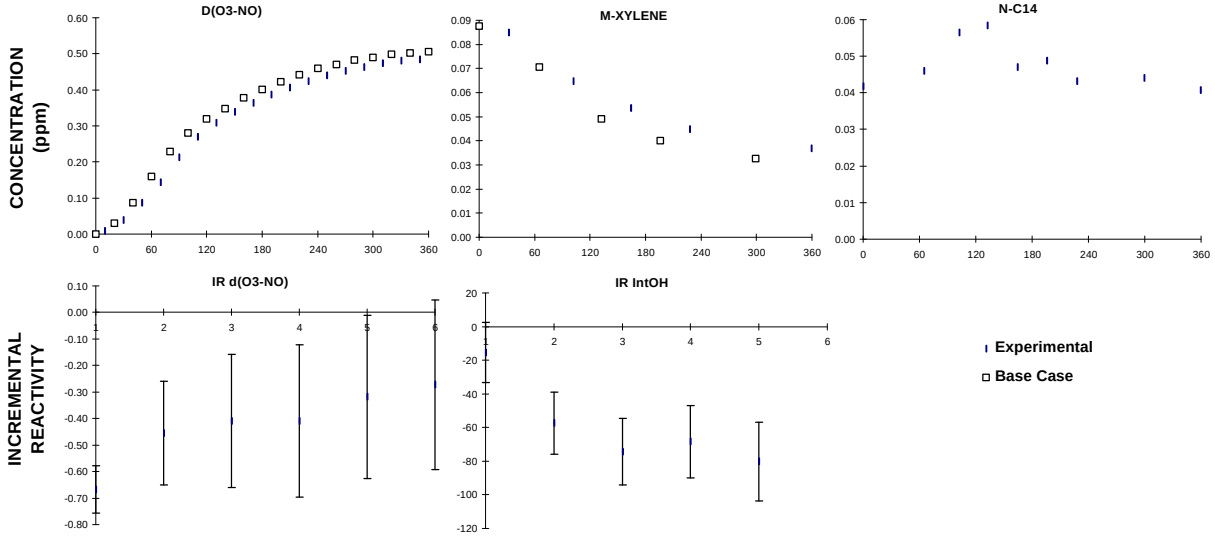

Figure B-14. Plots of selected results of the full surrogate + n-C_{14} experiment DTC-278. (The initial n-C_{14} was to uncertain for the run to be modeled.)

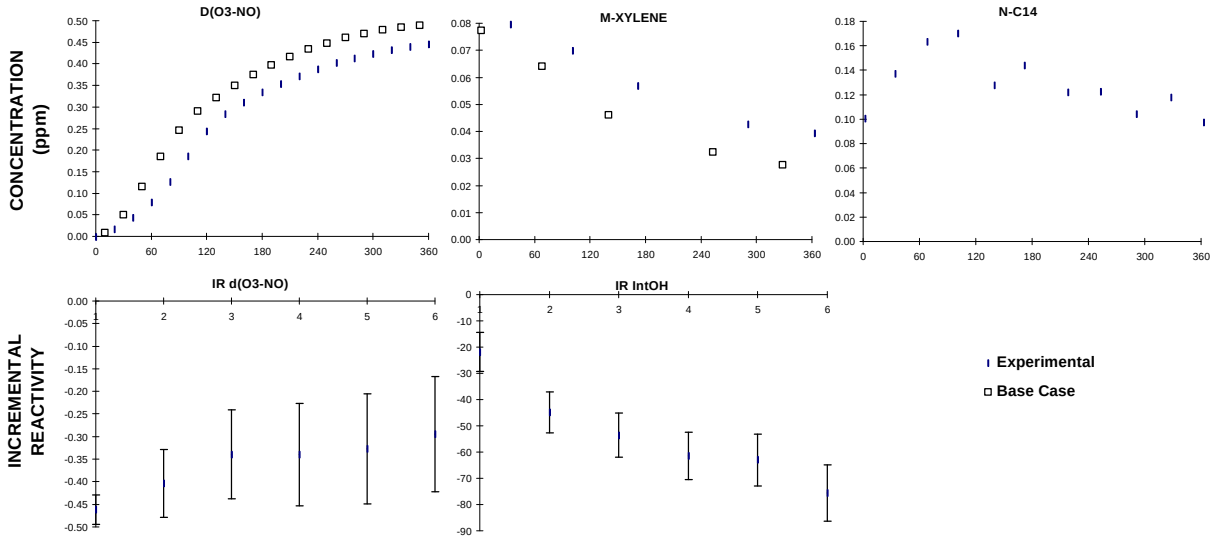

Figure B-15. Plots of selected results of the full surrogate + n-C_{14} experiment DTC-290. (The initial n-C_{14} was to uncertain for the run to be modeled.)

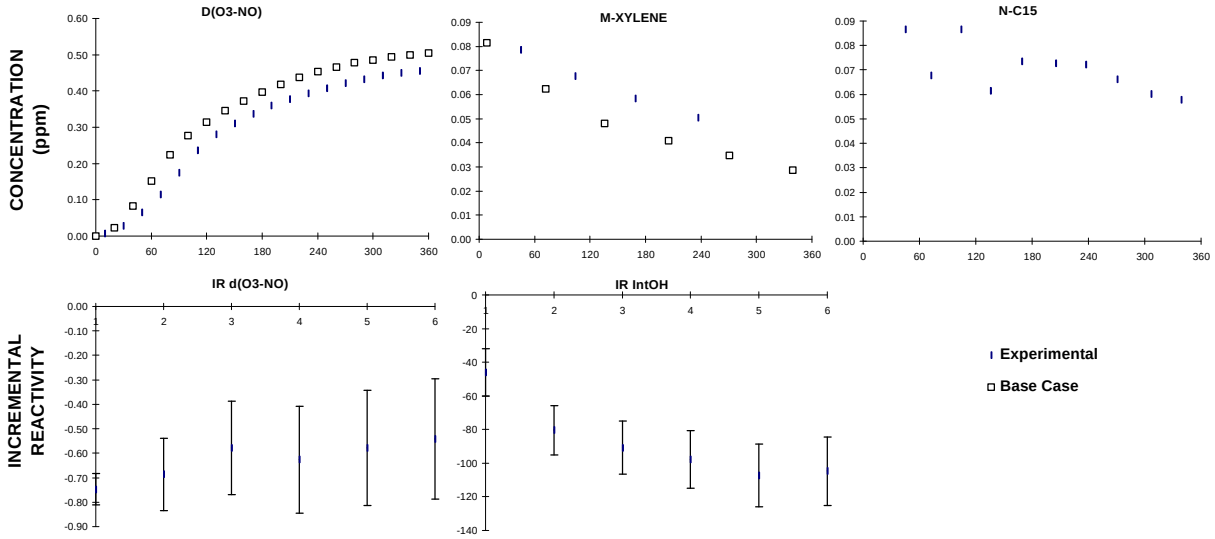

Figure B-16. Plots of selected results of the full surrogate + n-C_{15} experiment DTC-280. (The initial n-C_{15} was too uncertain for the run to be modeled.)

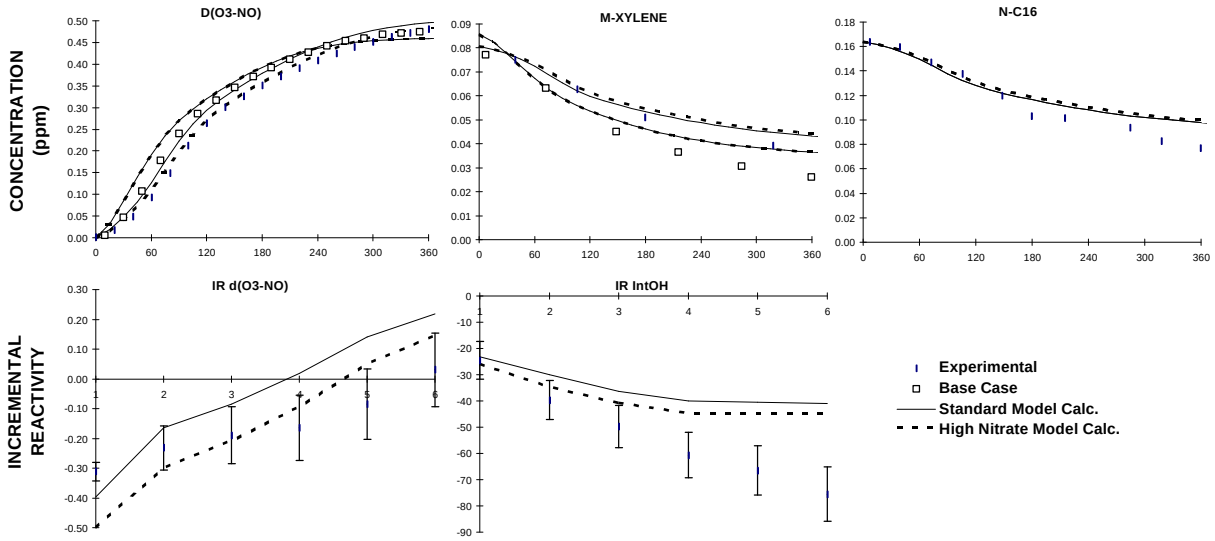

Figure B-17. Plots of selected results of the full surrogate + n-C_{16} experiment DTC-281.

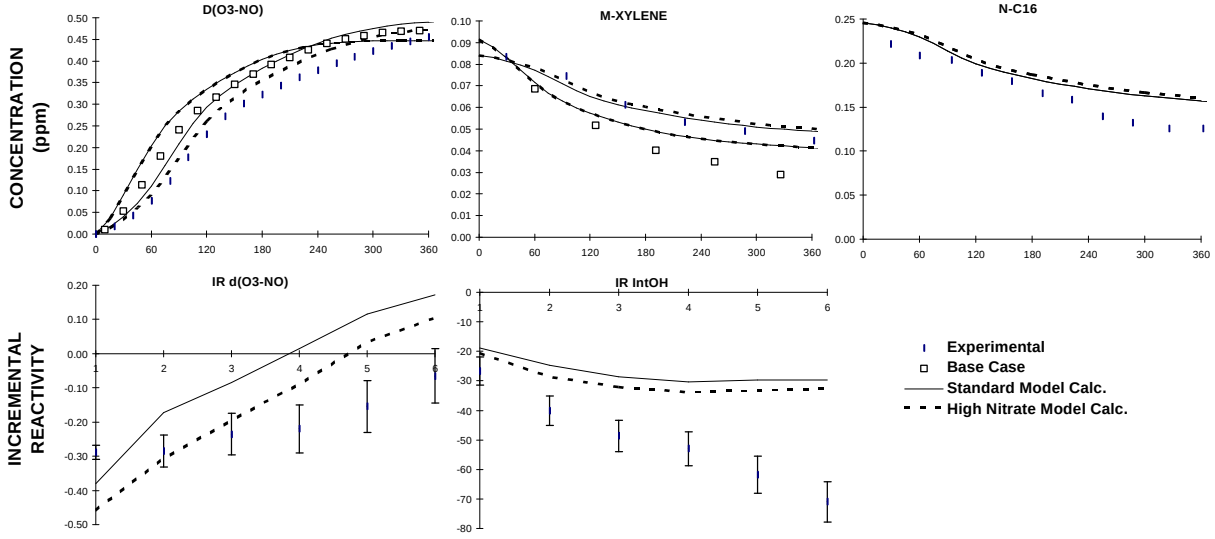

Figure B-18. Plots of selected results of the full surrogate + n-C_{16} experiment DTC-292.

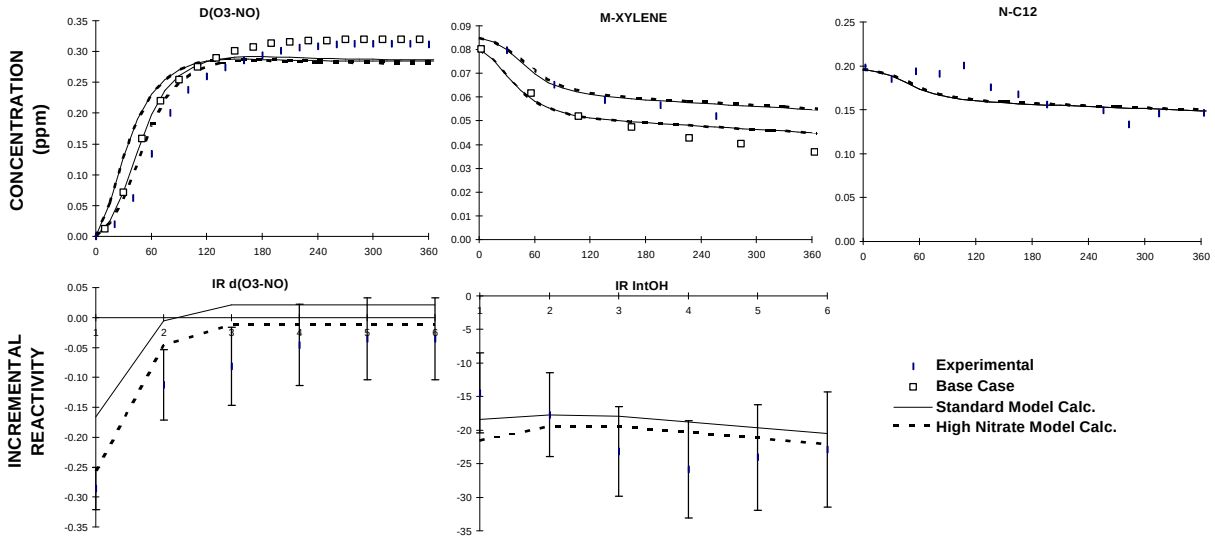

Figure B-19. Plots of selected results of the low NO_x full surrogate + n-C_{12} experiment DTC-293.

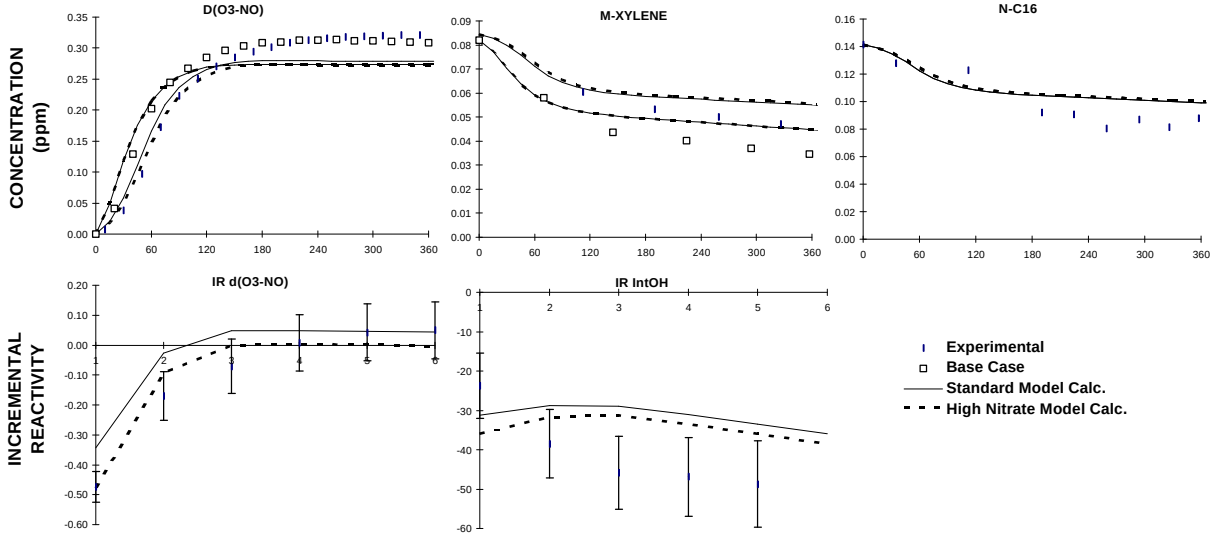

Figure B-20. Plots of selected results of the low NO_x full surrogate + n-C_{16} experiment DTC-298.

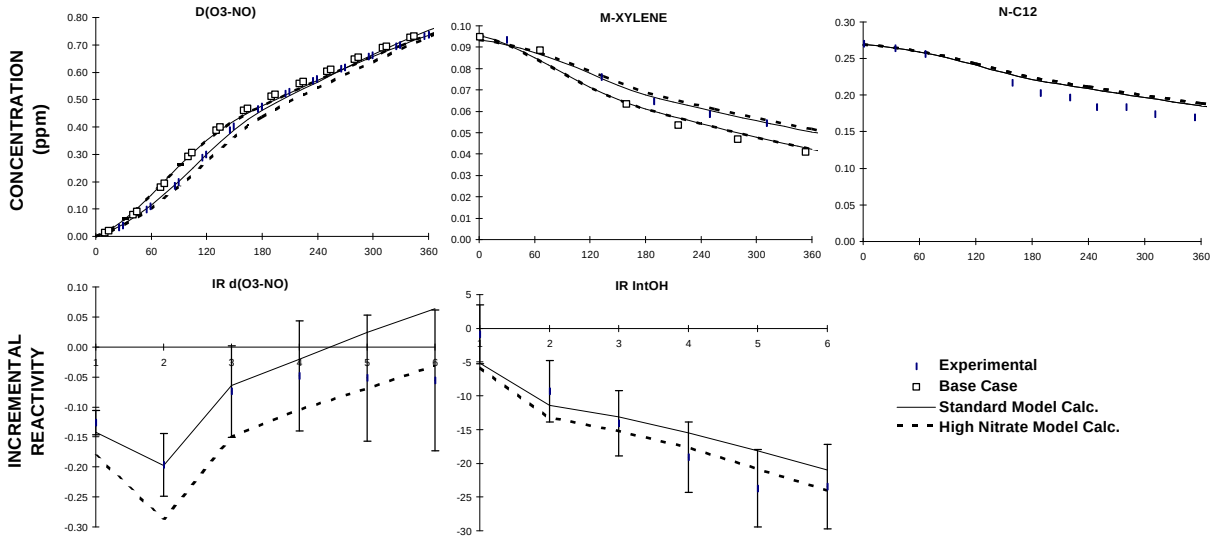

Figure B-21. Plots of selected results of the full surrogate + n-C_{12} experiment CTC-150, using the xenon arc light source.

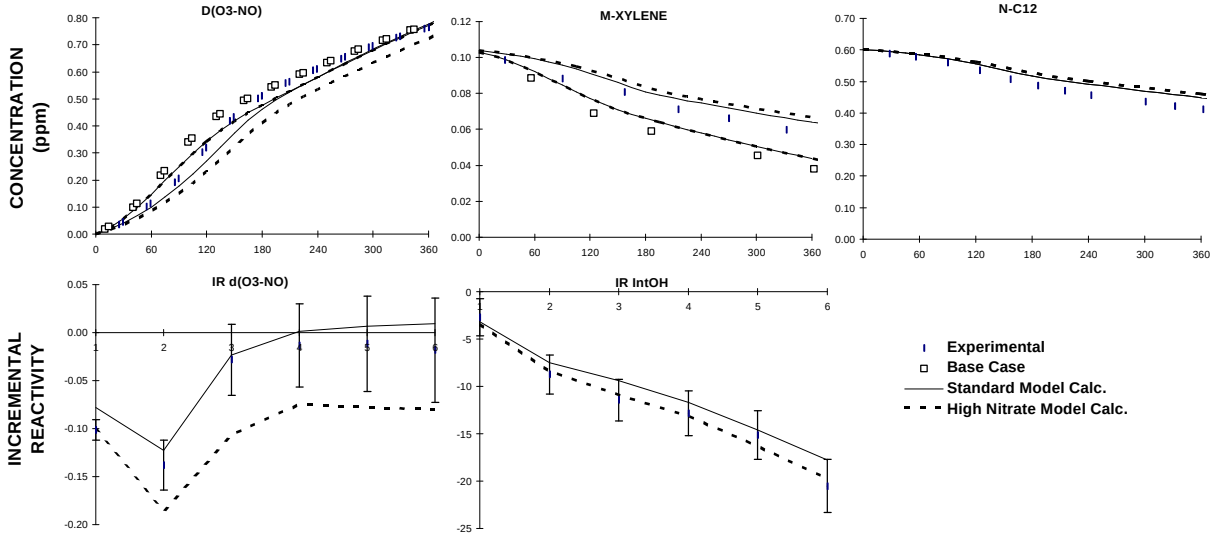

Figure B-22. Plots of selected results of the full surrogate + n-C_{12} experiment CTC-154, using the xenon arc light source.

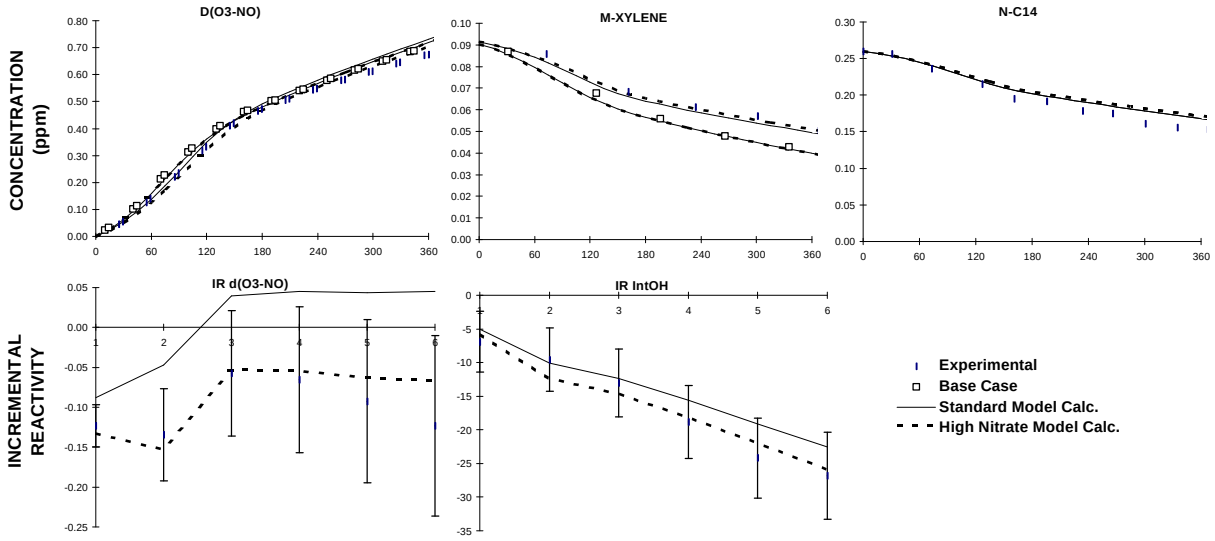

Figure B-23. Plots of selected results of the full surrogate + n-C_{14} experiment CTC-151, using the xenon arc light source.

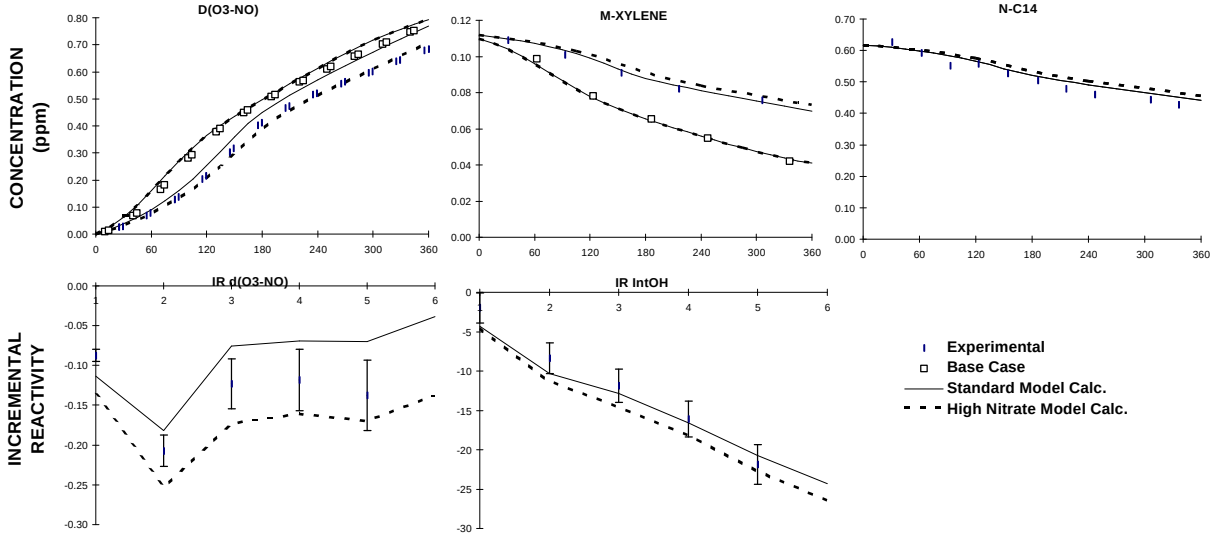

Figure B-24. Plots of selected results of the full surrogate + n-C_{14} experiment CTC-158, using the xenon arc light source.

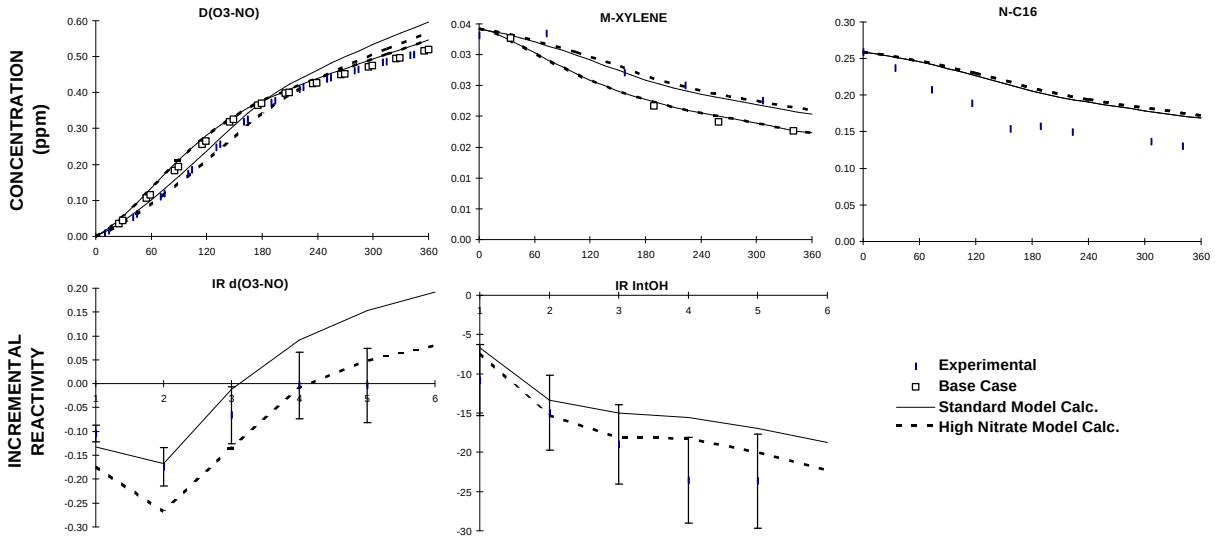

Figure B-25. Plots of selected results of the full surrogate + n-C_{16} experiment CTC-152, using the xenon arc light source.

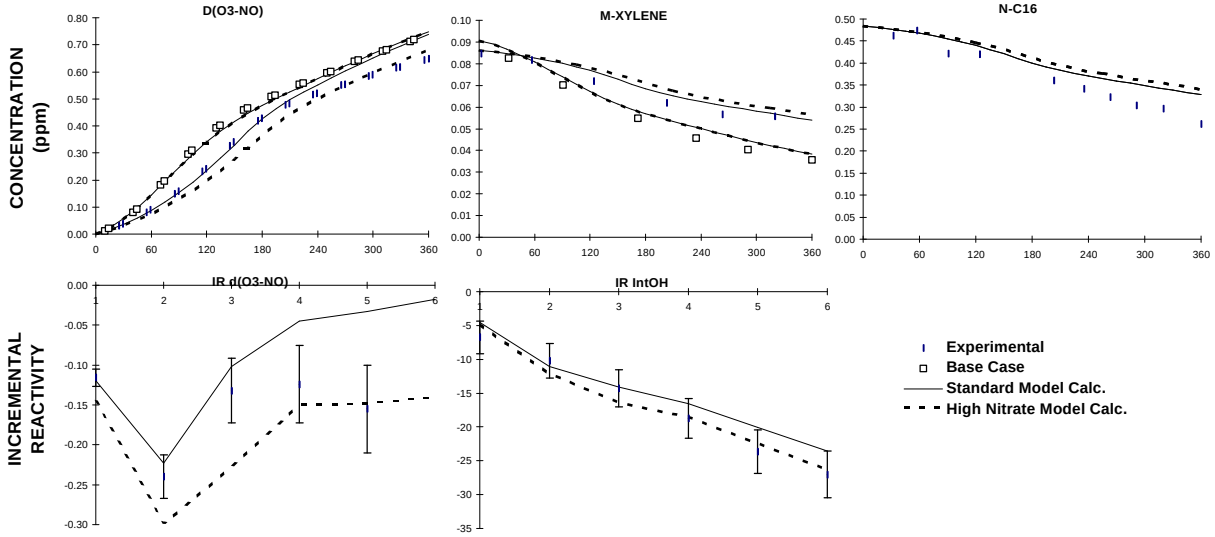

Figure B-26. Plots of selected results of the full surrogate + n-C_{16} experiment CTC-156, using the xenon arc light source.